Michael S. Triantafyllou
Antoine Bliek
Jim Burgess
Hyunkyoung Shin

Mooring Dynamics for Offshore Applications

Part II Applications

MIT Sea Grant
College Program

Massachusetts
Institute of Technology
Cambridge, MA 02139

MITSG
January

MOORING DYNAMICS FOR OFFSHORE APPLICATIONS

Part II APPLICATIONS

Michael S. Triantafyllou
Antoine Bliek
Jim Burgess
Hyunkyoung Shin

Sea Grant College Program
Massachusetts Institute of Technology
Cambridge, MA 02139

Index No. NA81AA-D00069
Project No. R/O-5

MITSG 86-2
January 1986

Acknowledgments

This research was supported by the MIT Sea Grant Program through the National Oceanic and Atmospheric Administration in the US Department of Commerce and by NAVSEA and a consortium of companies, including Conoco, Exxon, Gulf, HydroNorsk, Mobil and Shell.

Authors

The authors are all affiliated with the MIT Department of Ocean Engineering and held the following positions at the time this report was completed:

Michael S. Triantafyllou, Associate Professor
Antoine Bliek, Post-Doctoral Associate
Jim Burgess, Post-Doctoral Associate
Hyunkyoung Shin, Gruaduate Student

Table of Contents

List of Figures

List of Tables

Introduction

This is part II of the final report of a research effort conducted at the Ocean Engineering Department at M.I.T., supported jointly by the Sea Grant Program, NAVSEA and a consortium of offshore companies consisting of

Conoco Inc.

Exxon Production Research Company

Gulf Oil Exploration and Production Company

Norsk-Hydro

Mobil Research and Development Corporation

Shell Development Company

In part II a number of examples, relevant to the offshore industry, are given to illustrate the theory which was presented in part I. Examples were divided in three categories: linear dynamics, nonlinear dynamics and snap motions, and equivalent linearization techniques.

Chapter 1

NUMERICAL APPLICATIONS OF THE LINEAR DYNAMICS

1.1 Introduction

In this chapter, a number of applications of the solutions for linear cable dynamics are discussed, with the intention to illustrate the presented theory.

1.2 WKB Approximation of the Dynamics of Strings with Varying Tension

The accuracy of the WKB solution for strings with varying tension was tested for a linear tension variation. The legs of a tension leg platform were modeled as a string fixed at both ends. We consider two cases.

	Case A	Case B
Length (m)	549	549
Area (m^2)	0.00215	0.00215
Density (kg/m^3)	7870	7870
Lower tension (N)	$371\ 10^6$	$5\ 10^3$
Weight (N/m)	1449	1449
Mass (kg/m)	1907	1907

In the mass term the transverse added mass was included. The ratio of the top tension to the bottom tension was:

T_t/T_b	1.21	160

The second case was only selected to show the behavior of the WKB

method near the turning point.

Comparison of the eigenfrequencies

	Case A		Case B	
Eigenmode	Bessel	WKB	Bessel	WKB
1	0.83733	0.83744	0.18796	0.19963
2	1.67482	1.67488	0.39076	0.39925
3	2.51228	2.51231	0.59224	0.59888

The WKB method provides accurate results, even very close to the turning point of the solution. The approximation is increasingly better for higher frequencies. because the variation of the static quantities over a wave length is smaller. In addition to the eigenfrequencies, the eigenmodes are also well approximated. The "worst" case result is given in figure 1-1, which shows the approximation for the first mode of case B. Agreement in this case is still surprisingly good.

The extension of the above ideas to include bending rigidity (necessary for accurate analysis) has been carried out by [Kim 83], where similarly good agreement was found. First order WKB solutions can give very accurate results with a minimum of computational requirements.

1.3 Parametric Study of the Eigenfrequencies of a Two-Dimensional Cable

The eigenfrequencies of a two-dimensional cable hanging under its own weight have been studied extensively numerically, as well as experimentally.

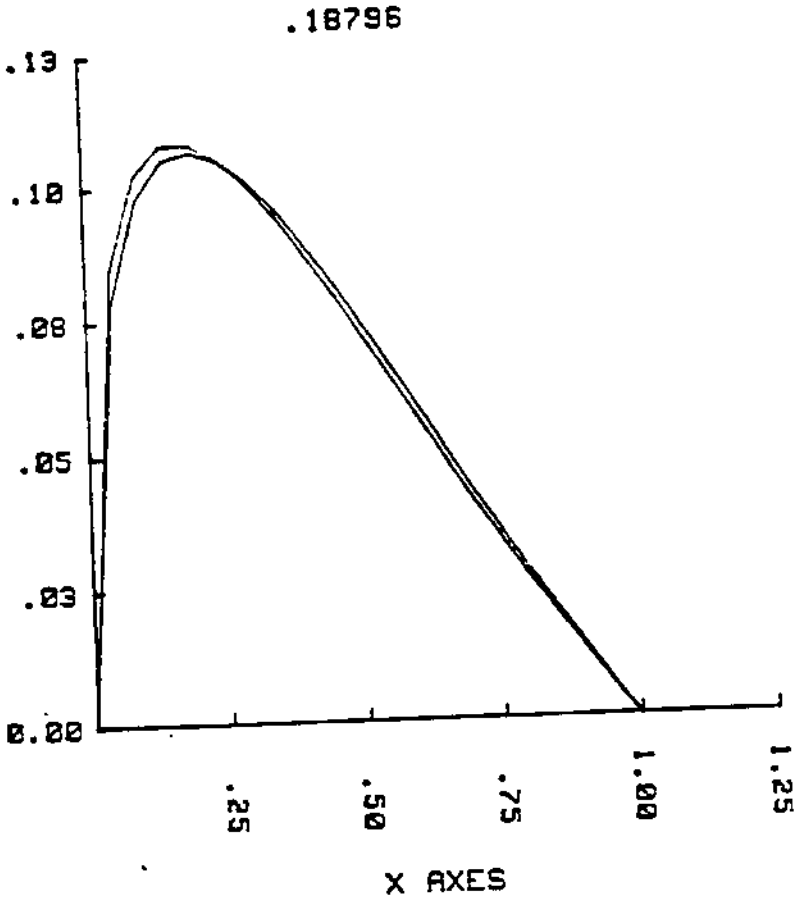

Figure 1-1: Comparison between the Mode Shapes of the WKB Solution and the Bessel Solution

Pugsley [Pugsley 49], Saxon and Cahn [Saxon 53] and Goodey [Goodey 61] studied the behavior of inextensible cables. Pugsley, and Saxon and Cahn performed also a limited number of experiments.

Irvine and Caughey [Irvine 74] predicted succesfully using approximate analytic techniques the cross-over phenomena for a small sag, horizontal cable. Among the most recent numerical contributions on eigenfrequencies of extensible cables are: West et al. [West 75], Gambhir and Batchelor [Gambhir 77] and Henghold et al. [Henghold 77]. Ramberg and Bartholomew [Ramberg 82] did some experiments on the vibration of inclined slack cables. Although all of the above authors were able to confirm the existence of cross-over phenomena for extensible cables in the horizontal case, the phenomena of hybrid modes were not detected. This is mainly due, in the author's opinion, to the very small transition region in the cases considered by the above researchers. Yamaguchi [Yamaguchi 79] used a Galerkin's expansion with sinusoidal terms to calculate the eigenfrequencies. He obtained hybrid modes and the non-crossing of the modes.

In the course of this report, a number of perturbation and numerical calculations of eigenfrequencies were carried out. We will briefly discuss some of the results.

1.3.1 Non-Dimensional Parameters

The governing equations in non-dimensional form depend only on 4 non-dimensional parameters when a uniform cable hanging under its own weight is considered. They can be written as:

1. The angle of inclination (ϕ_a) of the line connecting the two end

points with a horizontal.

2. The ratio of the total weight of the cable and the tension projected on the chord ($\alpha = w_0 L/H \cos\phi_a = w_0 L/H_*$).

3. The projected elastic strain: the ratio of the projected tension and the uniform stiffness of the cable ($\beta = H_*/E\cdot A$).

4. The ratio of the mass and the mass plus the added mass.

The non-dimensional frequency was selected as follows:

$$\bar{\omega} = \frac{\omega L (M/H_*)^{1/2}}{\pi} \tag{1.1}$$

where: ω is the frequency

L is the length of the cable

H_* is $H/\cos\phi_a$

M is the mass plus the added mass

H is the horizontal tension

In the case of string: $\bar{\omega} = n \qquad n = 1, 2, 3 \ldots$

The above non-dimensionalisation of the frequency has the advantage that it virtually eliminates the dependency of the eigenfrequencies on h. The influence of the variation of h on $\bar{\omega}$ is small and will not be discussed here. In the sequel, cables in air will be analysed (h = 1). The results, though, should be a good approximation for the eigenfrequencies in water when (1.1) is used.

1.3.2 Inextensible Cables

The non-dimensional parameters are in this case:

1. ϕ_a, the inclination angle

2. $\alpha = \frac{w_o L}{H_*}$, the non-dimensional weight parameter

Three representative inclination angles were selected: 0° , 30° , 60°. The non-dimensional weight parameter was varied between 0 and 5. The cables for high values of α are extremely slack (for a horizontal cable, $\alpha = 5$ corresponds to a top angle of 68°).

The results can be found in figure 1-2 – 1-4. The solid lines are the results obtained with the inextensible perturbation theory. The + marks denote the results obtained with the numerical central difference scheme (100 points). The numerical solution can be considered as an "exact" solution, considering the resolution of the graph. For small α, the shallow sag inextensible eigenfrequencies are recovered. The curves are tangential to a horizontal line for the small sag inextensible eigenfrequencies. The small sag results can, therefore, be extrapolated to moderately large values of α.

The perturbation theory predicts fairly accurately the eigenfrequencies for the whole range of α and ϕ_a. Only for very high values of α and/or high inclination angles the predictions are deteriorating. Due to the nature of the perturbation expansions the prediction will be more accurate for the higher modes. This can be clearly seen on figure 1-4.

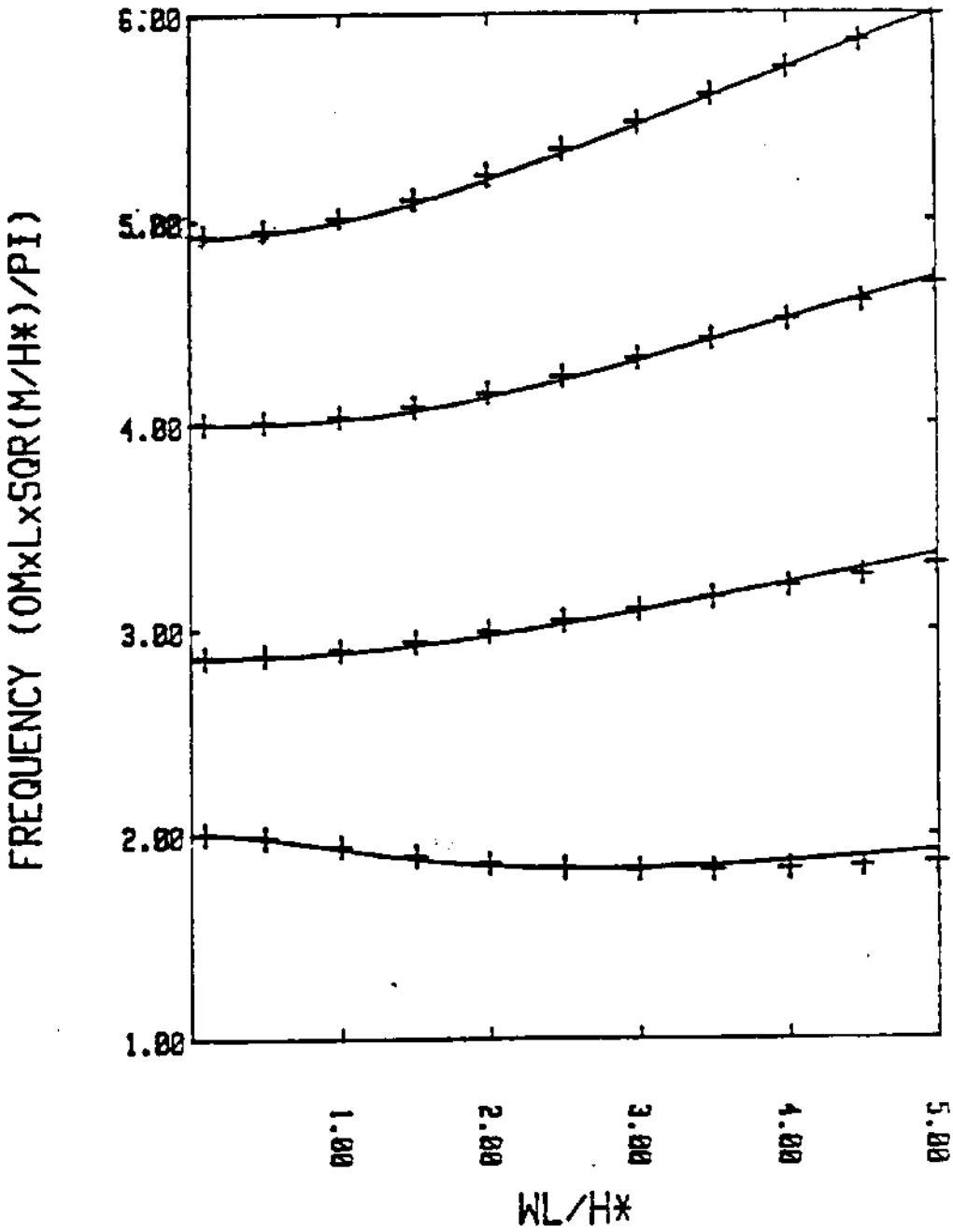

Figure 1-2: Eigenfrequencies for an Inextensible Cable, $\phi_a = 0^o$

(Solid line: inextensible perturbation theory)
(+ marks: numerical central difference scheme with 100 points)

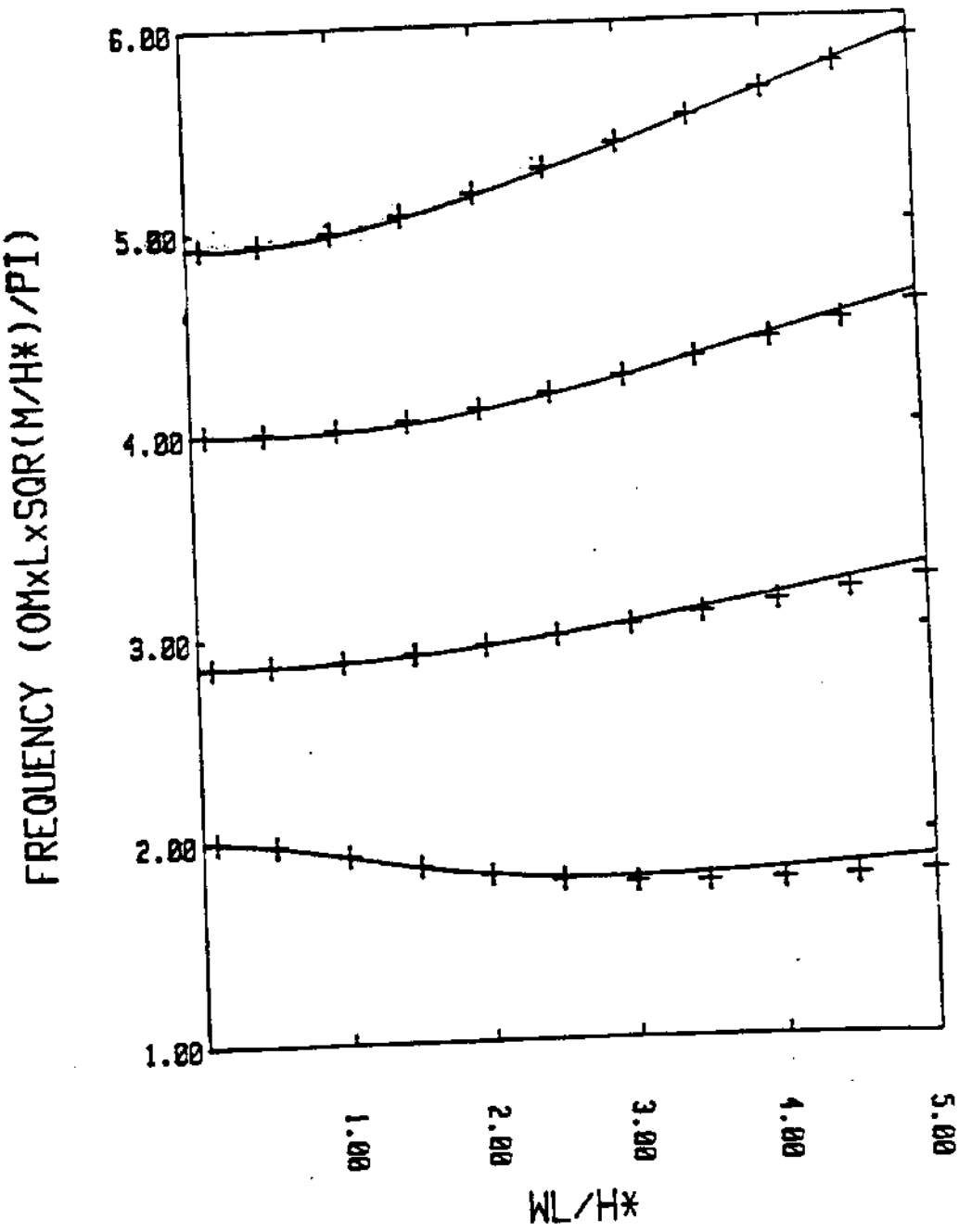

Figure 1-3: Eigenfrequencies for an Inextensible Cable, $\phi_a = 30^\circ$

(Solid line: inextensible perturbation theory)
(+ marks: numerical central difference scheme with 100 points)

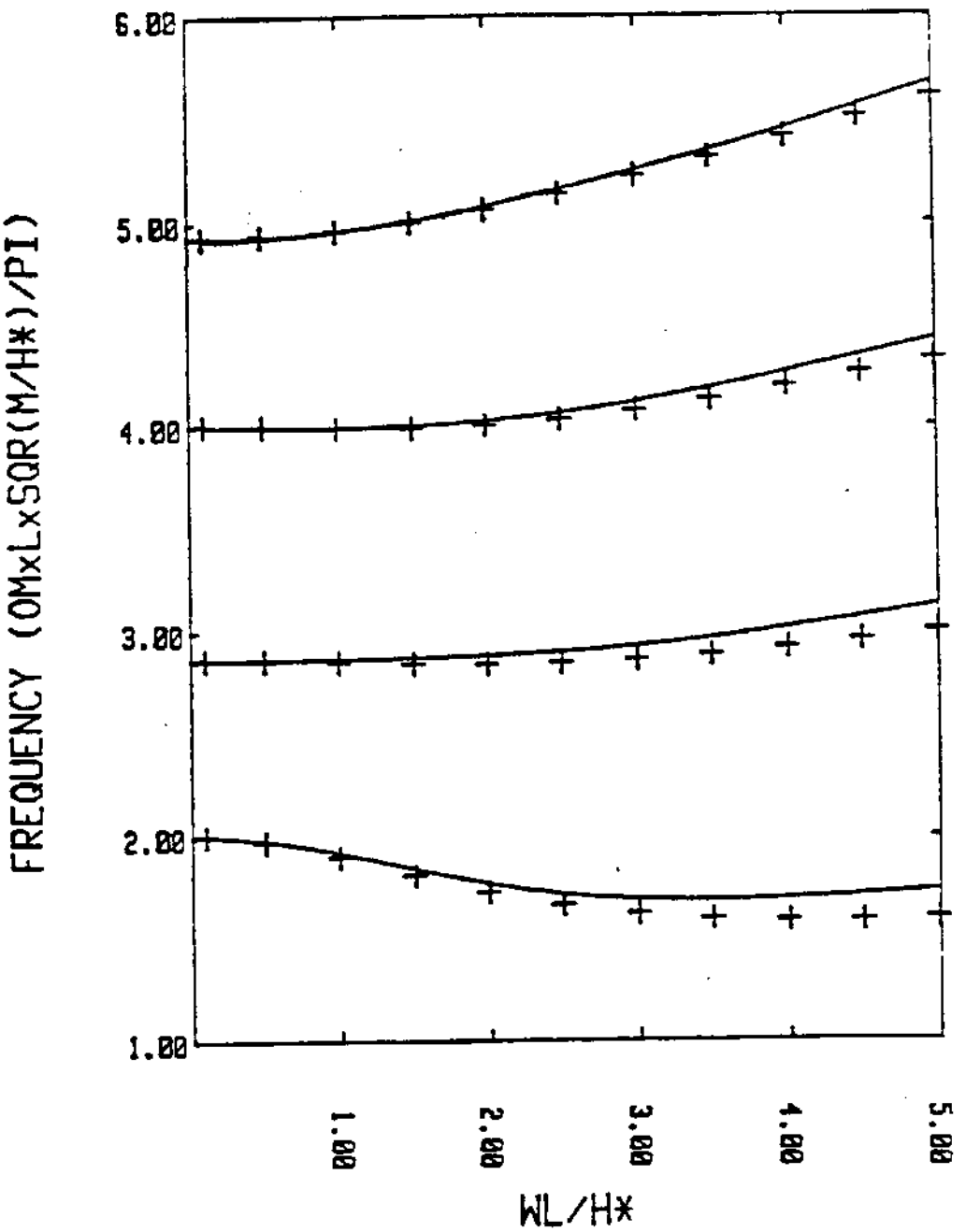

Figure 1-4: Eigenfrequencies for an Inextensible Cable, $\phi_a = 60^\circ$

(Solid line: inextensible perturbation theory)
(+ marks: numerical central difference scheme with 100 points)

1.3.3 Extensible Cables

The eigenfrequencies of extensible cables (with h = 1) depends on 3 non-dimensional parameters:

1. ϕ_a, the inclination angle

2. α, the non-dimensional weight parameter ($w_o L/H_*$)

3. β, the projected elastic strain ($H_*/E{\cdot}A$)

There are several possibilities to represent the variation of the eigenfrequencies in terms of these three parameters. We will briefly discuss two of them.

First, the projected elastic strain was selected as a fixed parameter. This corresponds to choosing the ratio of the elastic and the transverse wave speed. This is a fairly good choice, because the elastic strain is restricted in design applications to be within a certain range. Yamaguchi [Yamaguchi 79] used this approach in his paper, while the non-dimensional weight parameter was selected as the independent variable. This allows direct comparison with the inextensible cables (A good alternative to this could be λ_*^2.)

The following relation between the ratio of the wave speed and the projected elastic strain exists:

$$\frac{c_{el}^2}{c_{tr}^2} = \frac{E{\cdot}A}{H_*} = \frac{1}{\beta} \qquad (h = 1) \tag{1.2}$$

For steel cables, a value of 400 was selected for $1/\beta$ (wave speed ratio of 20). This can be considered to be close to the lowest acceptable value.

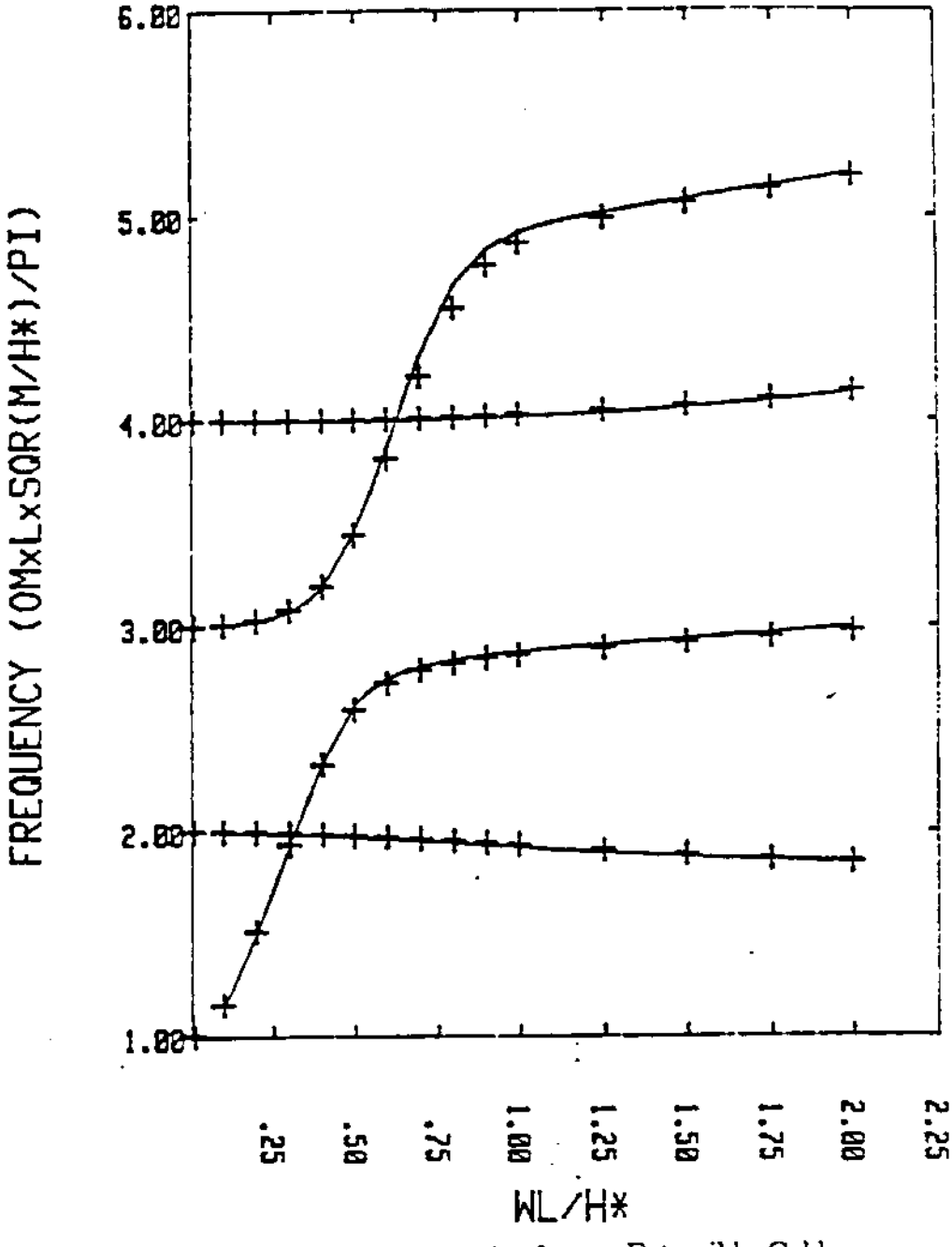

Figure 1-5: Eigenfrequencies for an Extensible Cable, $\phi_a = 0^\circ$, $\beta = 1/400$

(Solid line: extensible perturbation theory)
(+ marks: numerical central difference scheme)

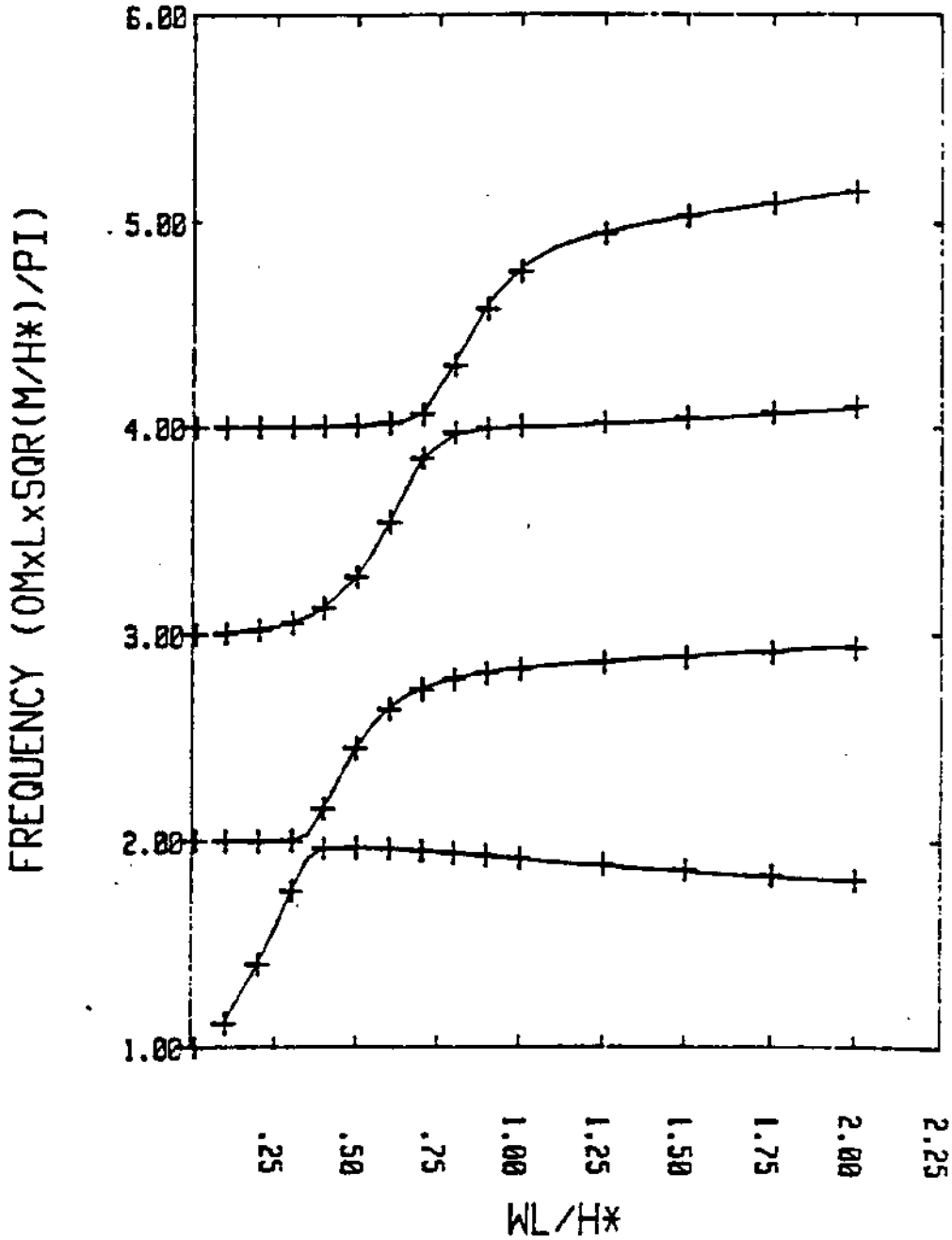

Figure 1-6: Eigenfrequencies for an Extensible Cable, $\phi_a = 30^\circ$, $\beta = 1/400$

(Solid line: extensible perturbation theory)
(+ marks: numerical central difference scheme)

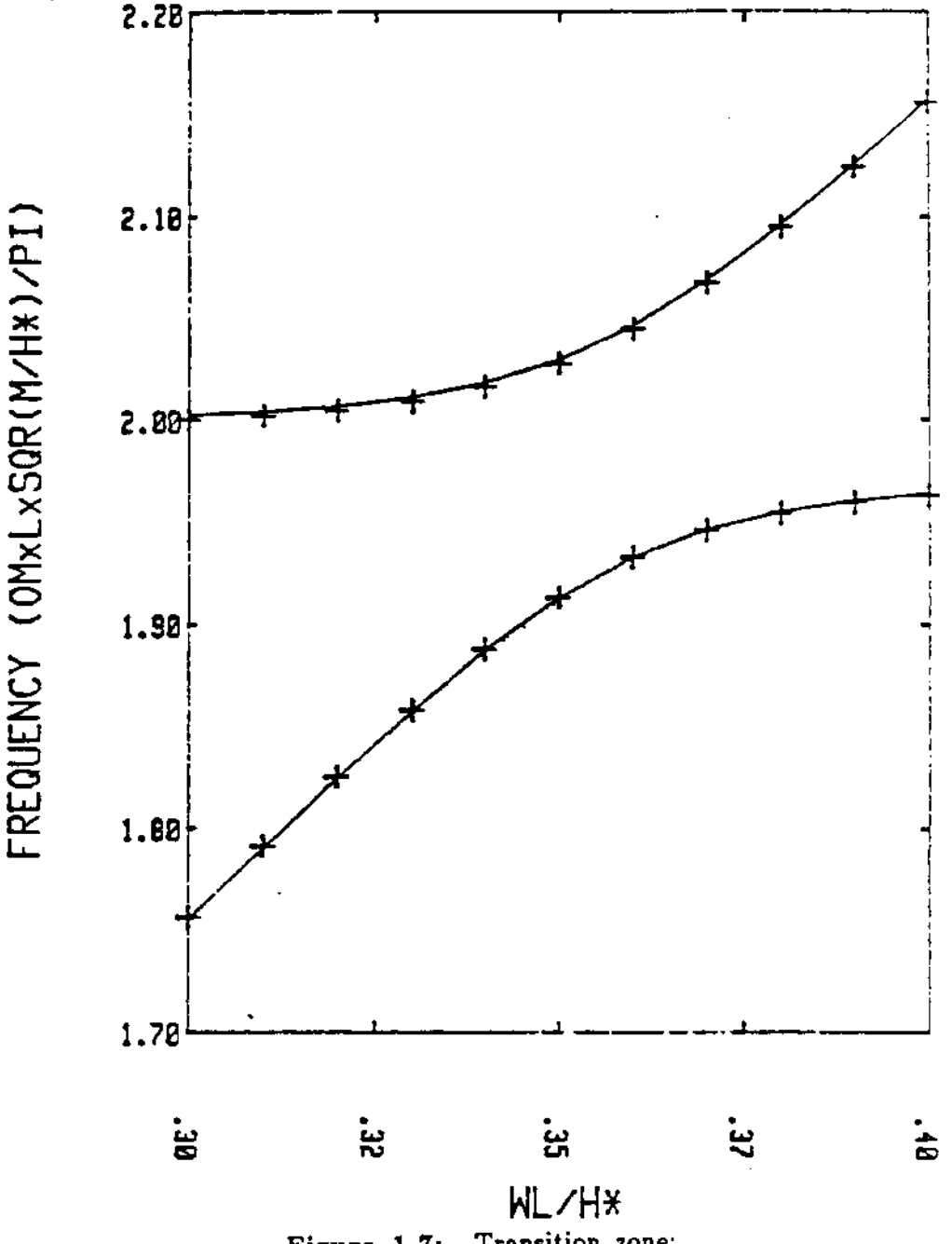

Figure 1-7: Transition zone:
Eigenfrequencies for an Extensible Cable.
$\phi_a = 30°$, $\beta = 1/400$

(Solid line: extensible perturbation theory)
(+ marks: numerical central difference scheme)

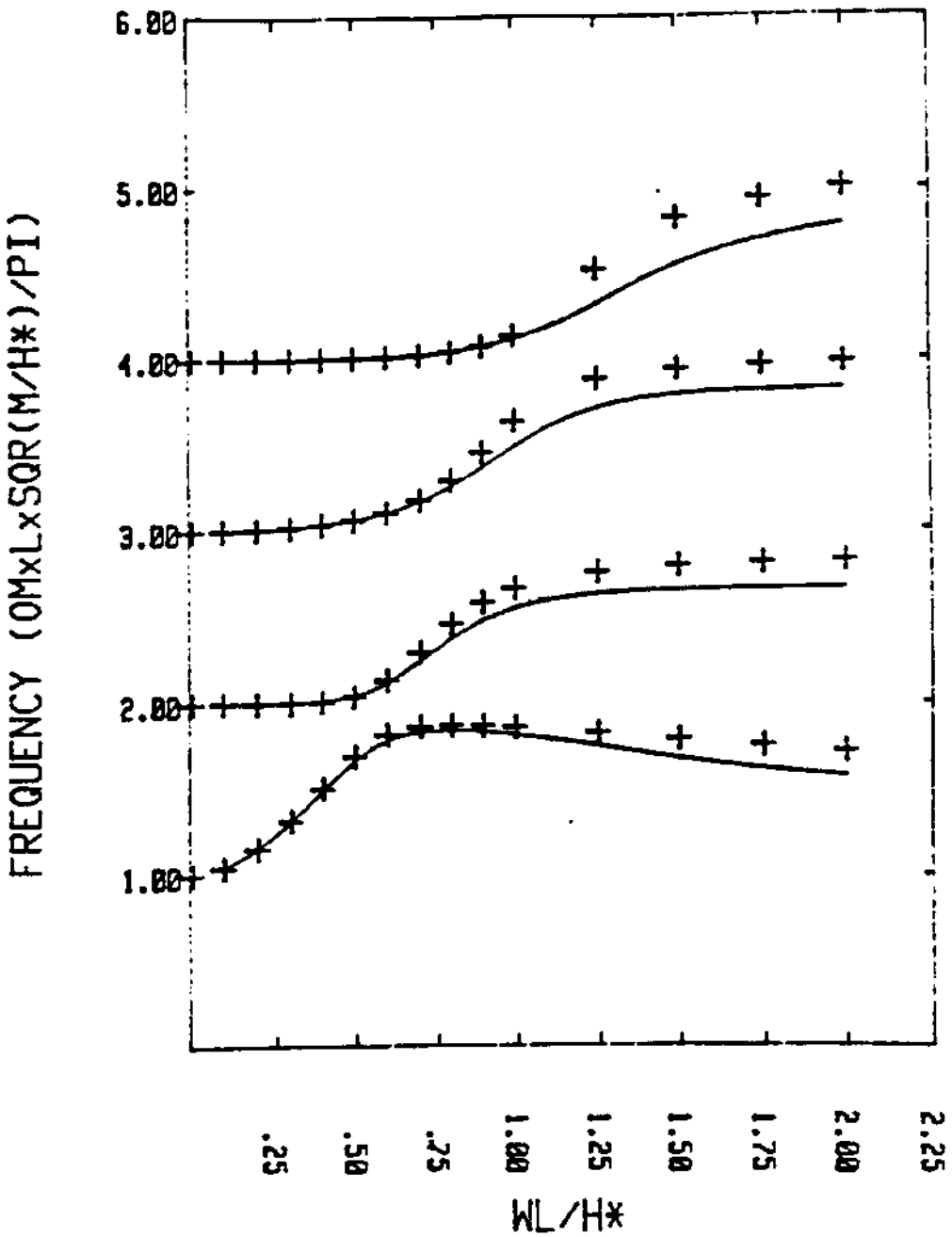

Figure 1-8: Eigenfrequencies for an Extensible Cable, $\phi_a = 60°$, $\beta = 1/400$

(Solid line: extensible perturbation theory)
(+ marks: numerical central difference scheme)

The results can be found in figures 1-5 through 1-8. The solid lines are the results obtained using the perturbation theory and assuming an extensible cable. For the slow solution, the first order approximation ($Q(\sigma) = Q_o$) was used, which provides exponential or sinusoidal slow solutions. The + marks denote the results obtained using a numerical central difference scheme (100 points). The cross-over is predicted accurately for an inclination angle of 0^o. For inclined cables the transition region is also well predicted by the perturbation theory. To prove clearly that no cross-over exists, an enlargement of the transition zone for an inclination angle of 30^o was made in figure 1-7. Again, the solution breaks down for large values of α and large inclination angles, as seen in figure 1-8. When the parabolic cylinder functions are used instead of the exponentials in the slow solution, a much better approximation for large α and large ϕ_a is obtained. This has a drawback in that the perturbation approximation becomes, of course, numerically more complicated. Overall, the simple exponential slow solution predicts the eigenfrequencies fairly accurately. The case selected here ($\beta = 1/400$) implies high straining of the cable and, therefore, for most applications the transition will occur for smaller values of α_*, for which the perturbation solution will be increasingly more accurate. For very low values of α_* the solution tends to the eigenfrequencies of the taut string, while for high values of α_* the eigenfrequencies of the inextensible cable are obtained.

The previous graphs have the drawback that the transition zone is strongly dependent on β. This can be reduced by plotting the eigenfrequencies versus λ_*^2. For small sag cables, as demonstrated in part I, the eigenfrequencies depend only on λ_*^2. For large sag cables this is not valid, but the representation in terms of λ_*^2 is still useful. λ_*^2 can be expressed as:

$$\lambda_*^2 = \left[\frac{w_o L}{H_*} \right]^2 \cdot \left[\frac{E \cdot A}{H_*} \right] \cdot \cos^2(\phi_a) \qquad (1.3)$$

$$= \frac{\alpha^2}{\beta}$$

In figure 1-9 and 1-10 the eigenfrequencies are plotted versus λ_*^2. The parameter α_* is kept fixed and is allowed to take three values (0 , 0.5 , 1). Figure 1-10 is an enlargement of the transition zone of the first and second modes. The eigenfrequency curves were cut off at $\beta = 1/100$. The cut-off value of λ_*^2 is higher for higher values of α_*^2, for which the transition zone becomes clearly more pronounced. With the exception of the transition zone, the shallow sag extensible theory gives a good approximation for values of $\alpha_* < 0.5$. Figure 1-11 provides the shallow sag eigenfrequencies and can be considered a fairly good approximation for $\alpha_* < 0.5$, outside the transition zone. For horizontal cables, the modes are crossing over and figure 1-11 will be approximately valid even for higher values of α_*.

1.4 Linear Dynamic Analysis of a Guy

The eigenfrequencies for the guy of a guyed tower were calculated using the finite differences and an approximate analytical method. The eigenmodes obtained by the finite difference scheme are also shown. Finally the undamped transfer functions for the guy, were calculated using both the perturbation method and the finite difference scheme (100 discretisation points).

The data for the guy are:

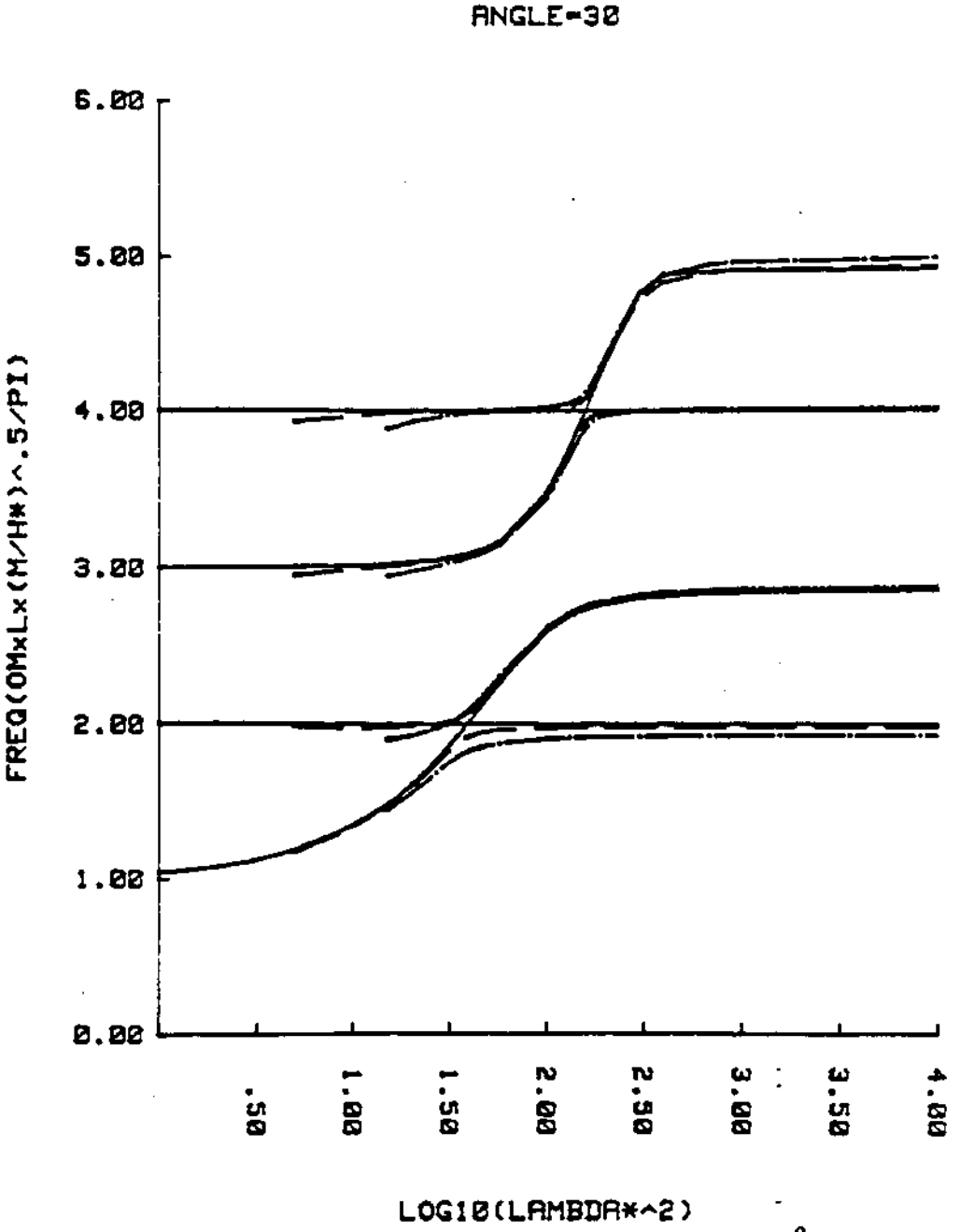

Figure 1-9: Eigenfrequencies of Extensible Cables vs. λ_*^2 ($\phi_a = 30$)

(solid line: $\alpha_* = 0$; dash line: $\alpha_* = 0.5$;
dot-dash line: $\alpha_* = 1$)

$$\lambda_*^2 = \left[\frac{w_o L}{H_*} \right]^2 \cdot \left[\frac{E \cdot A}{H_*} \right] \cdot \cos^2(\phi_a) \qquad (1.3)$$

$$= \frac{\alpha^2}{\beta}$$

In figure 1-9 and 1-10 the eigenfrequencies are plotted versus λ_*^2. The parameter α_* is kept fixed and is allowed to take three values (0 , 0.5 , 1). Figure 1-10 is an enlargement of the transition zone of the first and second modes. The eigenfrequency curves were cut off at $\beta = 1/100$. The cut-off value of λ_*^2 is higher for higher values of α_*^2, for which the transition zone becomes clearly more pronounced. With the exception of the transition zone, the shallow sag extensible theory gives a good approximation for values of $\alpha_* < 0.5$. Figure 1-11 provides the shallow sag eigenfrequencies and can be considered a fairly good approximation for $\alpha_* < 0.5$, outside the transition zone. For horizontal cables, the modes are crossing over and figure 1-11 will be approximately valid even for higher values of α_*.

1.4 Linear Dynamic Analysis of a Guy

The eigenfrequencies for the guy of a guyed tower were calculated using the finite differences and an approximate analytical method. The eigenmodes obtained by the finite difference scheme are also shown. Finally the undamped transfer functions for the guy, were calculated using both the perturbation method and the finite difference scheme (100 discretisation points).

The data for the guy are:

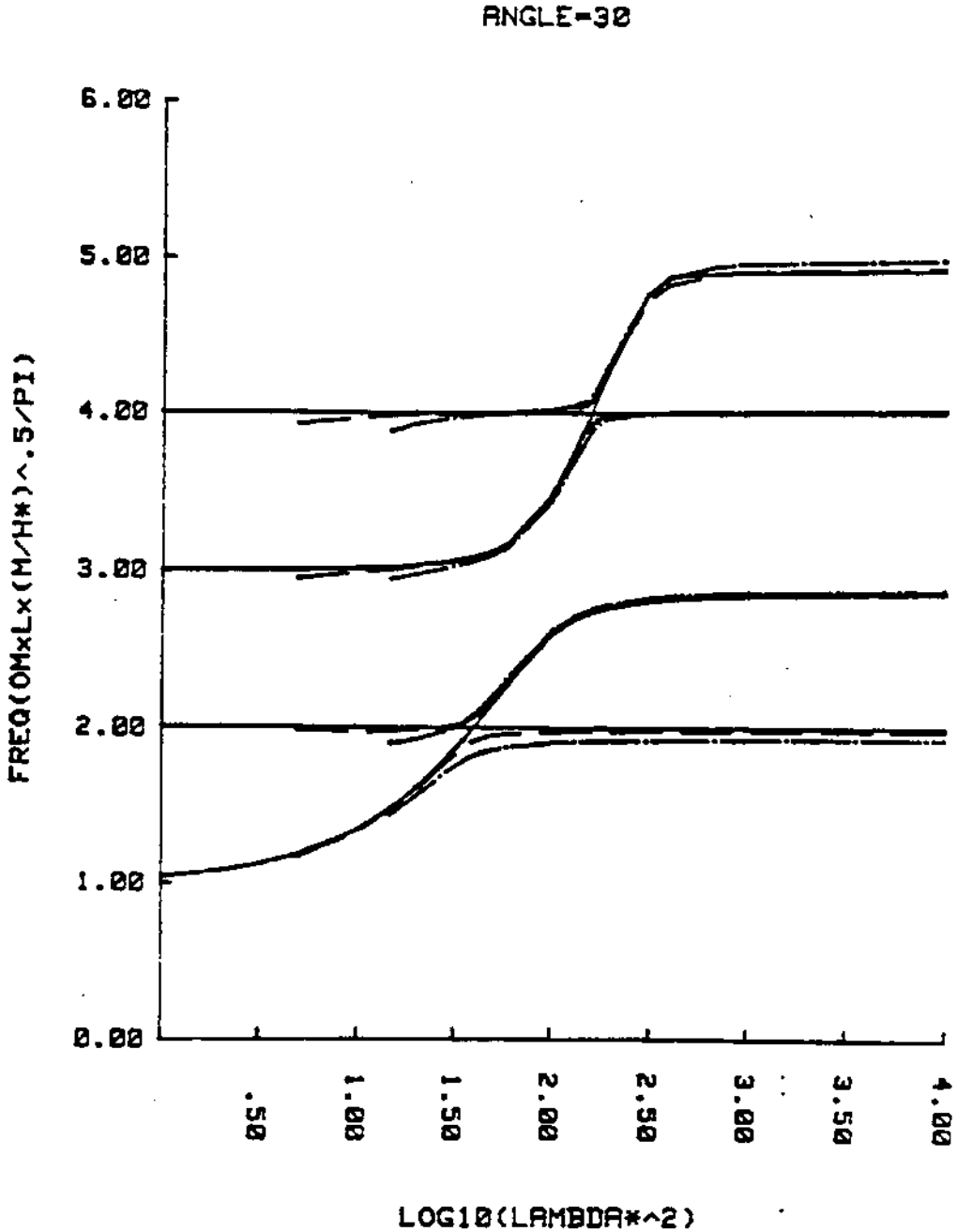

Figure 1-9: Eigenfrequencies of Extensible Cables vs. λ_*^2 ($\phi_a = 30$)

(solid line: $\alpha_* = 0$; dash line: $\alpha_* = 0.5$;
dot-dash line: $\alpha_* = 1$)

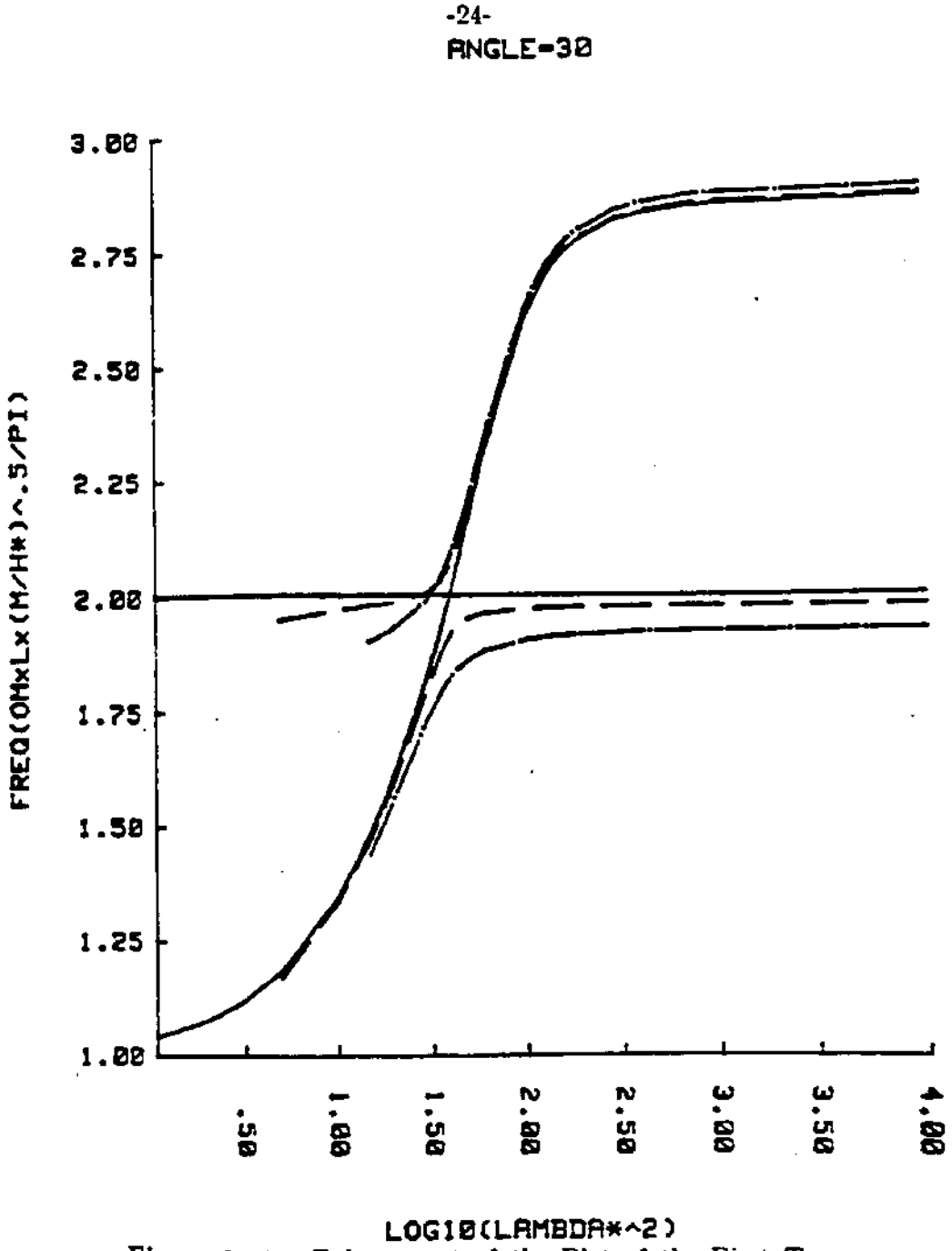

Figure 1-10: Enlargement of the Plot of the First Two Eigenfrequencies of Extensible Cables vs. λ_*^2 ($\phi_a = 30$)

(solid line: $\alpha_* = 0$; dash line: $\alpha_* = 0.5$;
dot-dash line: $\alpha_* = 1$)

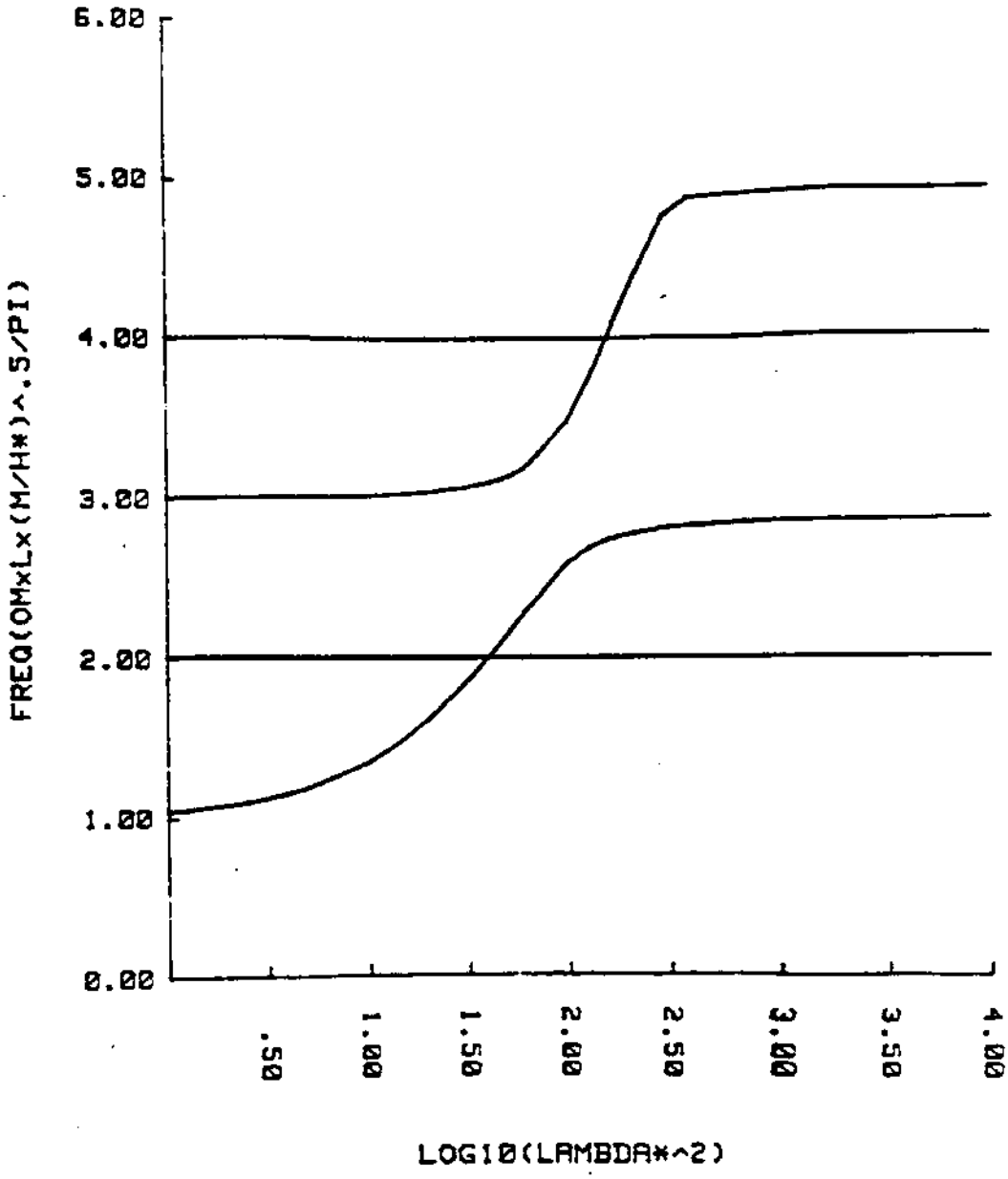

Figure 1-11: Eigenfrequencies for Shallow Sag Extensible Cables, Generalised for Inclination Angles

T_{top}	=	1 332 000 N
T_{bot}	=	1 155 096 N
Mass	=	48.7 kg/m
Added mass	=	6.3 kg/m
Net weight	=	414.98 N/m
D_o	=	0.0889 m
E·A	=	$1.30\ 10^9$ N
Length	=	1 036 m
Depth	=	426.70 m
C_{Dn}	=	1.2
C_{Dt}	=	0.05

No external current

A static analysis of the problem gives the following results: (see figure 1-12)

ϕ_{top}	=	33.056°
ϕ_{bot}	=	14.874°
Δx	=	940.68 m
ϕ_{av}	=	24.399°

ϕ_{av} is the angle formed between the cable chord and the horizontal.

The eigenfrequencies can be found in table 1-I. They were calculated using the finite difference scheme described in part I chapter 3. The mode configuration is only approximately symmetric or anti-symmetric, because the inclination angle destroys the symmetry about the cable midpoint. The results above were calculated numerically, but the perturbation theory and even Irvine's inclined cable results, predict essentially the same values for the eigenfrequencies.

To calculate the eigenfrequencies approximately with Irvine's modified theory for inclined angles, the methods described in part I, chapter 3.8.7 can be used. We obtain for symmetric modes:

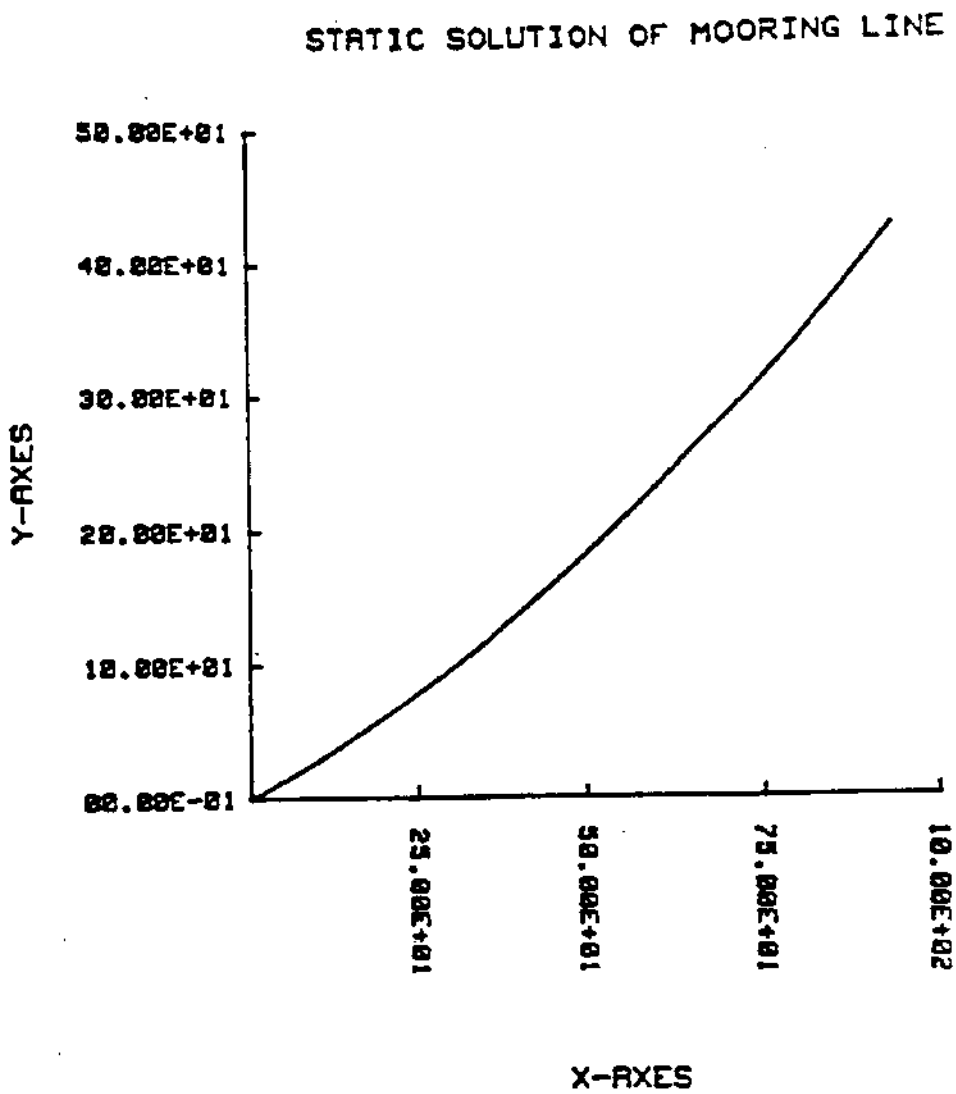

Figure 1-12: Static Shape of a Guy

The eigenfrequencies for the guy are:

calculated by finite differences (100 points)

	ω(rad/sec)	T(period)	mode shape
1	0.9011	6.937	anti-symmetric
2	1.1949	5.258	symmetric
3	1.6086	3.906	symmetric
4	1.8228	3.447	anti-symmetric
5	2.3115	2.718	symmetric
6	2.7527	2.283	anti-symmetric
7	3.2335	1.943	symmetric
8	3.7059	1.695	anti-symmetric

Table 1-I: Eigenfrequencies, Finite Differences

$$\tan\left[\frac{k_e L}{2}\right] - \left[\frac{k_e L}{2}\right] + \frac{4}{\lambda_e^2}\left[\frac{k_e L}{2}\right]^3 = 0 \qquad (1.4)$$

with: $k_e = \omega \left[\frac{M}{H_e}\right]^{1/2}$

$$\lambda_e^2 = \left[\frac{w_o L}{H_e}\right]^2 \frac{E A_o}{H_e} \cdot \cos^2\phi_a$$

$$H_e = \frac{H}{\cos\phi_a}$$

ϕ_a = inclination angle between the cable chord and the horizontal

For anti-symmetric modes:

$$\sin\left[\frac{k_* L}{2}\right] = 0 \qquad (1.5)$$

In the case of the guy we have:

H_* = 1 225 882 N
L = 1036 m
λ_*^2 = 108.17

The eigenfrequencies can now be calculated directly by using the above formulas. For the symmetric eigenfrequencies the transcendental equation has to be solved or looked up in a table [Irvine 81]. As result we obtain:

The eigenfrequencies for the guy are:

calculated by analytic method

antoine	ω(rad/sec)	T(period)	mode shape
1	0.9054	6.940	anti-symmetric
2	1.1861	5.297	symmetric
3	1.6072	3.909	symmetric
4	1.8109	3.470	anti-symmetric
5	2.2908	2.743	symmetric
6	2.7163	2.313	anti-symmetric
7	3.1736	1.980	symmetric
8	3.6218	1.735	anti-symmetric

Table 1-II: Eigenfrequencies, Analytic Method

The analytic method can give as shown in 1-II reliable estimates of the eigenfrequencies (and eventually also of the eigenmodes). To give the reader a

notion about the shape of the modes, some figures for the first four modes and for the quasi-static solution are presented. For the modes the solution has been normalised as described in part I, but with the amplitude written in non-dimensional form (normalised amplitude · $(M)^{1/2}$ L). The four essential quantities for each mode are plotted, i.e. the tangential displacement, the normal displacement, the dynamic tension and the dynamic angle.

The second and third modes are symmetric, which is explained by the fact that the cable is in the region where the first symmetric mode has shifted to a higher value than a taut string mode, while the third symmetric mode has not. The dynamic tension is nearly constant or slowly varying for the low modes shown. The quasi-static solution is the solution to an imposed unit motion at the top in the normal and tangential direction at the limit of zero frequency.

The impedance transfer functions at the top have also been calculated at the top. For a definition of the transfer functions see part I chapter 7. The transfer functions have been calculated by the perturbation method and by the numerical finite difference method. In the perturbation theory, the zeroth order slow solution was used. To leading order the slow solution is generating the dynamic tension and the fast solution is generating the dynamic angle.

In figures 1-37 through 1-39 a comparison of the transfer functions of the perturbation theory and the numerical, finite difference scheme is given.

The peaks corresponding to the anti-symmetric modes are very narrow and do not contribute to the transfer functions (anti-symmetric modes $\omega_{1a} = 0.90$ and $\omega_{2a} = 1.82$). The symmetric modes are solely responsible for the resonance phenomena ($\omega_{1s} = 1.19$, $\omega_{2s} = 1.61$, $\omega_{3s} = 2.31$). The

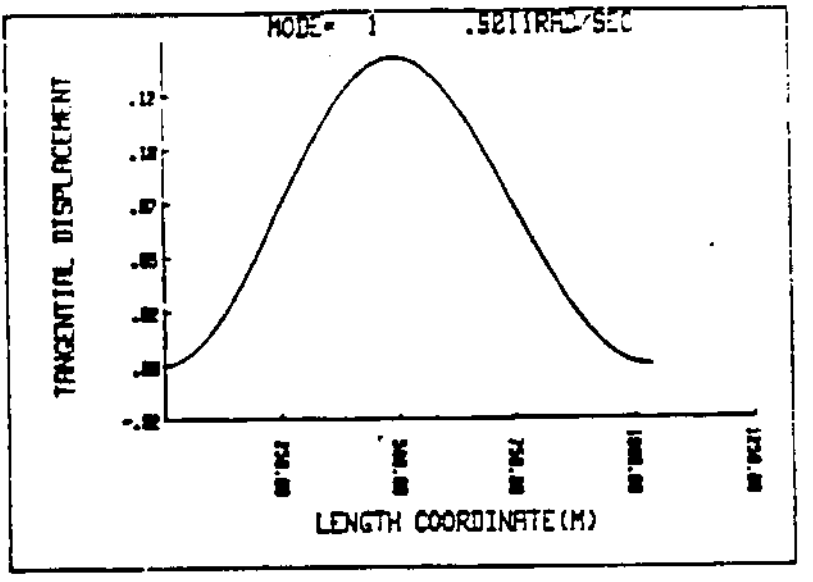

Figure 1-13: First Mode of a Guy: Tangential Displacement

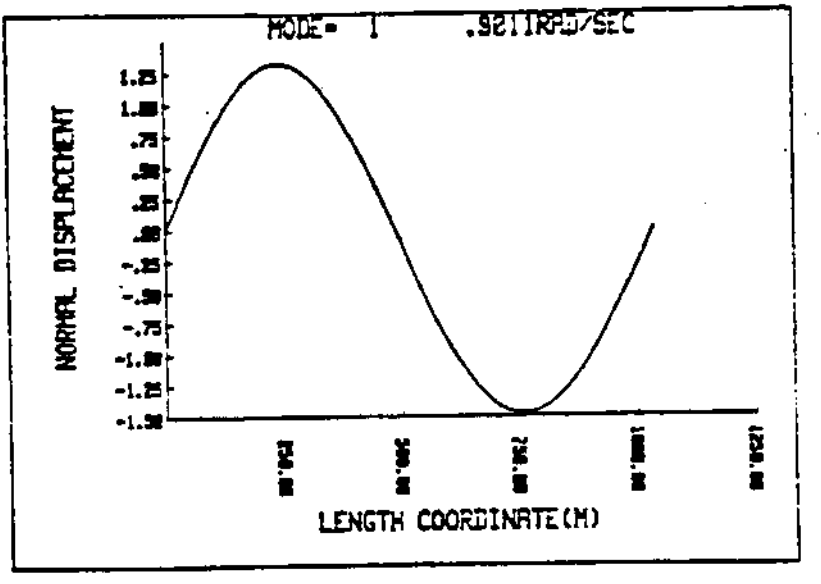

Figure 1-14: First Mode of a Guy: Normal Displacement

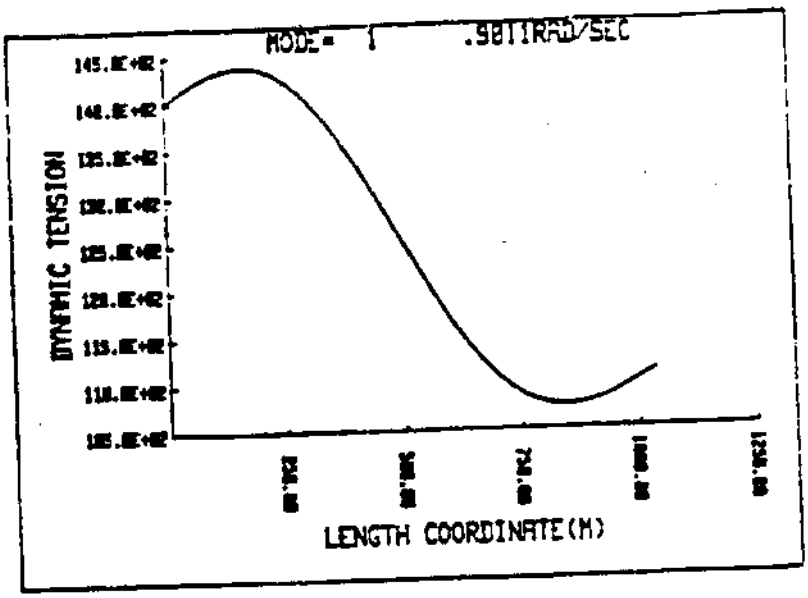

Figure 1-15: First Mode of a Guy: Dynamic Tension

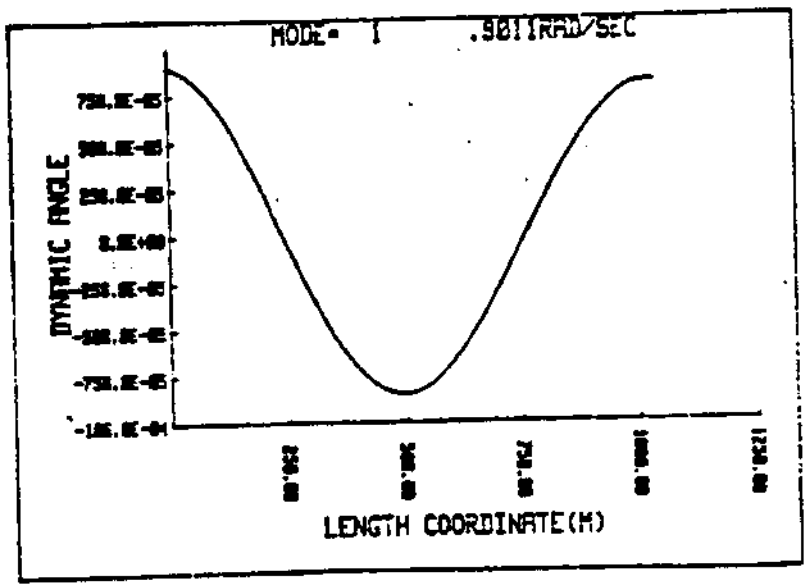

Figure 1-16: First Mode of a Guy: Dynamic Angle

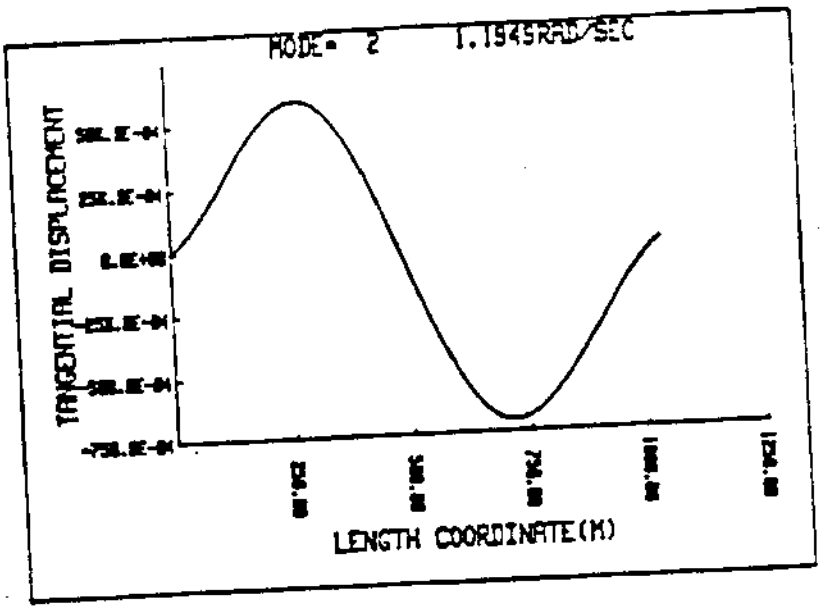

Figure 1-17: Second Mode of a Guy: Tangential Displacement

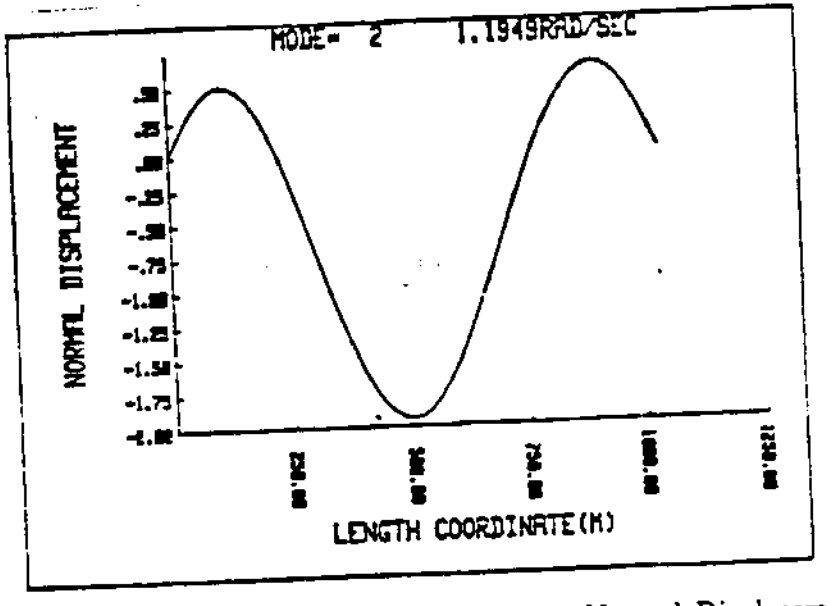

Figure 1-18: Second Mode of a Guy: Normal Displacement

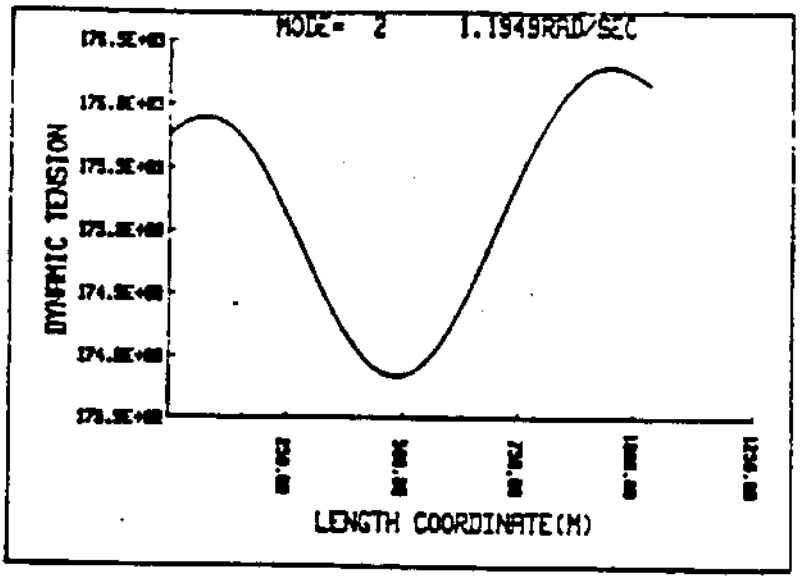

Figure 1-19: Second Mode of a Guy: Dynamic Tension

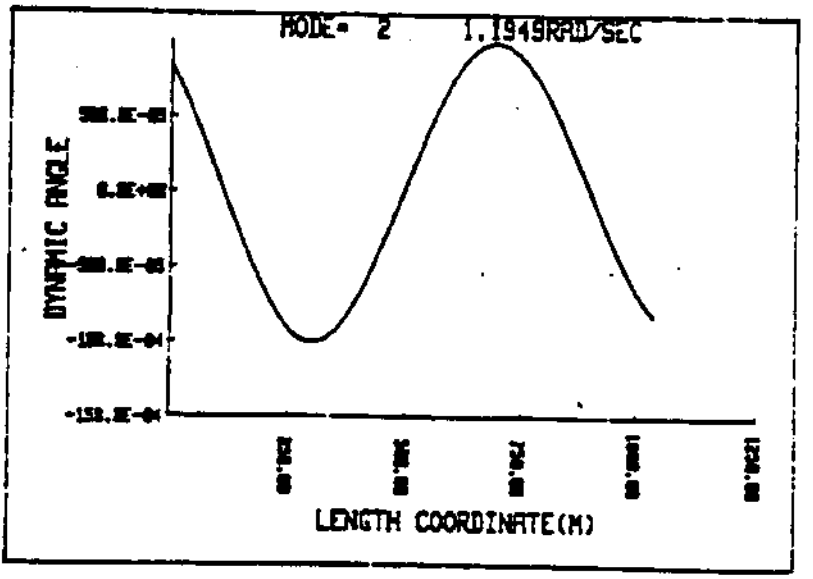

Figure 1-20: Second Mode of a Guy: Dynamic Angle

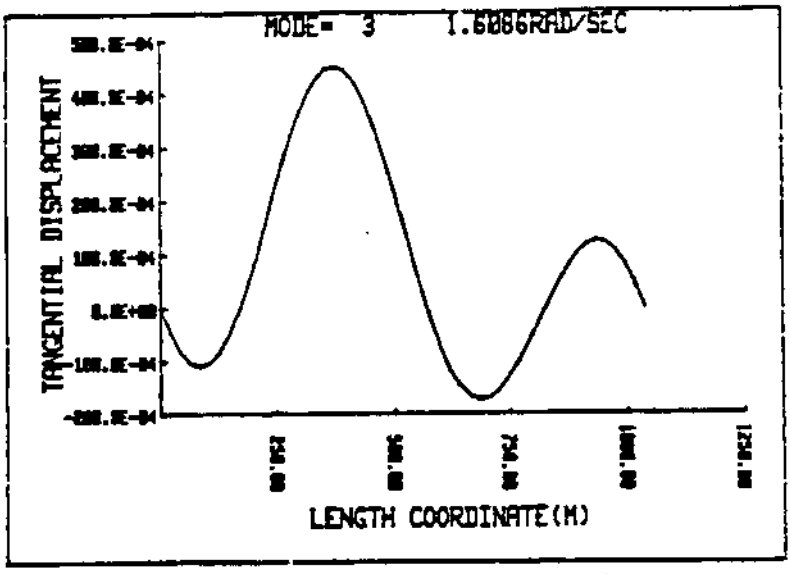

Figure 1-21: Third Mode of a Guy: Tangential Displacement

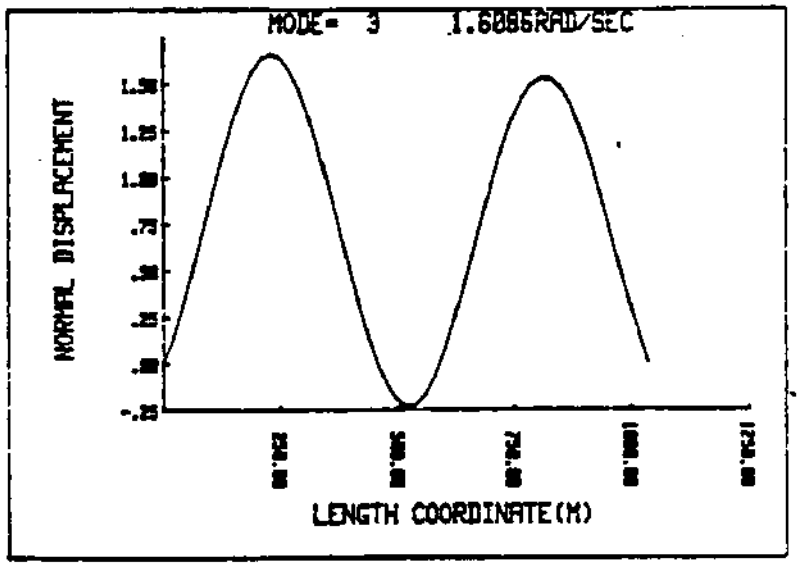

Figure 1-22: Third Mode of a Guy: Normal Displacement

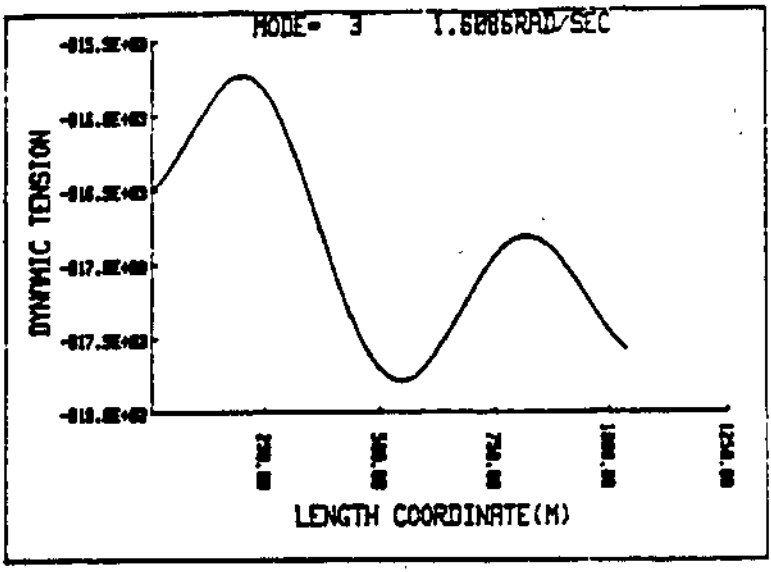

Figure 1-23: Third Mode of a Guy: Dynamic Tension

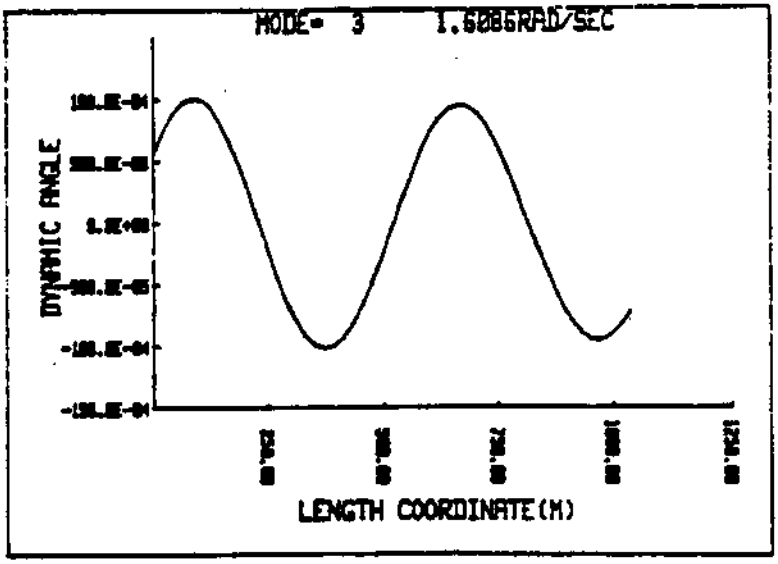

Figure 1-24: Third Mode of a Guy: Dynamic Angle

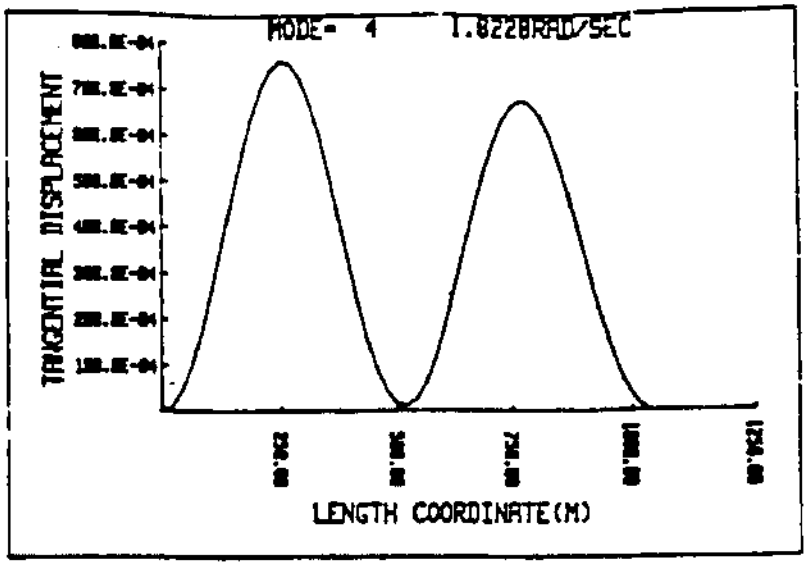

Figure 1-25: Fourth Mode of a Guy: Tangential Displacement

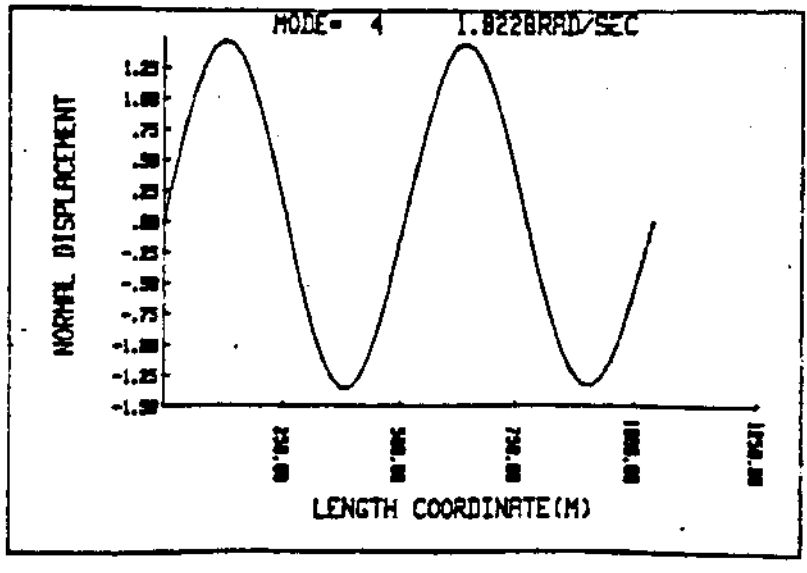

Figure 1-26: Fourth Mode of a Guy: Normal Displacement

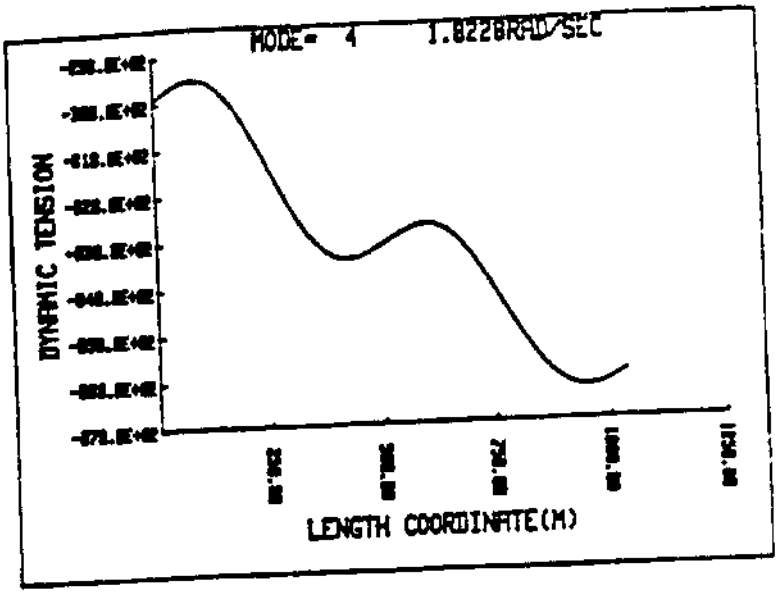

Figure 1-27: Fourth Mode of a Guy: Dynamic Tension

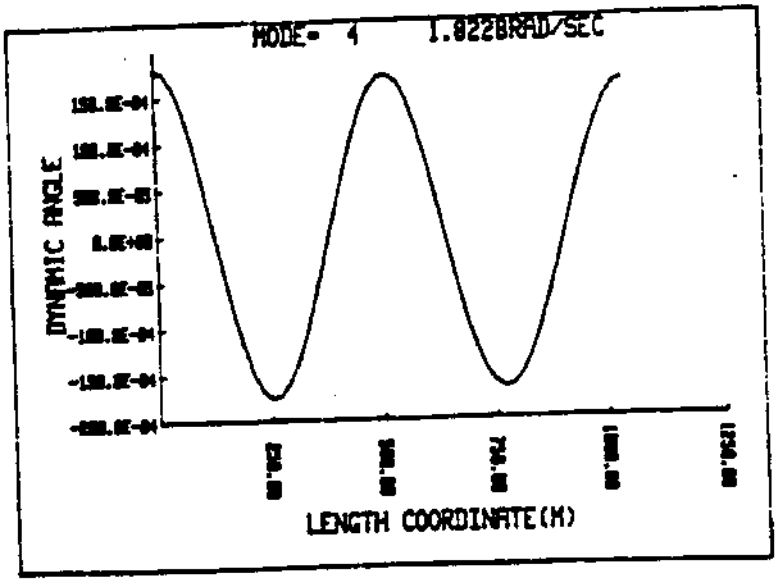

Figure 1-28: Fourth Mode of a Guy: Dynamic Angle

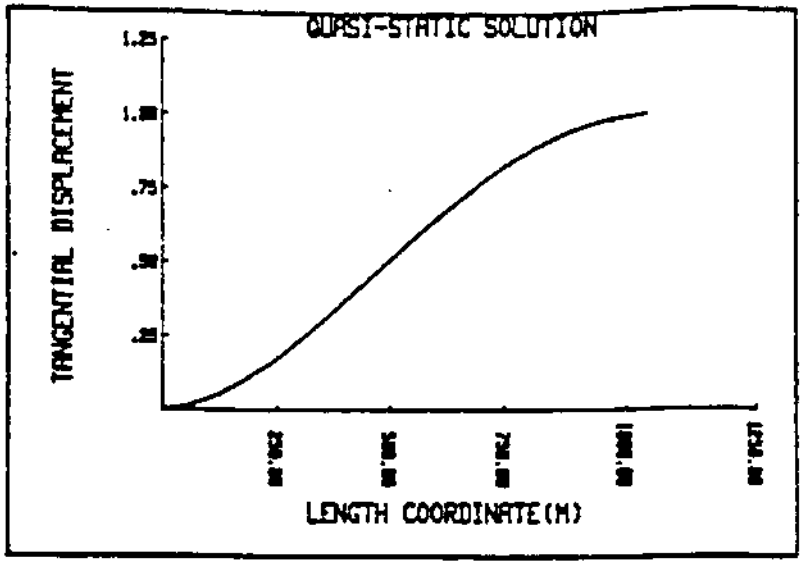

Figure 1-29: Tangential Quasi-Static Solution: Tangential Displacement

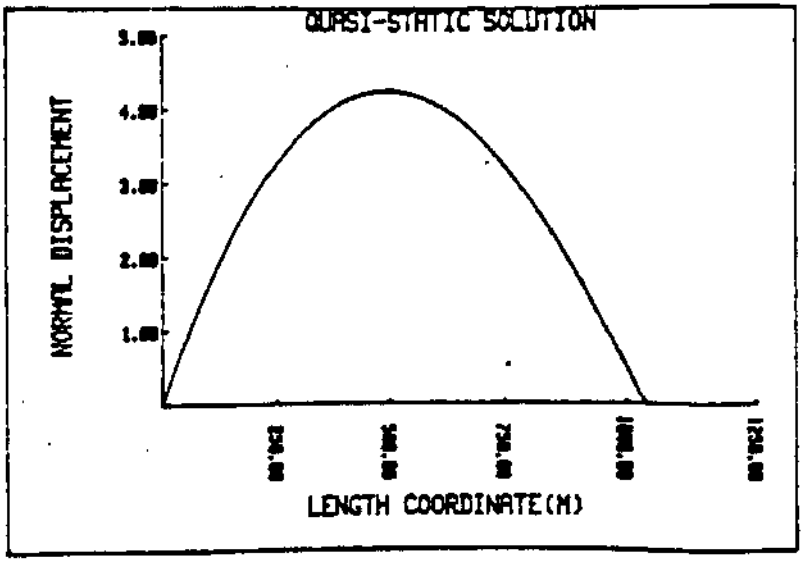

Figure 1-30: Tangential Quasi-Static Solution: Normal Displacement

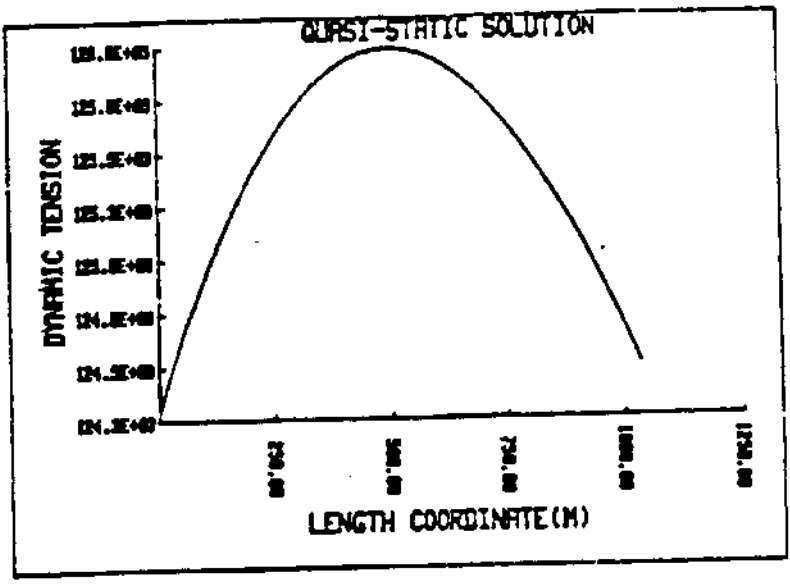

Figure 1-31: Tangential Quasi-Static Solution: Dynamic Tension

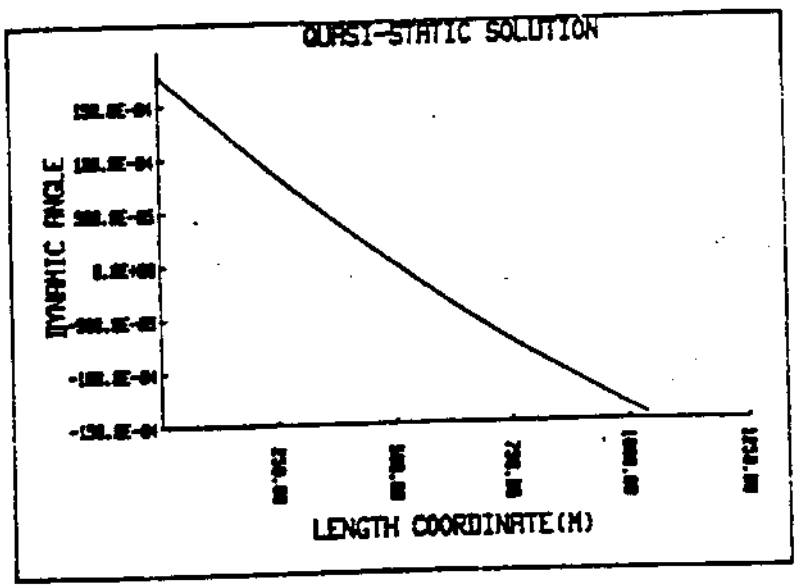

Figure 1-32: Tangential Quasi-Static Solution: Dynamic Angle

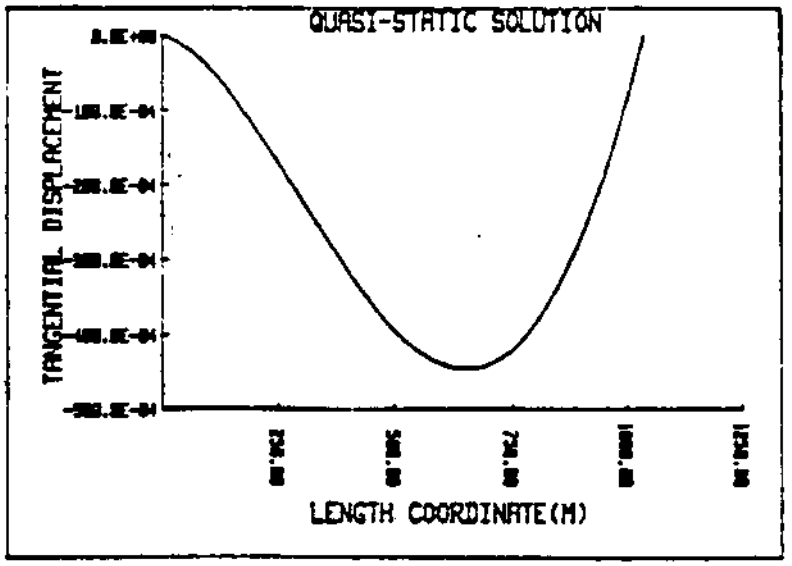

Figure 1-33: Normal Quasi-Static Solution: Tangential Displacement

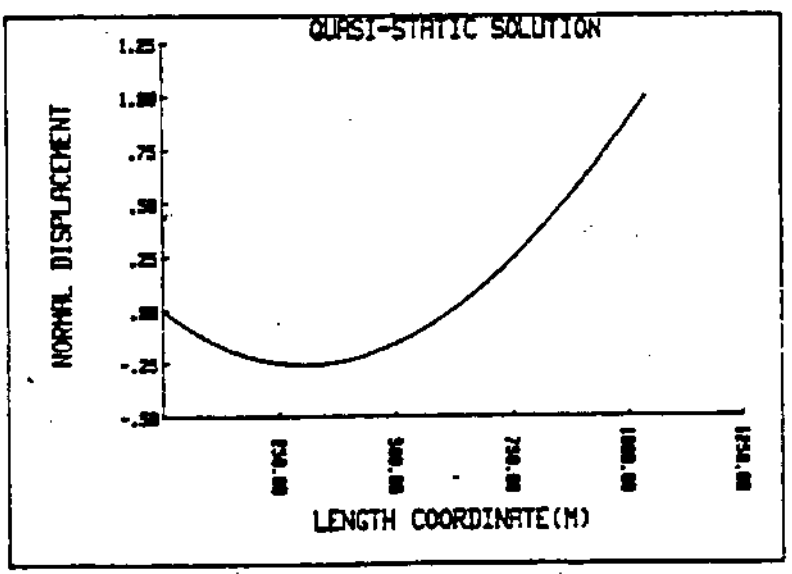

Figure 1-34: Normal Quasi-Static Solution: Normal Displacement

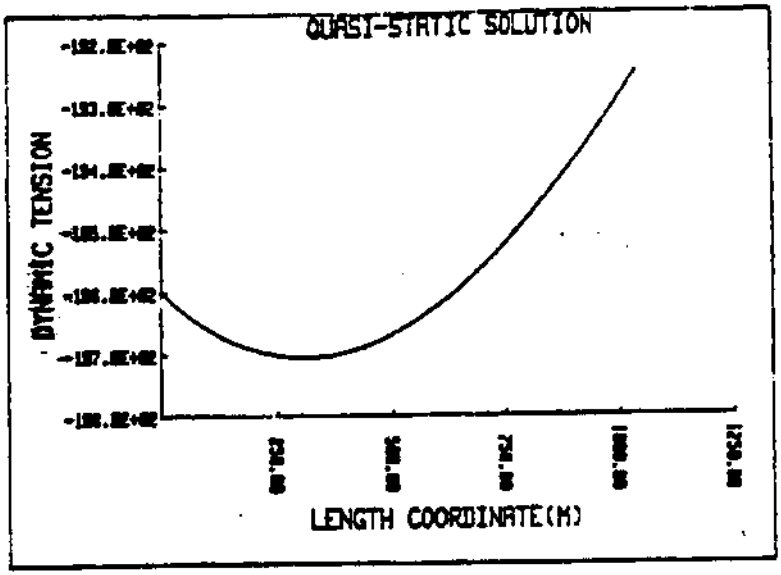

Figure 1-35: Normal Quasi-Static Solution: Dynamic Tension

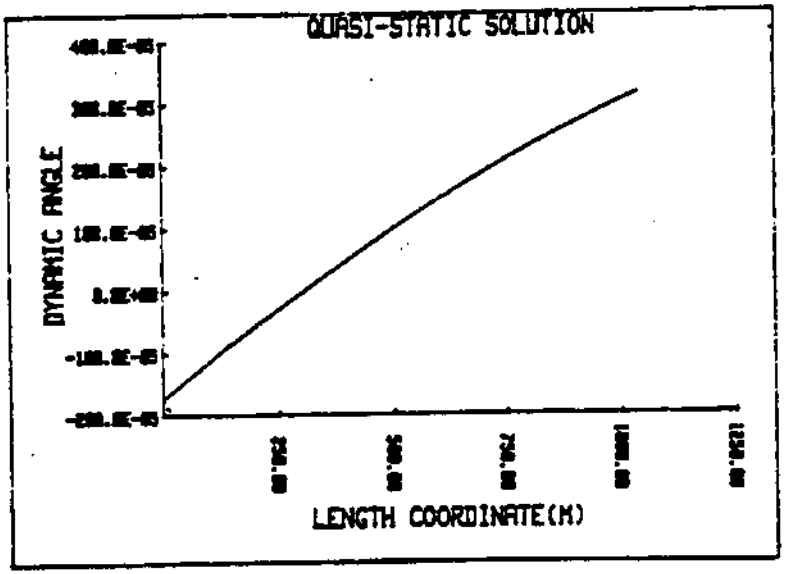

Figure 1-36: Normal Quasi-Static Solution: Dynamic Angle

List of Figures of Eigenmodes and Quasi-Static Shapes

	tangential	normal	dyn. tension	dyn. angle
first mode	1-13	1-14	1-15	1-16
second mode	1-17	1-18	1-19	1-20
third mode	1-21	1-22	1-23	1-24
fourth mode	1-25	1-26	1-27	1-28
tangential quasi-static	1-29	1-30	1-31	1-32
normal quasi-static	1-33	1-34	1-35	1-36

agreement between perturbation and numerical solution, in the range considered, is very good.

1.5 Impedances of a Two-leg System

As a simple example of impedances of a multi-leg system, the impedances of a two-leg system are analysed. For the symmetric configuration the impedance function S_{xx} is simply twice the individual leg impedance function. In this example the guy data described in the previous section are used for the individual legs (See figure 1-40). In the assymetric two-leg system (figure 1-41) the static tension in one of the legs was diminished by 200 000 N. The total impedance function S_{xx} is the addition of the individual impedance functions. The symmetric eigenfrequencies of both leg appear in the total impedance function.

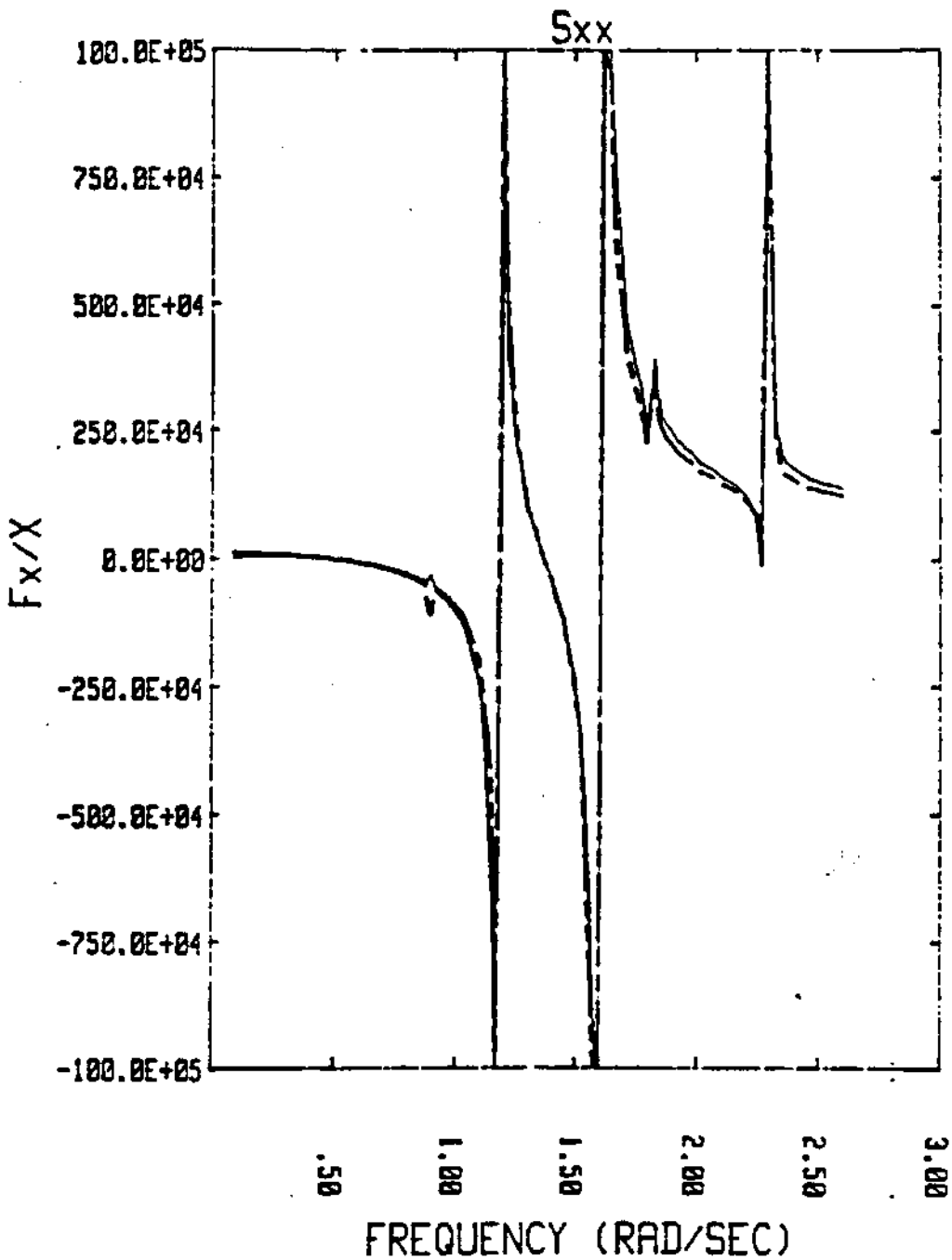

Figure 1-37: S_{xx} for a Guy of a Guyed Tower

(Solid line: perturbation theory)
(Dashed line: finite difference scheme)

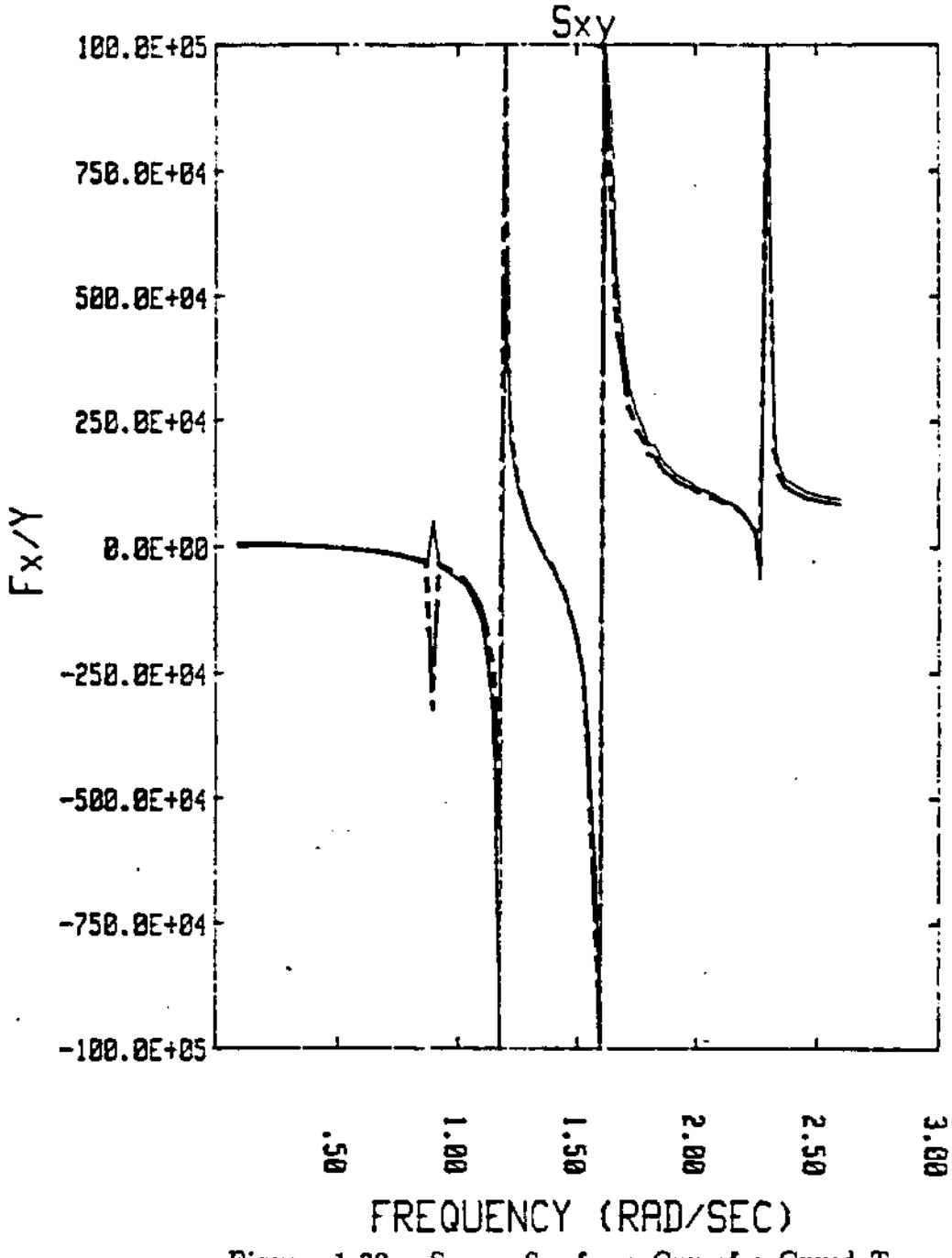

Figure 1-38: $S_{xy} = S_{yx}$ for a Guy of a Guyed Tower

(Solid line: perturbation theory)
(Dashed line: finite difference scheme)

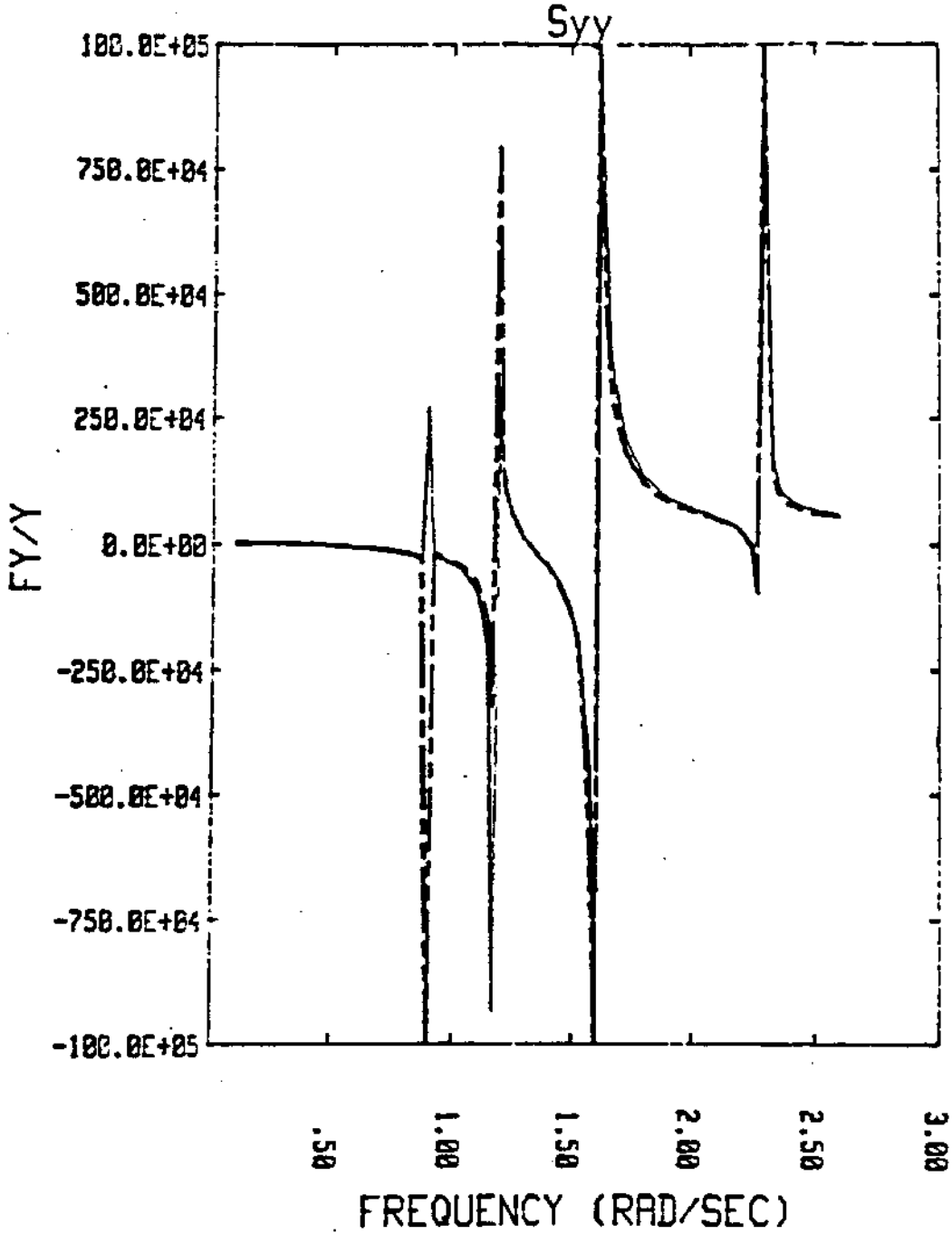

Figure 1-39: S_{yy} for a Guy of a Guyed Tower

(Solid line: perturbation theory)
(Dashed line: finite difference scheme)

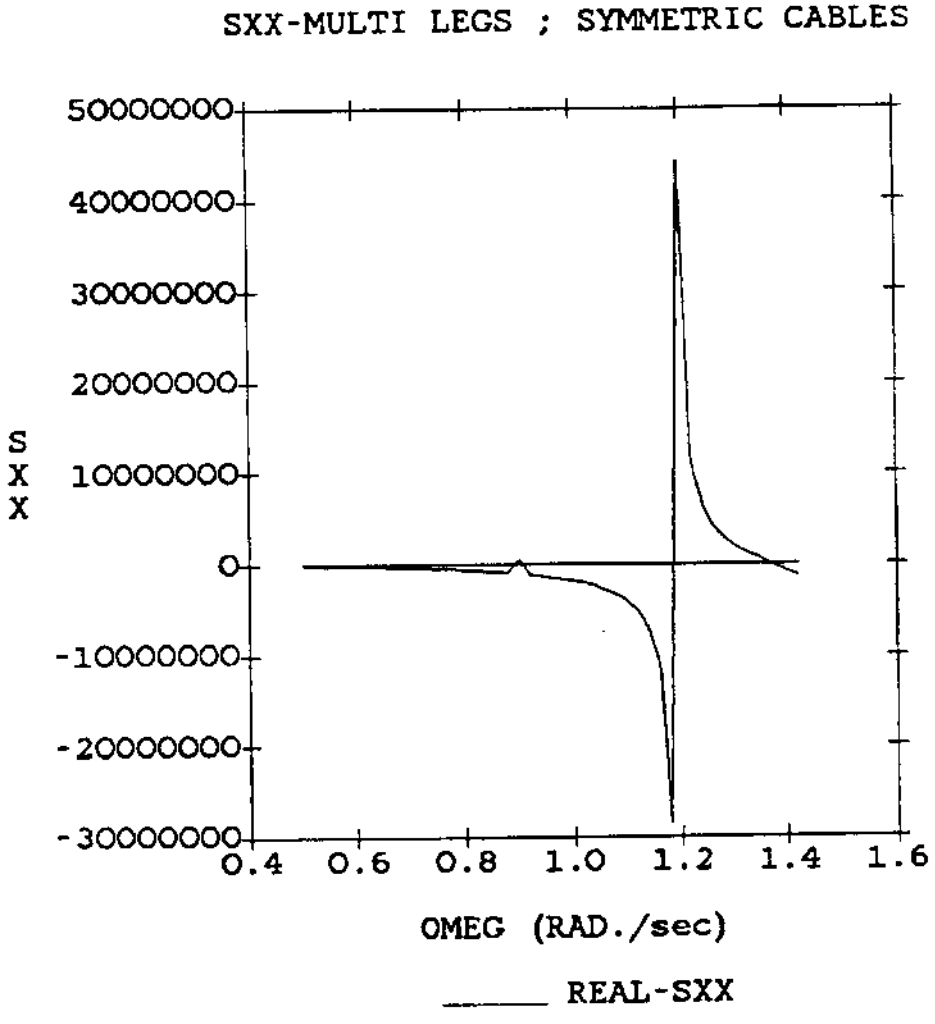

Figure 1-40: S_{xx} for a Symmetric Two-leg System

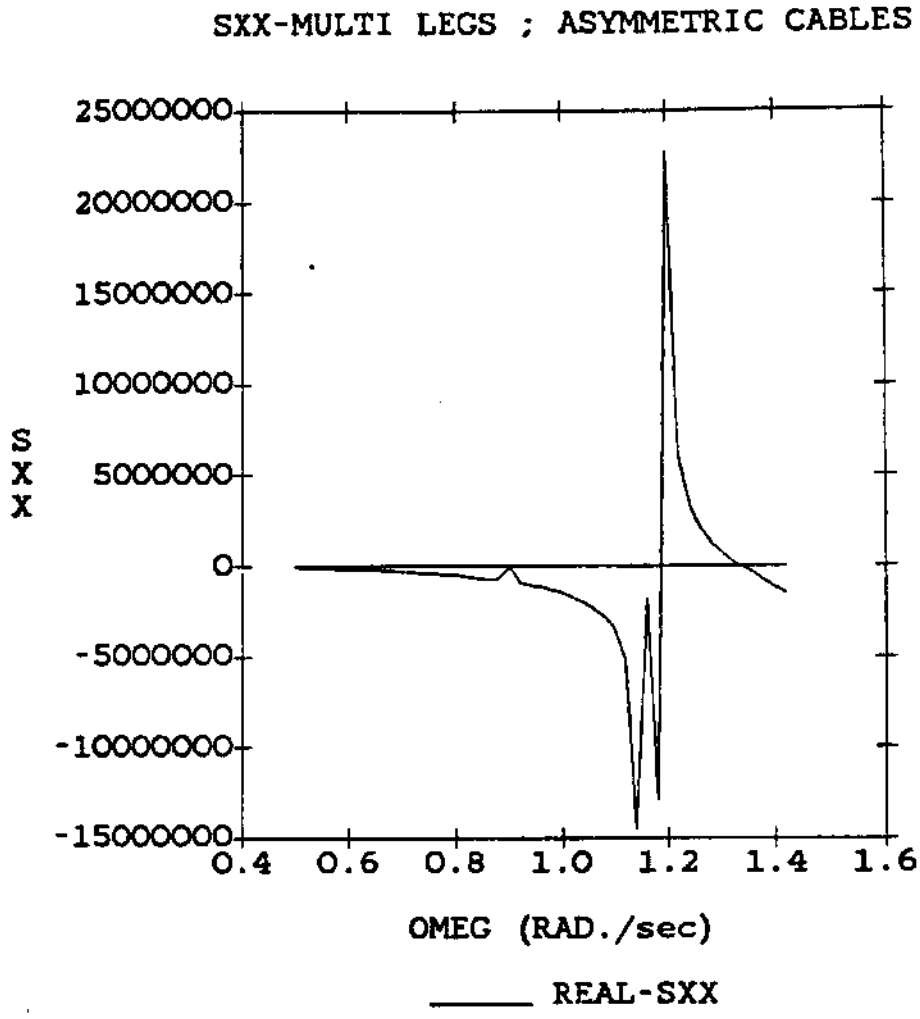

Figure 1-41: S_{xx} for a Assymmetric Two-leg System

1.6 References

[Gambhir 77] Gambhir, M. L. and de Batchelor, B.
A Finite Element for 3D Prestressed Cable Nets.
International Journal for Numerical Methods in Engineering 2:1699-1718, 1977.

[Goodey 61] Goodey, W. J.
On the Natural Modes and Frequencies of a Suspended Chain.
Quarterly Journal of Mechanics and Applied Mathematics 14(1):118-127, 1961.

[Henghold 77] Henghold, W. M., Russell, J. J. and Morgan, J. D.
Free Vibrations of Cable in 3D.
Journal of the Structural Division, ASCE 103(ST5):1127-1136, May, 1977.

[Irvine 74] Irvine, H. M. and Caughey, T. K.
The Linear Theory of Free Vibrations of a Suspended Cable.
Proceedings of the Royal Society Series A 341:299-315, 1974.

[Irvine 81] Irvine, H. M.
Cable Structures.
MIT Press, Cambridge, MA and London, England, 1981.

[Kim 83] Kim, Y.C.
Nonlinear Vibrations of Long Slender Beams.
PhD thesis, MIT, 1983.

[Pugsley 49] Pugsley, A. G.
On the Natural Frequencies of Suspension Chains.
Quarterly Journal of Mechanics and Applied Mathematics 2(4):412-418, 1949.

[Ramberg 82] Rambert, S. E. and Bartholomew, C. L.
Vibrations of Inclined Slack Cables.
Journal of the Structural Division, ASCE 108(ST7):1662-1664, July, 1982.

[Saxon 53] Saxon, D. S. and Cahn, A. S. .
Modes of Vibration of Suspension Chain.
Quarterly Journal of Mechanics and Applied Mathematics 6:273-285, 1953.

[West 75] West, H. H., Geschwindner, L. F. and Suhoski, J. E.
Natural Vibrations of Suspended Bridges.
Journal of the Structural Division, ASCE 101(ST11):2277-2291, November, 1975.

[Yamaguchi 79] Yamaguchi, H. and Ito, H.
Linear Theory of Free Vibrations of an Inclined Cable in Three Dimensions.
Proceedings Japanese Society of Civil Engineers (286):29-36, June, 1979.
In Japanese, Summary in English, Transactions Japanese Society of Civil Engineers 1979.

Chapter 2

NUMERICAL APPLICATIONS OF NON-LINEAR DYNAMICS

2.1 Introduction

In this chapter, a number of applications are provided, to demonstrate the practical implications of the theory presented in part I, and to validate the theoretical predictions by comparing them with experimental data and previous solutions.

2.2 The Non-Linear String

The use of modal expansions was first tested on a non-linear string. First, some calculations were performed including non-linear drag, which introduces an amplitude dependent damping. The results obtained can be seen as a special case of the second numerical application presented in this chapter (drag forces on a cable) and are therefore omitted. The study of a string with geometric non-linearity, as discussed in part I chapter 4, was the second case considered, and is presented in the sequel.

The dimensions of a guy of a guyed tower were used for the taut string, for demonstration purposes.

String characteristics: $T = 1\ 000\ 000$ N
$M = 48.7$ kg/m
$L = 1\ 036.32$ m

$$EA = 0.214\ 10^{11}\ N$$

The eigenfrequencies in air can be obtained as:

$$\omega = \frac{n\pi\ (T/M)^{1/2}}{L} \rightarrow 0.434,\ 0.861,\ \ldots$$

The string was subject at one end to a transverse sinusoidal excitation with frequency equal to the first natural frequency. The coefficient of the geometric non-linearity is selected as (see part I chapter 4):

$$\tau = \frac{E \cdot A}{T_o} \cdot \frac{1}{2} \frac{(Ampl)^2}{L^2} = 0.01$$

For a realistic strain in the string, of the order of 10^{-3}, this corresponds to an A/L ratio of approximately $4.5\ 10^{-3}$. The case considered was selected because it can be compared with Oplinger's theoretical results. [Oplinger 60]

	Time step as a fraction of the exiting period	Damping	number of modes	τ
Fig.7-1–7-2	1/1000	–	3 - 6	0.01
Fig.7-3	1/20	0.05	1 -3 - 6	0
Fig.7-4–7-5	1/100	0.05	1 - 3 - 6	0.01
Fig.7-6	1/100	0.05	1 - 3 - 6	0-0.01

Table 2-I: Geometric Non-Linearity

Note: The time steps are the minimum required to ensure convergence and accurate response calculations. Except for the case with no damping, the expansion using one mode gave essentially the same result as the expansion with more

modes.

Several time simulation runs were performed. A linear modal damping was also introduced. The simulation results can be seen in Table 2-1. The amplitude of the imposed motion is taken as equal to 1 , and the amplitude at the middle of the cable is given in the graphs. Also the tension variation is calculated.

In figures 2-1 and 2-2 the effect of a pure geometric non-linearity is studied. Because no damping is present, a beating phenomenon, caused by the non-decaying transient solution, is obtained. The dynamic tension oscillates at double the exciting frequency as expected.

Figure 2-3 shows the response with linear damping only. Figures 2-4 and 2-5 show the effect of the geometric non-linearity with some damping included. Figure 2-6 presents a comparison between the motion without geometric non-linearity and the motion with geometric non-linearity. The geometric non-linearity is clearly limiting the amplitude of the motion. The final value of the response with geometric non-linearity is around 3 at resonance, which agrees well with Oplinger's theoretical and experimental investigation.

2.3 Linear Cable Model with the Non-Linear Drag Force

In order to study the effect of the drag force on the motions of a cable, it was decided to use the linearised cable model, with the drag forces treated as external forces. In this example a guy of a guyed tower was excited in the normal direction, at the top.

The data for the guy are:

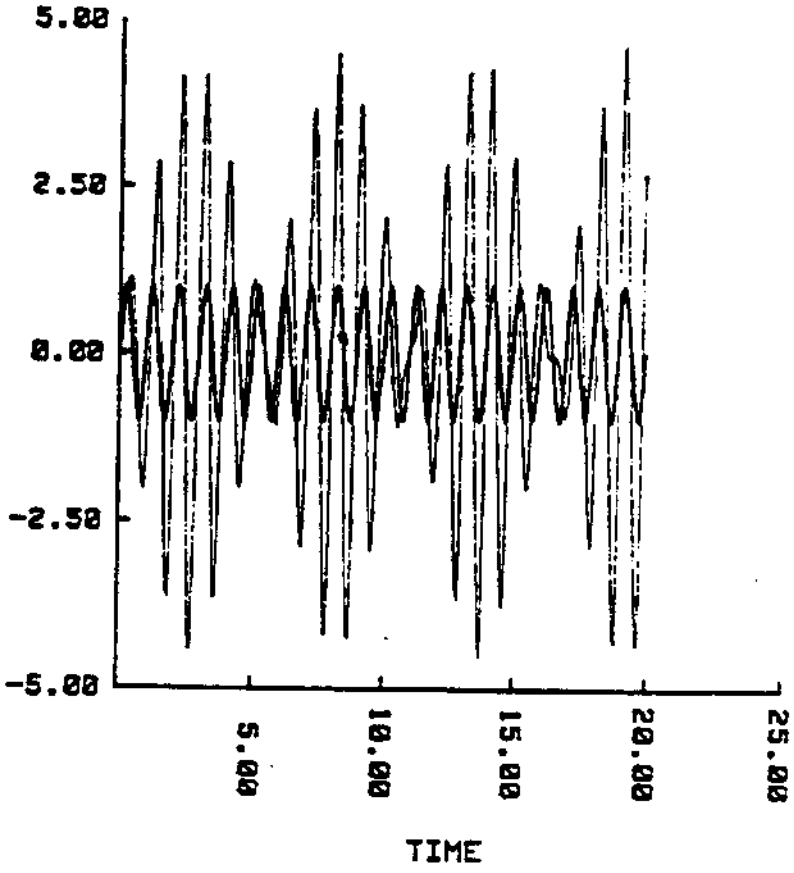

Figure 2-1: Non-Linear String; Motion at Midlength

Comparison with Unit Motion at the Top
$\tau = 0.01$
damping = 0
$\Delta T = 1/1000\ T_{per}$
3 modes

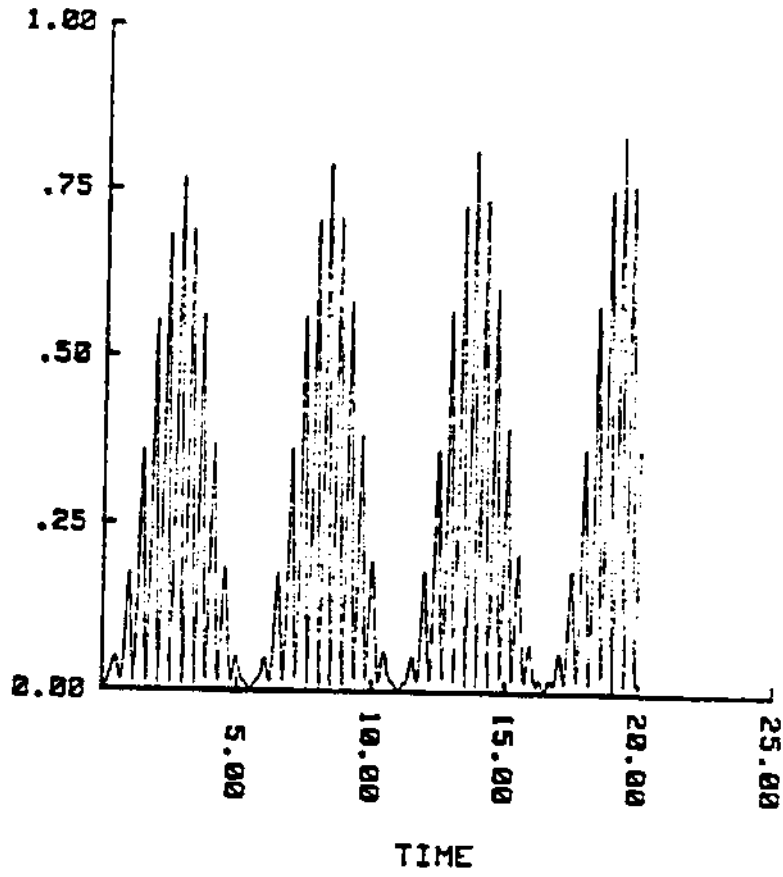

Figure 2-2: Non-Linear String; Dynamic Tension

(Dynamic Tension is given as a fraction of the Static Tension)

$r = 0.01$

damping $= 0$

$\Delta T = 1/1000\ T_{per}$

3 modes

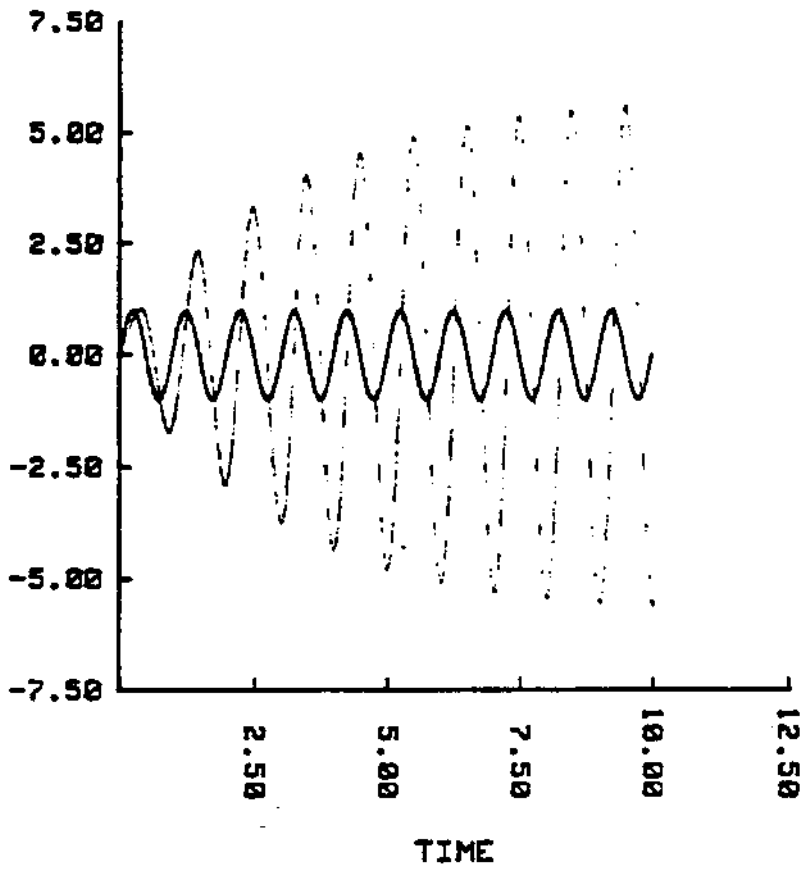

Figure 2-3: Non-Linear String; Motion at Midlength

Comparison with Unit Motion at the Top
$\tau = 0$
damping $= 0.05$
$\Delta T = 1/20\ T_{per}$
3 modes

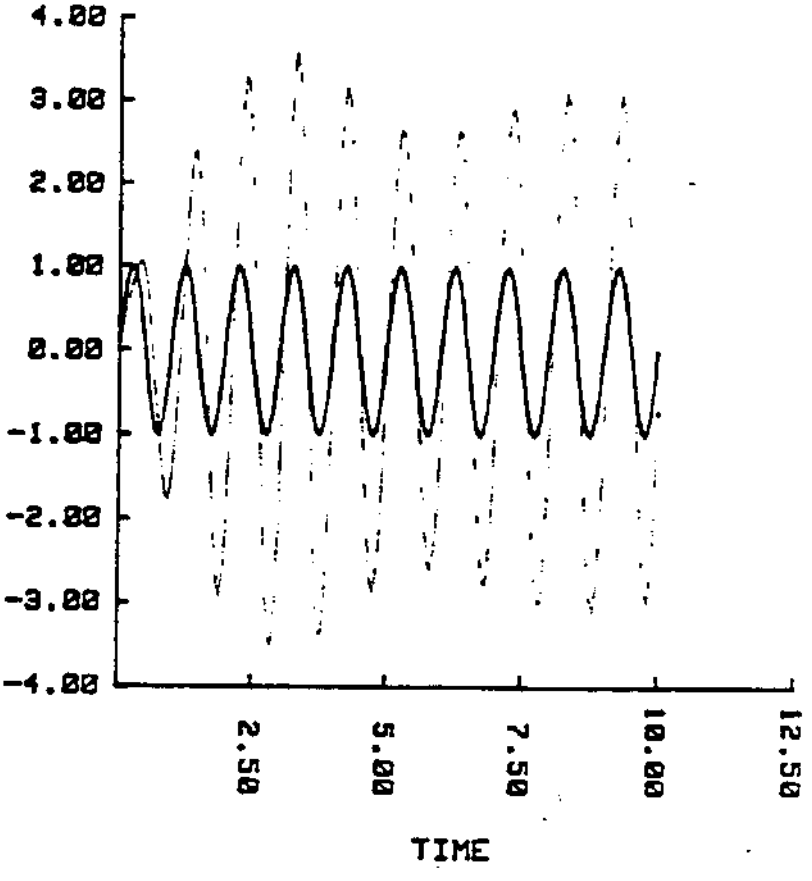

Figure 2-4: Non-Linear String; Motion at Midlength

Comparison with Unit Motion at the Top
$\tau = 0.01$
damping $= 0.05$
$\Delta T = 1/100\ T_{per}$
3 modes

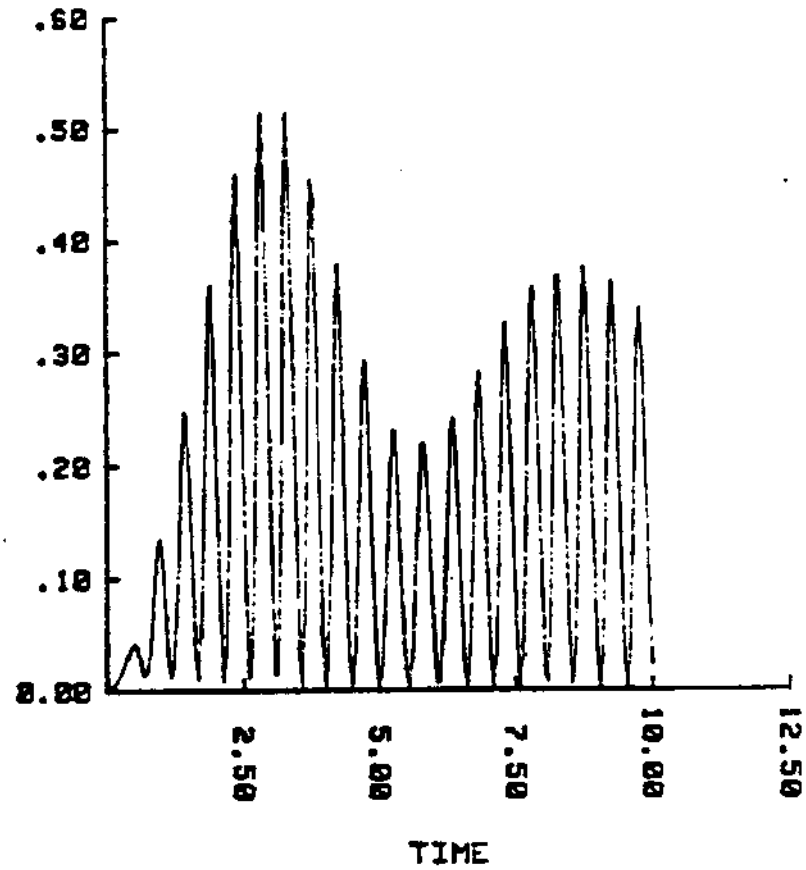

Figure 2-5: Non-Linear String; Dynamic Tension

(Dynamic Tension is given as a fraction of the Static Tension)
$\tau = 0.01$
damping = 0.05
$\Delta T = 1/100\ T_{per}$
3 modes

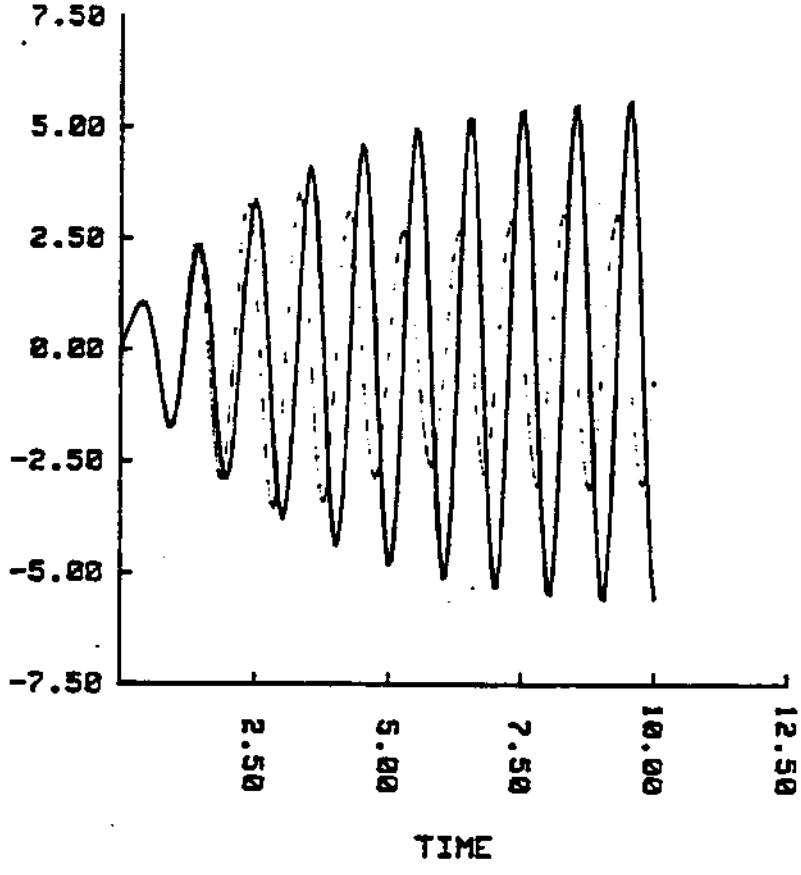

Figure 2-6: Non-Linear String; Motion at Midlength;
Comparison between responses with and without geometric non-linearity
(solid line)

$\tau = 0.01$
damping $= 0.05$
$\Delta T = 1/100\ T_{per}$
3 modes

T_{top}	=	1 332 000 N
T_{bot}	=	1 155 096 N
Mass	=	48.7 kg/m
Added mass	=	6.3 kg/m
Net weight	=	414.98 N/m
D_o	=	0.0889 m
E·A	=	1.30 10^9 N
Length	=	1 036 m
Depth	=	426.70 m
C_{Dn}	=	1.2
C_{Dt}	=	0.05

No external current

A static analysis of the problem gives the following results:

ϕ_{top}	=	33.056°
ϕ_{bot}	=	14.874°
Δx	=	940.68 m
ϕ_{av}	=	24.399°

ϕ_{av} is the angle formed between the cable chord and the horizontal.

The linear dynamics of this example were already discussed in chapter 1 Using the modes, described in chapter 1 the influence of the drag forces was studied by exciting the cable with a top motion in the normal direction. The simulations were done using 4 - 8 - 16 modes. The results for 8 modes are shown here. The simulation with four modes gave a similar envelope curve except for the high amplitude motions. The results are given in figures 2-7 through 2-10. The excitation frequency was equal to the first resonance frequency except for figure 2-7, for which excitation causes quasi-static motion. The plots represent the superposition of the shapes of the cable obtained at different time steps, so that an envelope of the transverse response of the cable is obtained. (This envelope contains also the transient phenomena) The plots give the motion normal to the static shape at each point expressed as a fraction of the A/D ratio, which was varied between 1.5 and 100. The

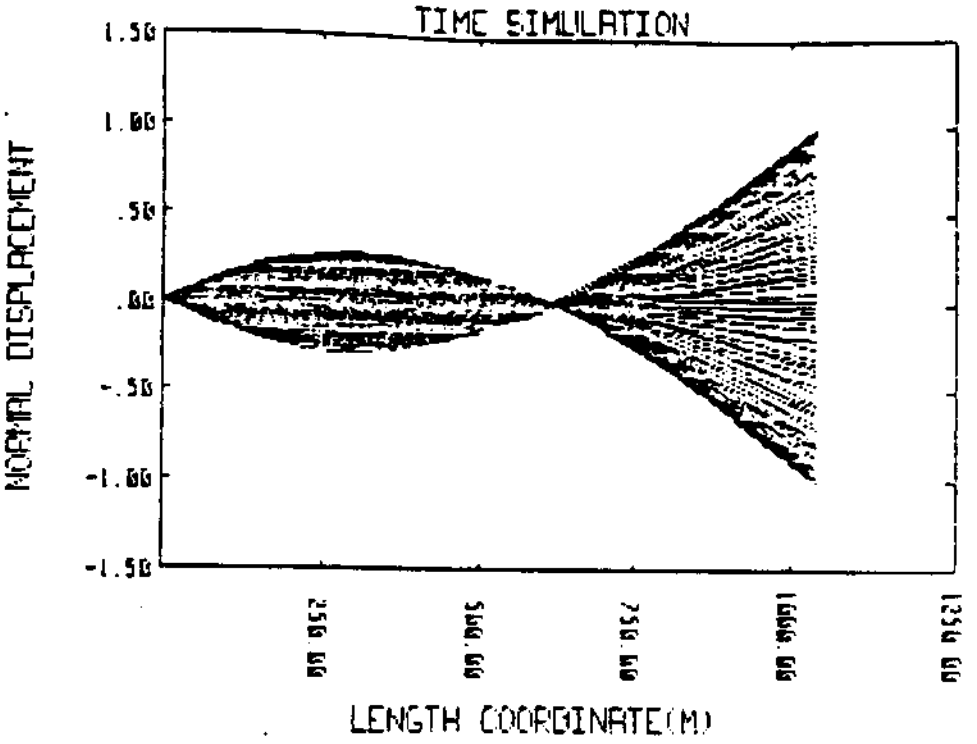

Figure 2-7: Quasi-Static Motion at very Low Frequency

Normal displacement along the guy.
Top motion has unit amplitude in the normal direction.
(A/D=1)
$\Delta T = 1/100\ T_{per}$

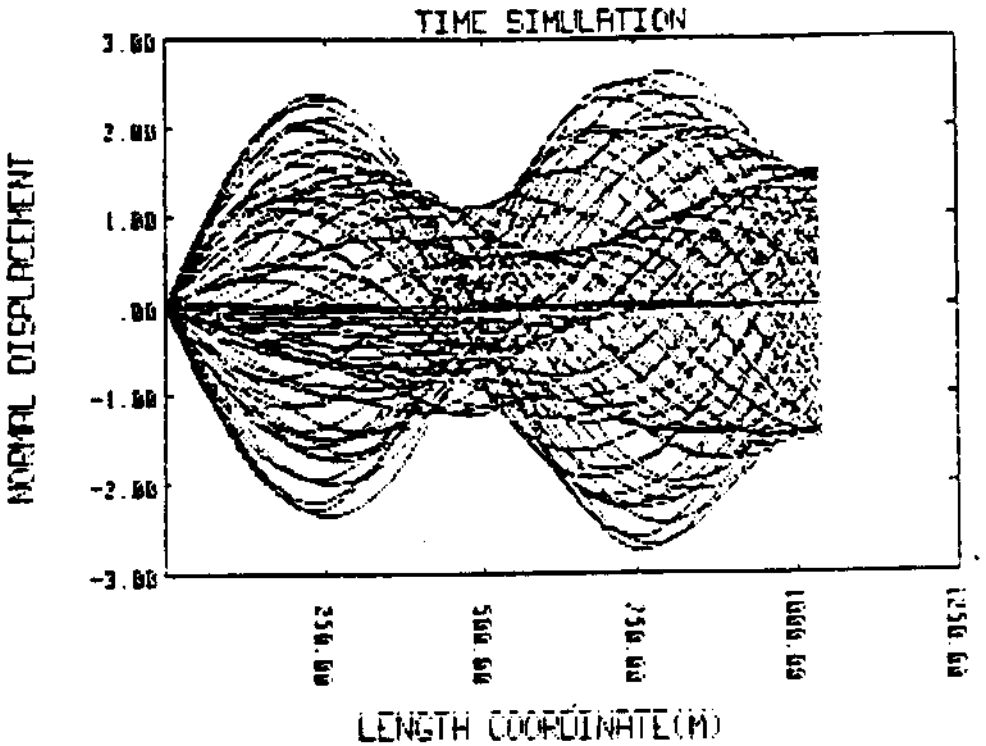

Figure 2-8: Response to Top Excitation at First Resonance Frequency, A/D = 1.5

Normal displacement along the guy.
Top motion A/D = 1.5 in the normal direction.
$\Delta T = 1/100\ T_{per}$

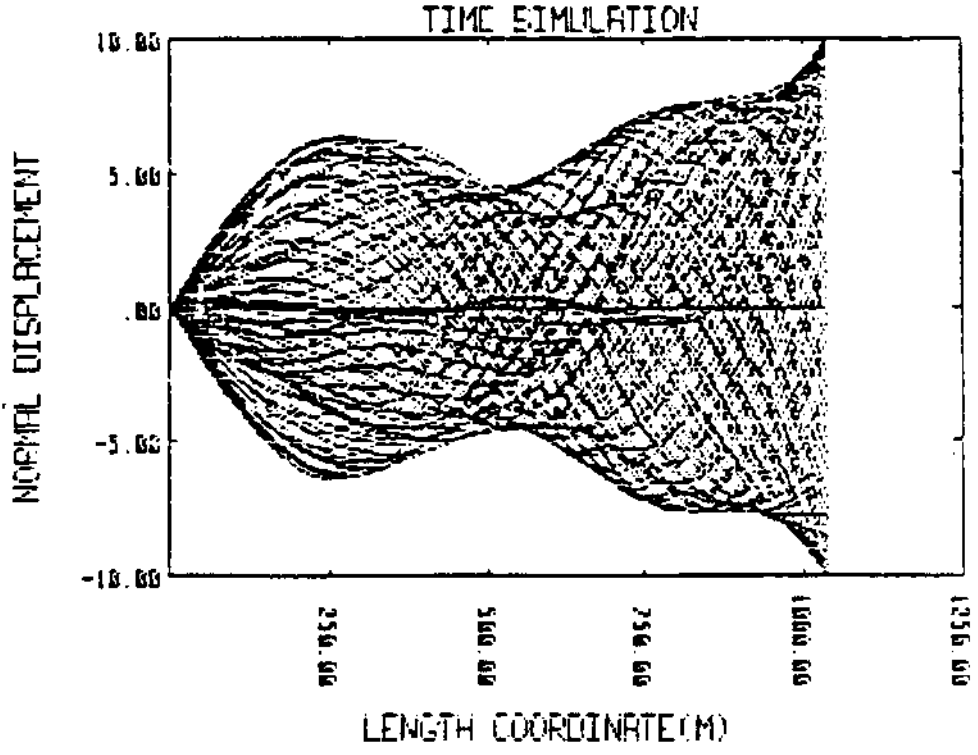

Figure 2-9: Response to Top Excitation at First Resonance Frequency, A/D = 10

Normal displacement along the guy.
Top motion A/D = 10 in the normal direction.
$\Delta T = 1/100\ T_{per}$

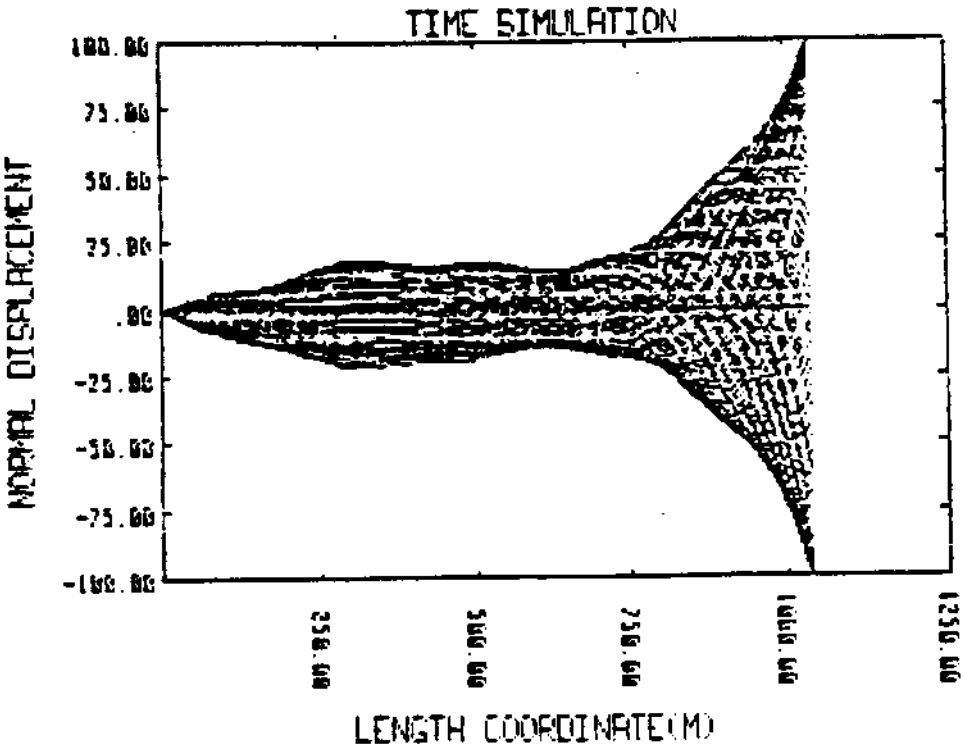

Figure 2-10: Response to Top Excitation at First Resonance Frequency A/D = 100

Normal displacement along the guy.
Top motion A/D = 100 in the normal direction.
$\Delta T = 1/100\ T_{per}$

dominant effect of the drag force at high amplitudes becomes clear.

The increasing importance of the drag force can simply be explained by looking at the ratio of inertia versus drag forces:

$$\frac{F_{dr}}{F_{in}} = \frac{0.5\ \rho_w\ C_D\ D\ \omega^2\ A^2}{\rho_{tot}\ 1/4\ \pi\ D^2\ \omega^2\ A}$$

$$= \frac{2}{\pi}\ \frac{\rho_w}{\rho_{tot}}\ C_D\ \frac{A}{D}$$

2.4 Comparison of Non-Linear Cable Model Results with Davenport's Experiments

A computer code using the non-linear modal expansions, described in part I chapter 5 was developed. The results of the code were compared with experimental data obtained by Davenport [Davenport 65].

Davenport's experiments consisted of moving the top of a guy cable sinusoidally in the horizontal direction through an excentric mechanism driven by an electric motor. The horizontal tension was measured by strain gauges. The horizontal motion at the top was also measured (See figure 2-11). The cable consisted of a piano wire of 0.026 inch diameter with cylindrical weights attached, to obtain the correct total weight to tension ratio. The cable was immersed in different liquids (oil or water) during the experiments to obtain different damping characteristics. Only one experiment (case 2.1 in water) was considered in this comparison.

The horizontal amplitude of excitation in the experiment was set at 0.01 inch. The data for the experiment are ;

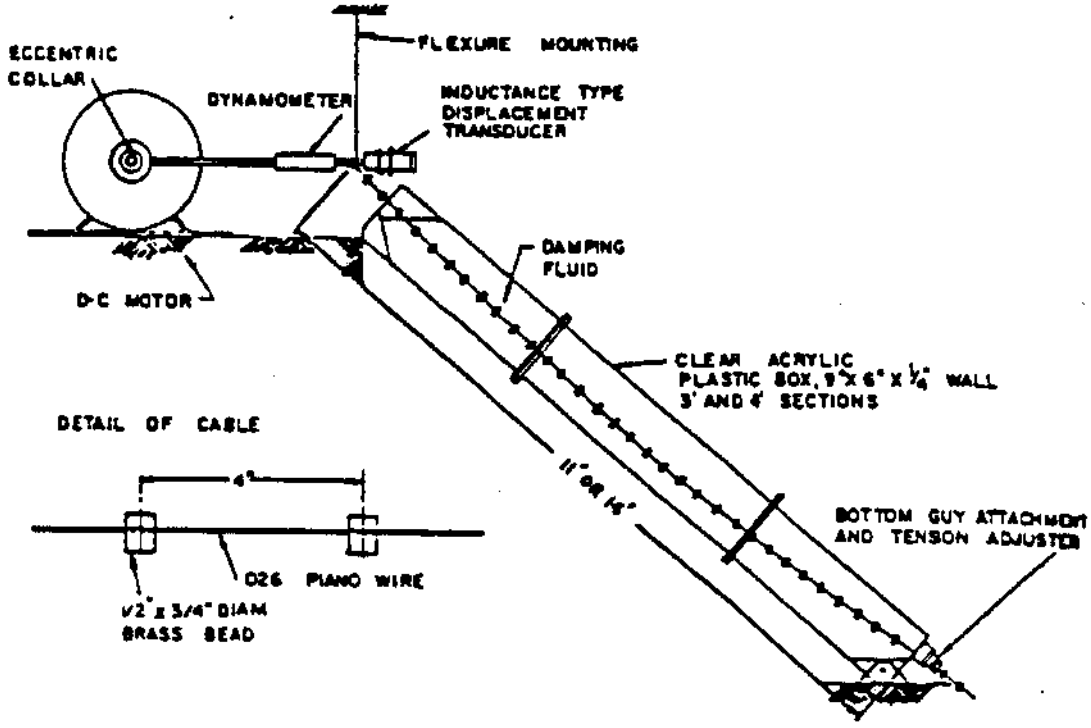

Figure 2-11: Experimental Arrangement for Dynamic tests

[Davenport 65]

$L = 11$ ft

$\phi_a = 41.06^\circ$

$H_*/AE = 0.000671$

$WL/H_* = 0.202$ (W is weight in air)

Davenport measured the horizontal component of the dynamic tension caused by an imposed horizontal motion at the top for various frequencies. The amplitude of the motion was 0.01 inch. The measured tension can be viewed, apart from a scale factor, as the impedance function S_{xx} discussed in part I. For the given amplitude, the geometric non-linear effects are not important and the damping forces are linear. The linear damping is due to the very low Reynolds number for both the oscillating cable and the attached cylindrical weights.

A number of time simulations, using the data of Davenport's experiment, were performed using the non-linear cable code. A linear modal damping was included in the code to simulate the linear damping of the cable. A damping coefficient of 4%, as suggested by Davenport, was used. This agrees approximately with the range of damping coefficients suggested by Ramberg and Griffin [Ramberg 77]. The selected damping coefficient should only be considered as a best estimate given the complicated configuration of the cable with the attached cylindrical weights. The time simulations were continued until a steady state was reached (10-20 periods).

The results are plotted on the graphs provided by Davenport. The frequency has been non-dimensionalised with respect to the first natural frequency of the equivalent string and the transfer function has been non-dimensionalised with respect to the horizontal dynamic stiffness coefficient of

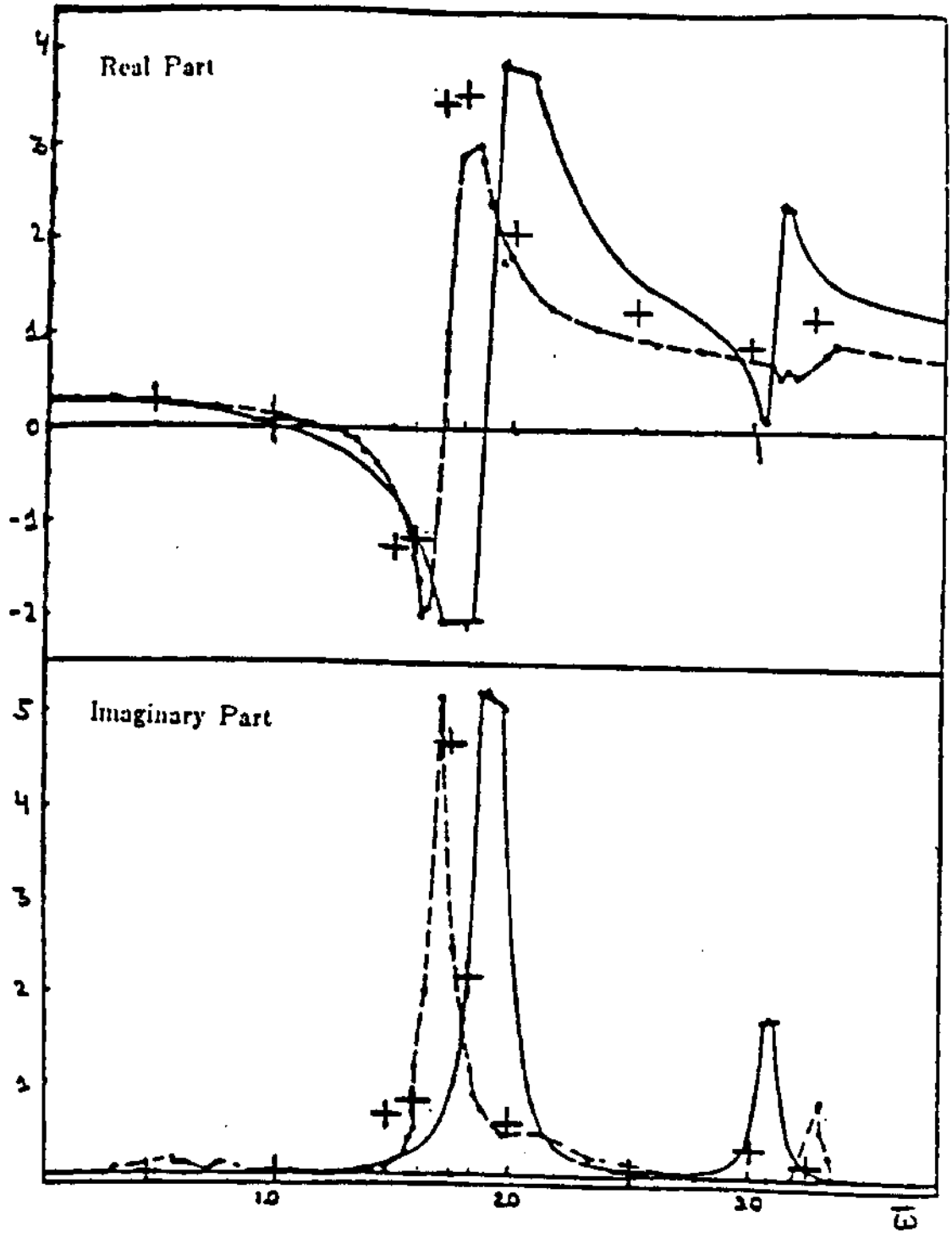

Figure 2-12: Impedance Function in the Horizontal Direction [Davenport 65]

the equivalent string.

$$\bar{S}_{xx} = S_{xx}/k \quad \text{with } k = EA/L \cos^2\phi_a$$

$$\bar{\omega} = \omega/\omega_o \quad \text{with } \omega_o = \pi (H_*/M)^{1/2}/L$$

Using the linear cable theory the eigenfrequencies were calculated as (see part I):

$\bar{\omega}_1 = 1.73$ symmetric

$\bar{\omega}_2 = 2.04$ anti-symmetric

$\bar{\omega}_3 = 3.06$ symmetric

$\bar{\omega}_4 = 4.02$ anti-symmetric

The transfer function obtained by the time simulations can be found in figure 2-12. The solid line represents Davenport's theoretical calculations. The dotted line shows the experimental results and the line annotated by plus(+) symbols shows the results obtained from the simulations. The simulation results agree fairly well with the experimental data considering the rough estimation of the damping coefficient. The location of the eigenfrequencies is predicted accurately using the linear cable theory outlined in this report. The symmetric modes are the only ones which contribute significantly to the transfer function, as expected. The time simulations predicted a steady state sinusoidal response, which was actually observed experimentally by Davenport.

2.5 A Comparison between the Non-linear Cable Model and Non-linear String Model

The results of the previous section were all within the linear regime. To test the code in the non-linear regime, the string example discussed in section 2.1 was simulated using the non-linear cable model. The data used can be found in section 2.1. The results can be found in figures 2-13 and 2-14, where it can be seen that the strings results are recovered. The major difference between the string and the cable analysis lies in the fact that in the string analysis the assumption is made, a priori, that the dynamic tension is constant over the length. If such an assumption is not made, the elastic modes seem to play an essential role in the redistribution of the dynamic tension over the cable, and they must be included to obtain a dynamic tension which is almost constant throughout the cable. This means that in the non-linear geometric regime elastic vibration modes must be included to get accurate results. The prediction of the motion in the middle, though, can be predicted accurately even when the elastic modes are left out of the response calculations.

To show the influence of sag on the geometric non-linearity, a cable weight term was added to the equations used in the previous example, which causes the cable to sag. This of course causes an asymmetric behavior of the cable: The dynamic tension when the cable is below its equilibrium position is larger for a cable than for a string, while the opposite is true when the cable moves above its equilibrium position. This can be seen in figures 2-15 and 2-16. The total cable weight to length ratio is still very small in this case ($WL/H_o = 0.005$). For a larger sag, the peak in the upward direction of the non-linear tension will disappear completely. Also, the linear component of the

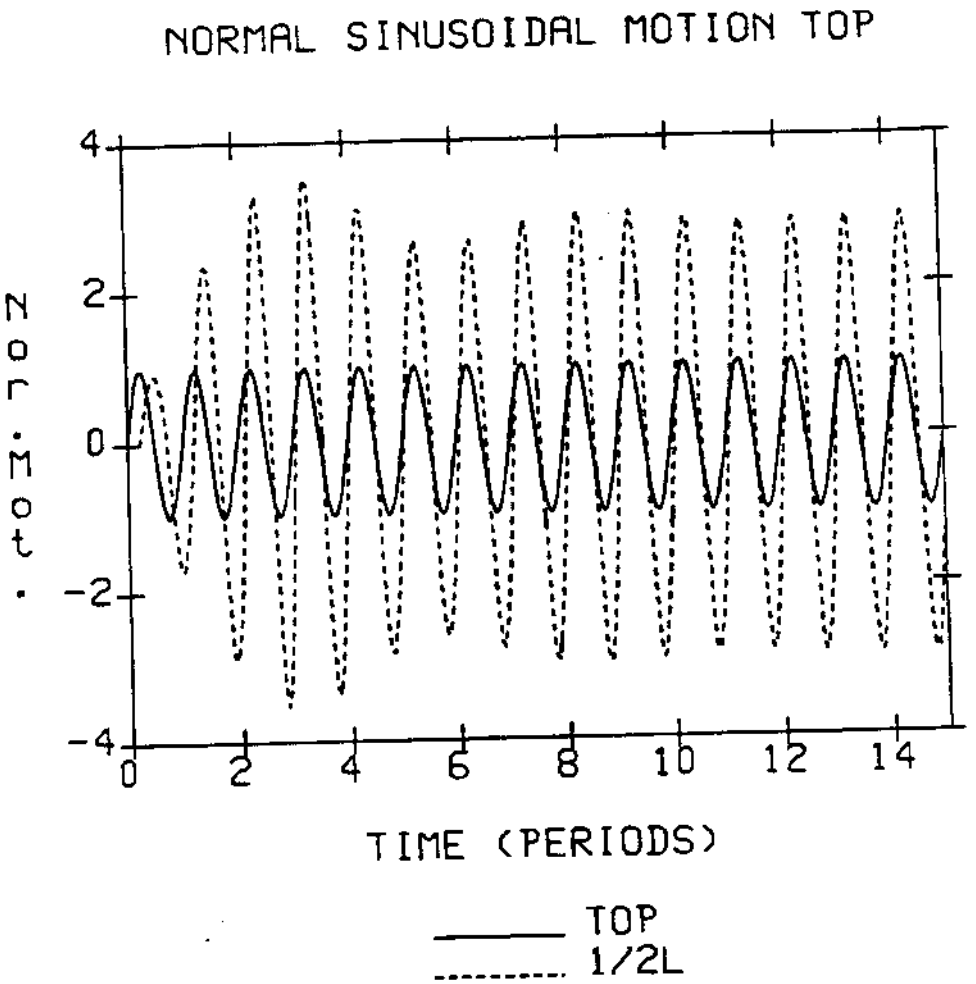

Figure 2-13: Non-linear String; Motion at midlength(cable model)

Comparison with unit motion at the top
$\tau = 0.01$
damping $= 0.05$
$\Delta T = 1/100\ T_{per}$
8 modes

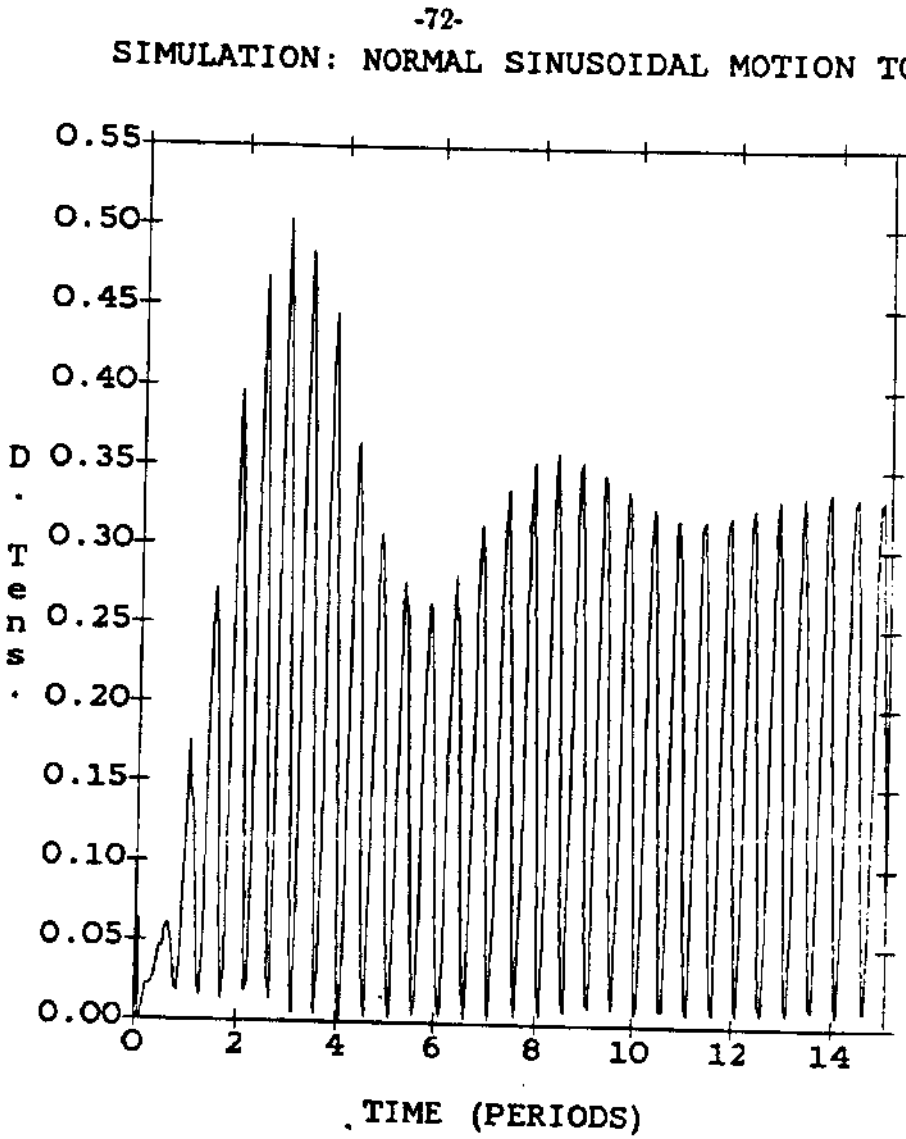

Figure 2-14: Non-linear String; Dynamic Tension (cable model)

(Dynamic Tension is given as fraction of the Static Tension)
$\tau = 0.01$
damping = 0.05
$\Delta T = 1/100\ T_{per}$
8 transverse modes, 3 elastic modes

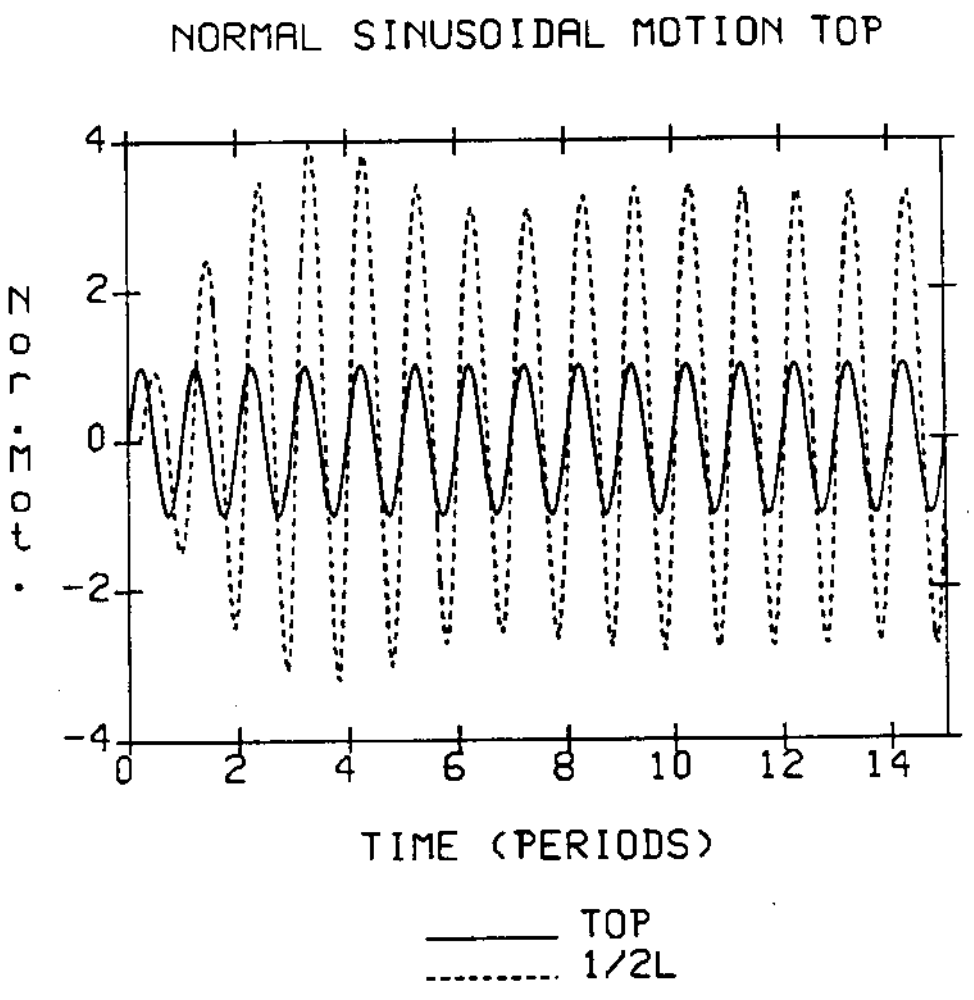

Figure 2-15: Non-linear Cable; Motion at midlength

Comparison with unit motion at the top
$\tau = 0.01$
damping = 0.05
$\Delta T = 1/100\ T_{per}$
8 modes

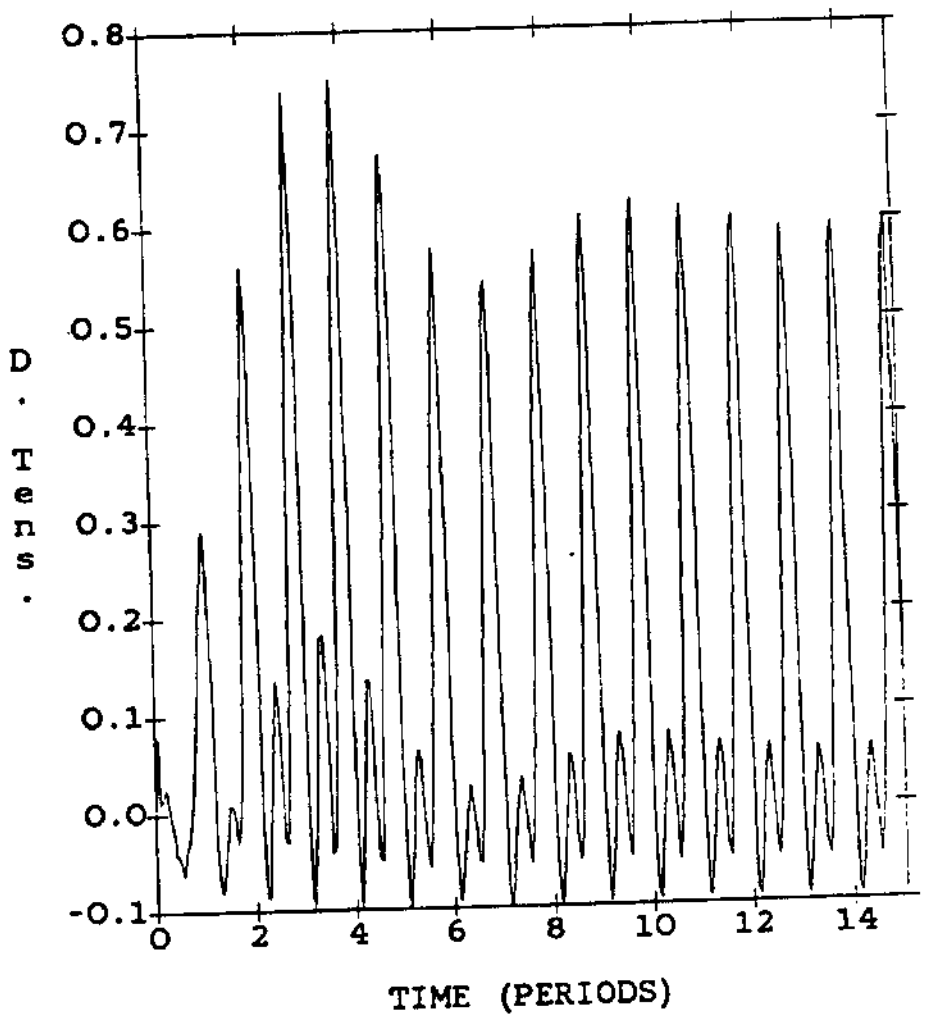

(Dynamic Tension is given as fraction of the Static Tension)

$r = 0.01$

damping = 0.05

$\Delta T = 1/100\ T_{per}$

8 transverse modes,3 elastic modes

tension plays a significant role when the amplitude of the motion is small.

2.6 Nonlinear Boundary Condition

To illustrate the effect of a non-linear boundary condition, a sinusoidal motion was imposed on a string which is laying for one third of its length on a horizontal surface. The data for the string are again the values used in section 2.1. For the timesimulation a linear spring stiffness of 1000 N/m and a damping of 2000 N s/m was used. A timestep of 1/200th of the period gave accurate results for the motions along the length (see figure 2-17). In this case the motions are highly dependent on the stiffness and damping selected. Further investigation how this selection influences the calculated response of mooring lines will certainly be required.

2.7 Snap motions

A horizontal cable was subjected to a horizontal motion of one of its end points. The data for the cable considered are:

H	=	88 300 N
Mass	=	8.84 kg/m
E·A	=	$1.2\ 10^8$ N
Length	=	365 m
Depth	=	0 m

No drag forces, no added mass considered

Figure 2-18 and 2-19 present the simulated time history at point 1/5th of the cable length from the fixed end with the excitation consisting of a harmonic oscillation of the form:

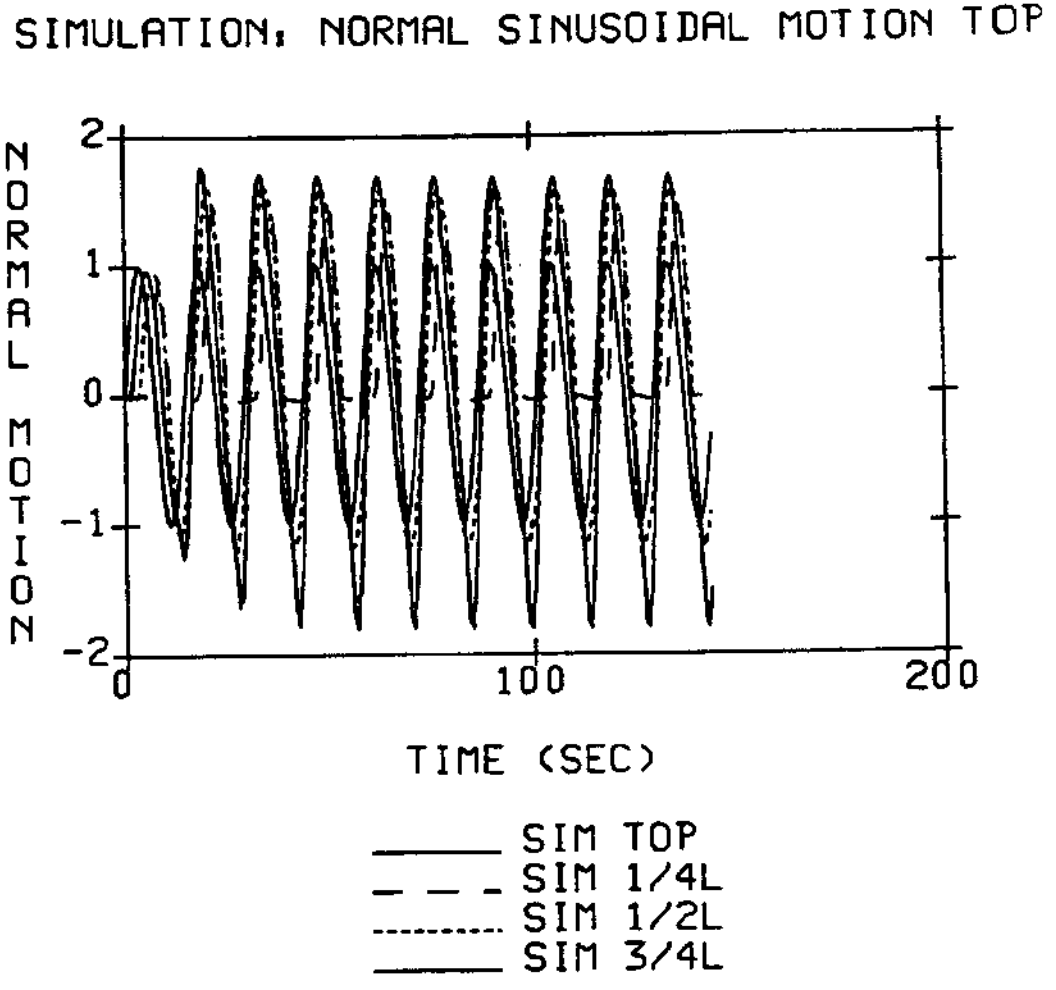

Figure 2-17: String with Nonlinear Boundary Condition

Bottom over 1/3 of the length of the string

$$p = 0.0003 \sin\omega_e t \tag{2.1}$$

In figure 2-18 the frequency is at the first elastic frequency and in figure 2-19 the excitation is at the first transverse natural frequency. The simulations were carried out using the first ten transverse mode shapes and the first five elastic mode shapers neglecting all other modes except the one bracketing the elastic modes (See part I chapter 8). The time step was set at 0.0012 second, after some trial and error determined this to be a safe and stable value.

The interesting feature in both of these figures is the time lag before the start of any significant motion. If the elastic waves travelled at a speed equal to the pure elastic wavespeed,

$$c_{el} = \left(\frac{EA}{m} \right)^{0.5} = 3\ 683\ m/S \tag{2.2}$$

it should take the motion 0.079 seconds to reach the point being studied. Careful study of the figures reveals that this is indeed the case which confirms the succesful inclusion of the elastic waves in the simulation.

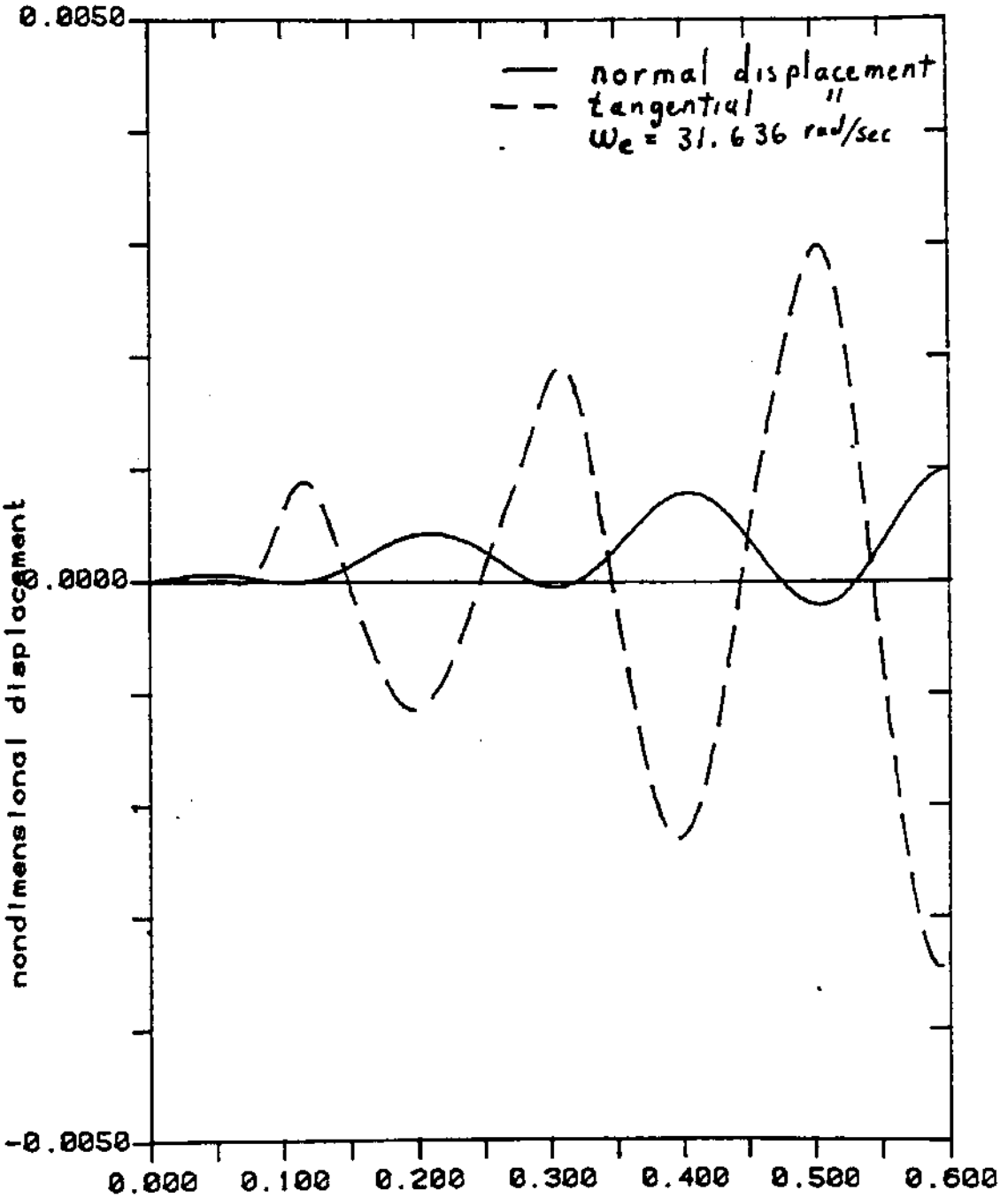

Figure 2-18: Snap Motion: Excitation at First Elastic Frequency

Response of Cable Point at s=1/5

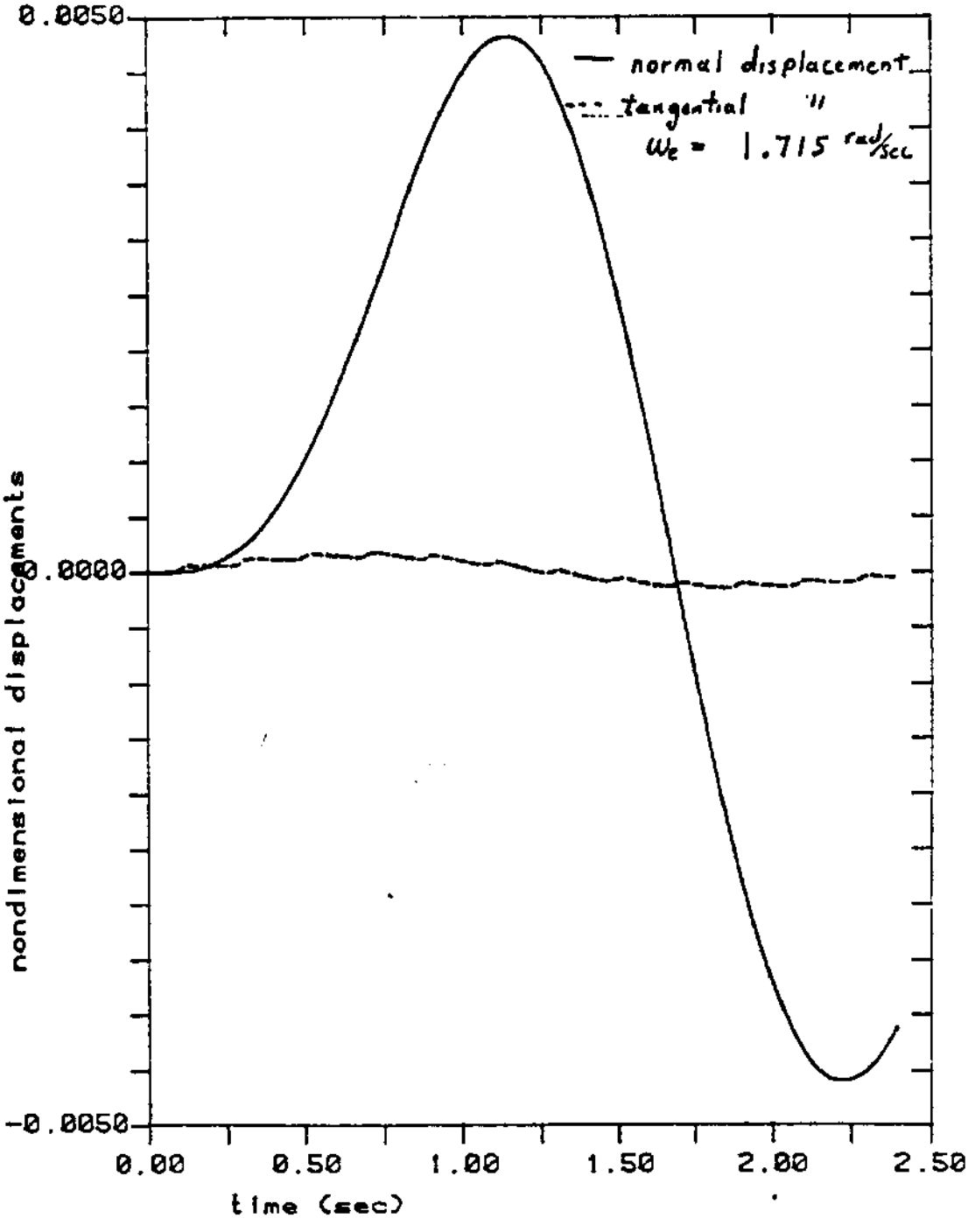

Figure 2-19: Snap Motion: Excitation at First Transverse Frequency

Response of Cable Point at s=1/5

2.8 References

[Davenport 65] Davenport, A. G. and Steels, G. N.
Dynamic Behavior of Massive Guy Cables.
Journal of the Structural Division, ASCE 91(ST2):43-70, April, 1965.

[Oplinger 60] Oplinger, D. W.
Frequency Response of a Nonlinear Stretched String.
Journal of the Acoustic Society of America 32(12):1529-1538, December, 1960.

[Ramberg 77] Ramberg, S. E. and Griffin, O. M.
Free Vibrations of Taut and Slack Marine Cables.
Journal of the Structural Division, ASCE 103(ST11):2079-2092, November, 1977.

Chapter 3

NUMERICAL APPLICATIONS OF LINEARIZATION TECHNIQUES

3.1 Introduction

In this chapter, a number of comparison between the drag linearization results and time simulation calculations are provided. For relative small motions the agreement is relatively good. For larger motions geometric nonlinearities become important and the linearization technique underestimates the tension generated. It will be shown that the dynamic tension generated due to a unit amplitude is significantly affected by the drag nonlinearity. Also the effect of the mooring line stiffness on the dynamic tension will be briefly discussed.

3.2 Comparison of Linearization Results and Nonlinear Time Simulations

In this section, the motions predicted by the linearized code and the nonlinear time domain code are compared directly. For this purpose a string and a cable were excited at one end in the transverse direction at the resonance frequencies. The importance of the hydrodynamic drag has been demonstrated in the previous chapter.

3.2.1 String Results

The data for the string analysed are:

T	=	1 000 000 N
Total Mass	=	48.7 kg/m
Net weight	=	0 N/m
D_o	=	0.0889 m
E·A	=	1.30 10^9 N
Length	=	1 036 m
Depth	=	0 m
C_{Dn}	=	1.2
C_{Dt}	=	0.05

No external current

One end of the string was moved sinusoidally at the first string resonance frequency which is a symmetric mode. The comparison between the linearized theory and the time simulation can be found in figures 3-1, 3-2 and 3-3. The figures are the superposition of one period of the time simulations at steady state and the linearized results for different ratios of amplitude to diameter. The agreement between the linearized solution and the time simulation is acceptable even for large ratios of amplitude to diameter. In figures 3-4, 3-5 and 3-6 the normal displacement along the string are given. This normal displacements have been obtained by the full nonlinear code.

3.2.2 Cable Results

The data for the cable analysed are (identical to guy in previous chapters):

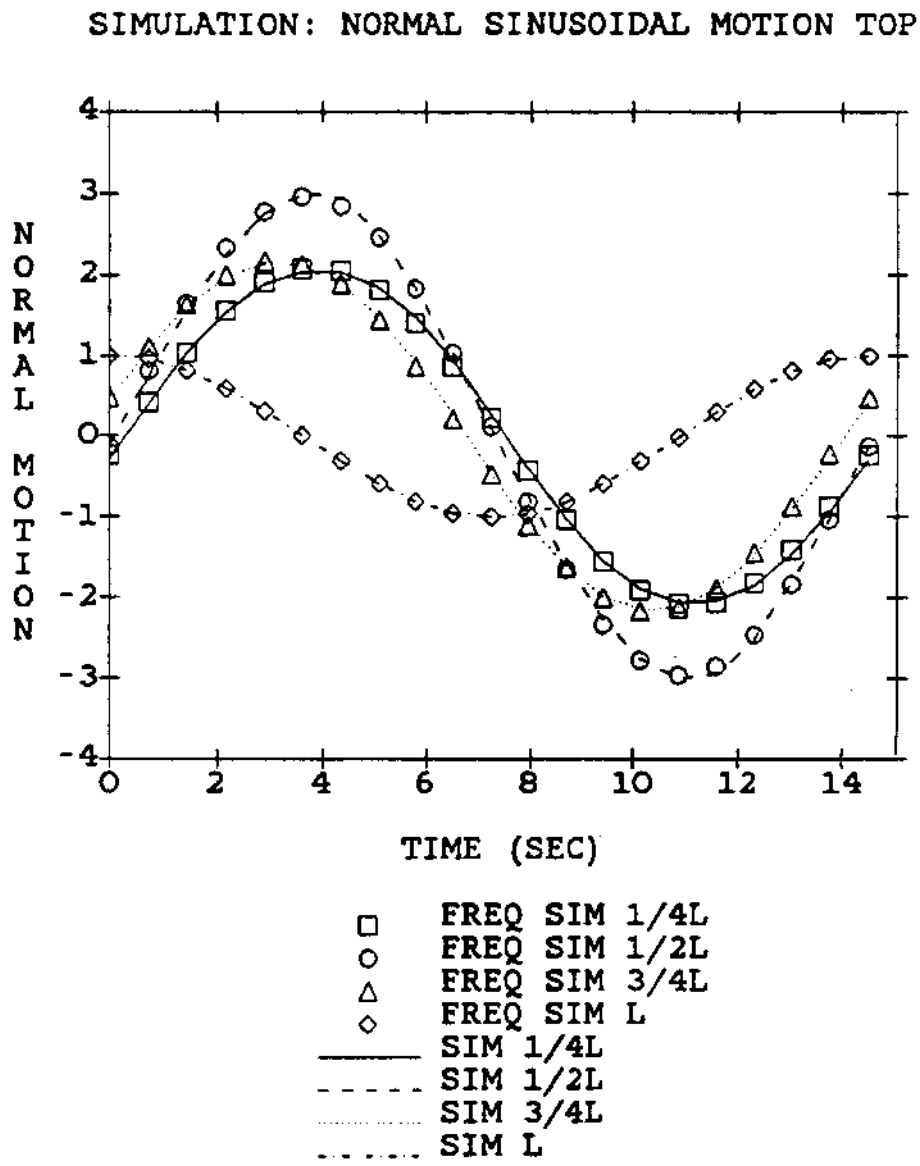

Figure 3-1: Linearization of the Drag Forces: String 1D

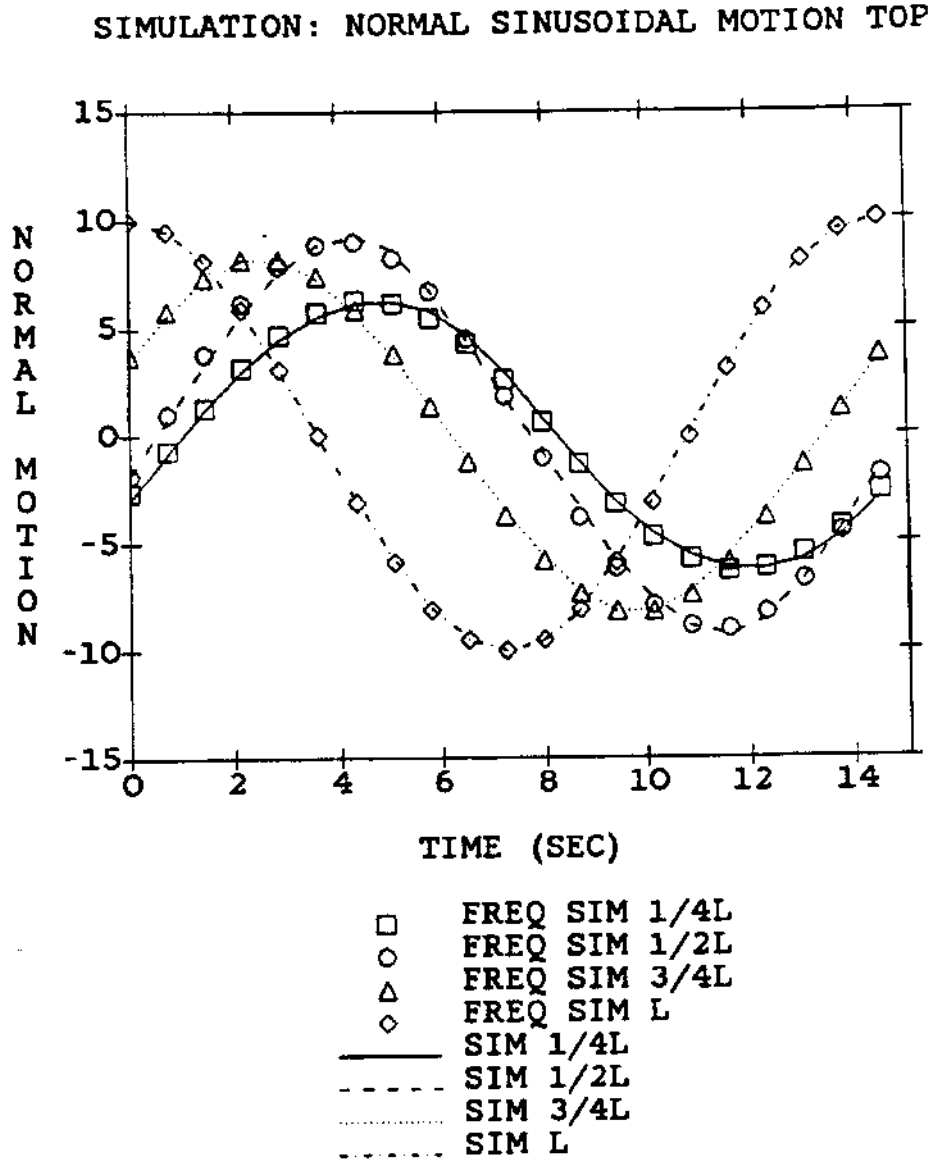

Figure 3-2: Linearization of the Drag Forces: String 10D

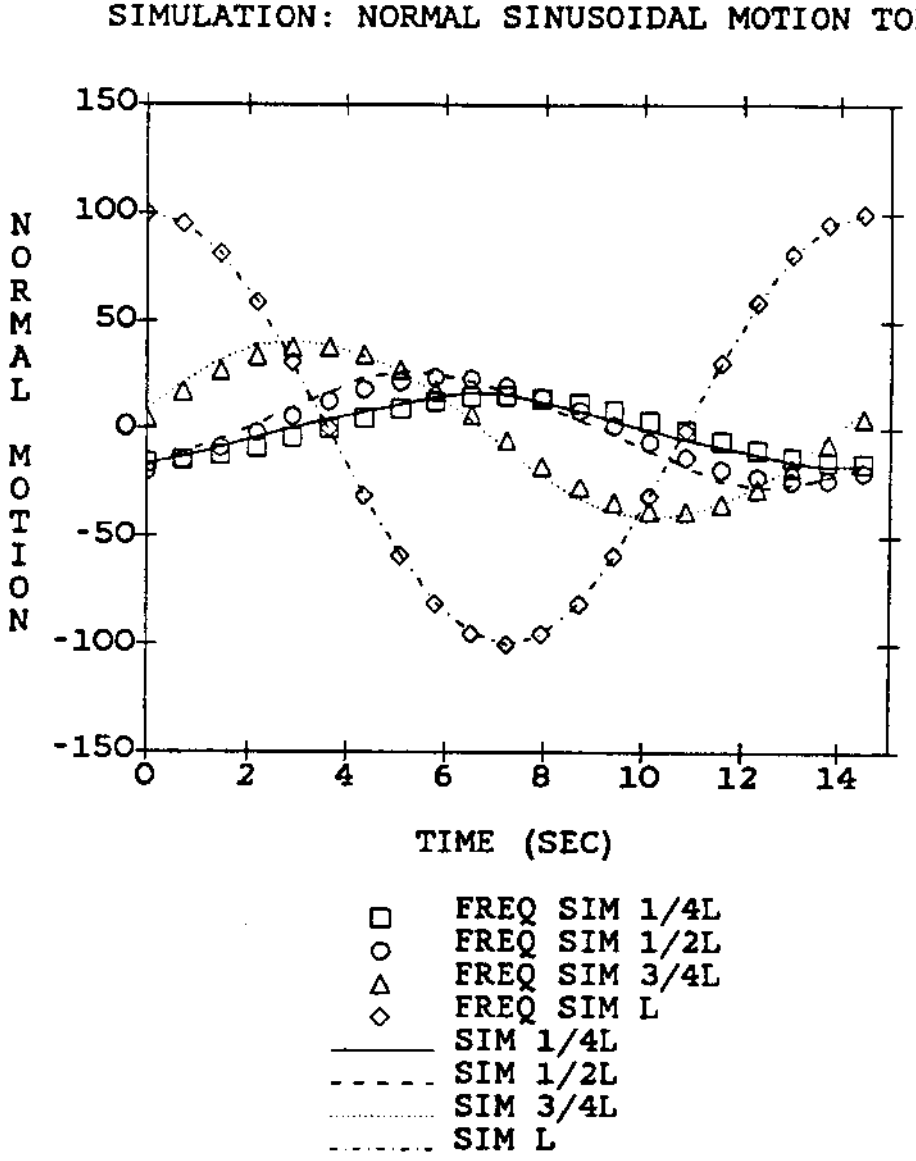

Figure 3-3: Linearization of the Drag Forces: String 100D

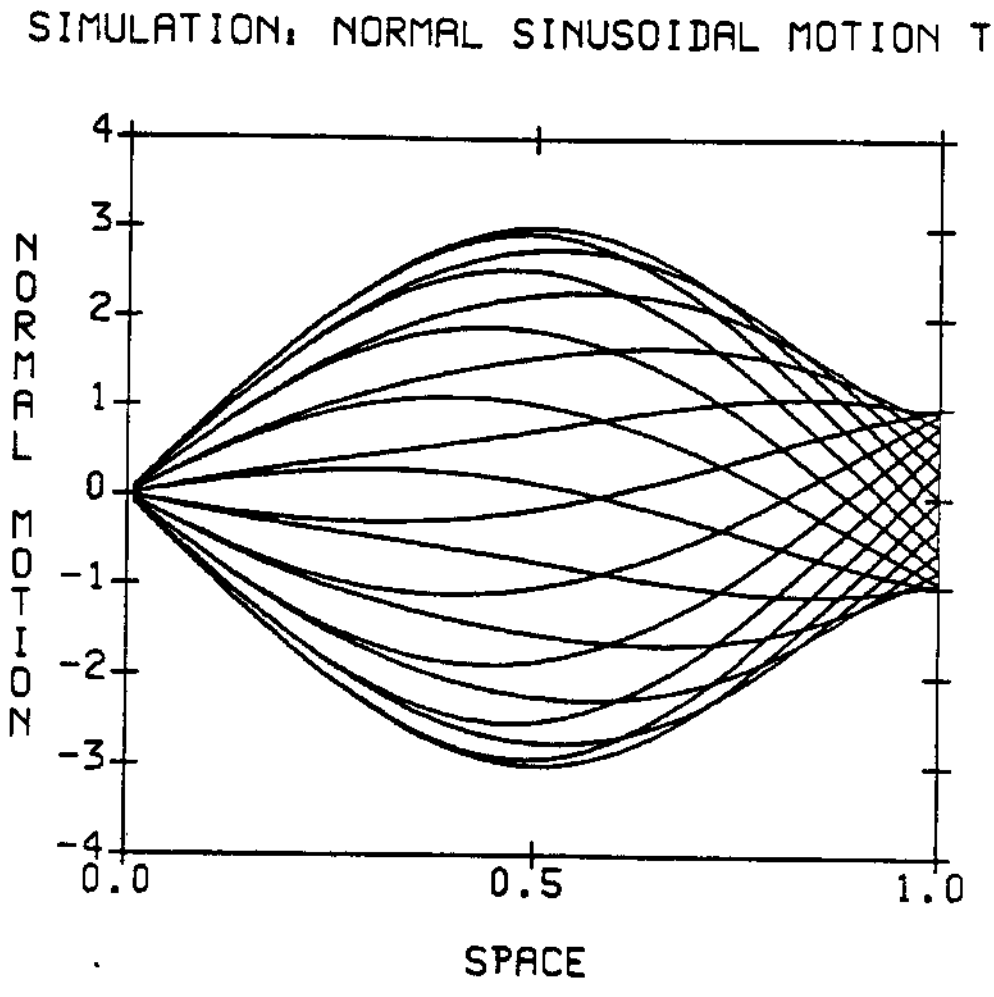

Figure 3-4: Displacement: String 1D

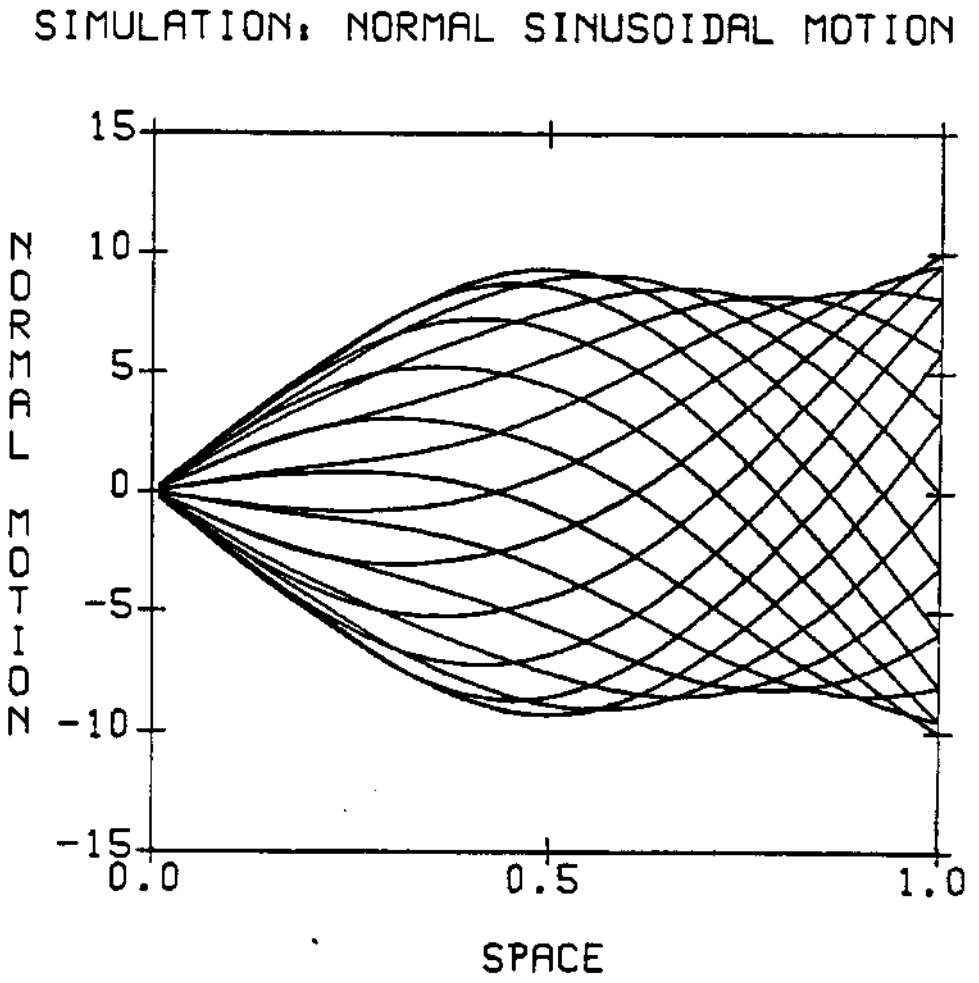

Figure 3-5: Displacement: String 10D

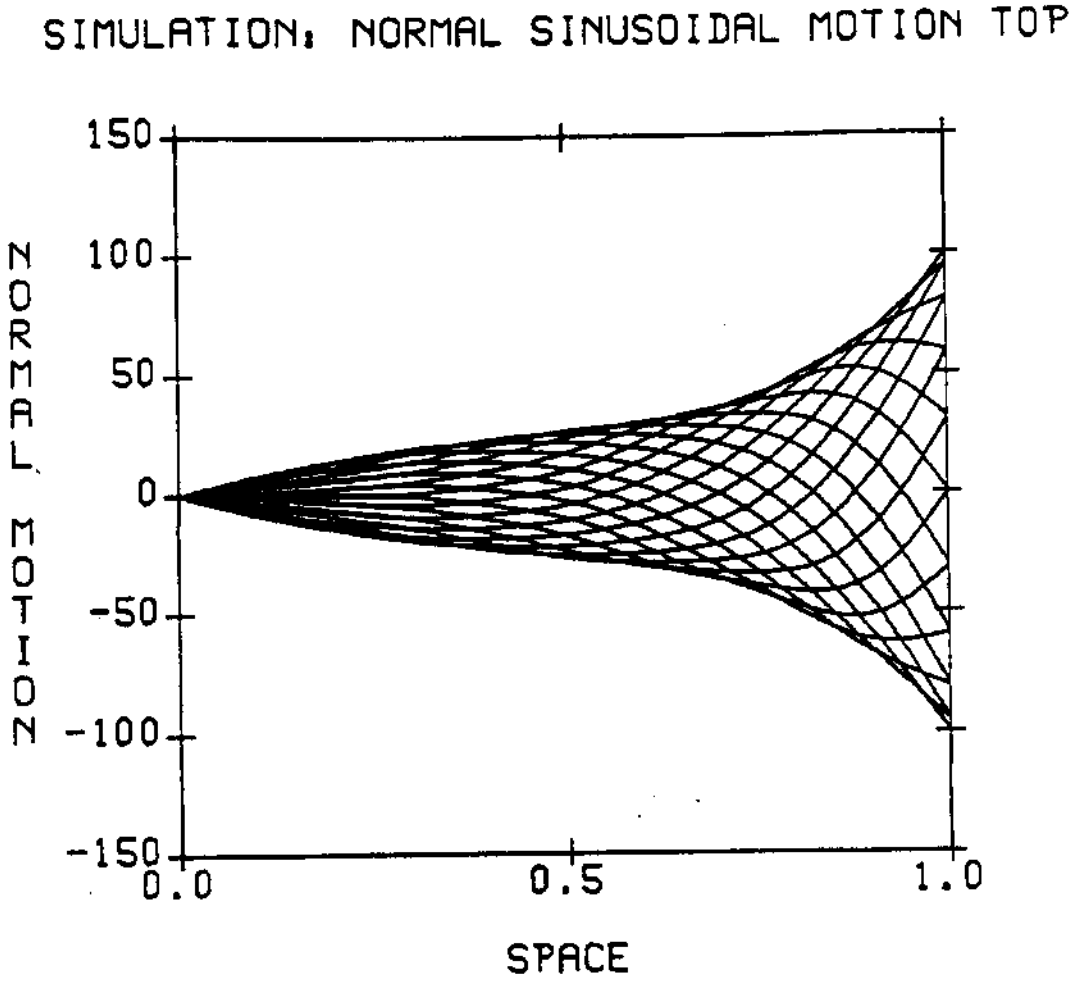

Figure 3-6: Displacement: String 100D

T_{top}	=	1 332 000 N
T_{bot}	=	1 155 096 N
Mass	=	48.7 kg/m
Added mass	=	6.3 kg/m
Net weight	=	414.98 N/m
D_o	=	0.0889 m
E·A	=	1.30 10^9 N
Length	=	1 036 m
Depth	=	426.7 m
C_{Dn}	=	1.2
C_{Dt}	=	0.05
ϕ_{top}	=	33.056°
ϕ_{bot}	=	14.874°
ΔX	=	940.68 m
ϕ_{av}	=	24.399°

No external current

One end of the cable was moved sinusoidally at the first string resonance frequency which is a assymmetric mode. The comparison between the linearized theory and the time simulation can be found in figures 3-7, 3-8 and 3-9. The figures are the superposition of one period of the time simulations at steady state and the linearized results for different ratios of amplitude to diameter.

The agreement between the linearized solution and the time simulation is also acceptable in this case. In figures 3-10, 3-11 and 3-12 the normal displacements along the cable are given. This normal displacements have been obtained by the full nonlinear code. In section 2.3 equivalent envelopes where obtained by using the linearized equations with a nonlinear drag force. Here the geometric nonlinear effects are included in the analysis. The non symmetric motion of the cable due to geometric stiffening can clearly be observed for the 100 D case. This should be compared with the result in section 2.3

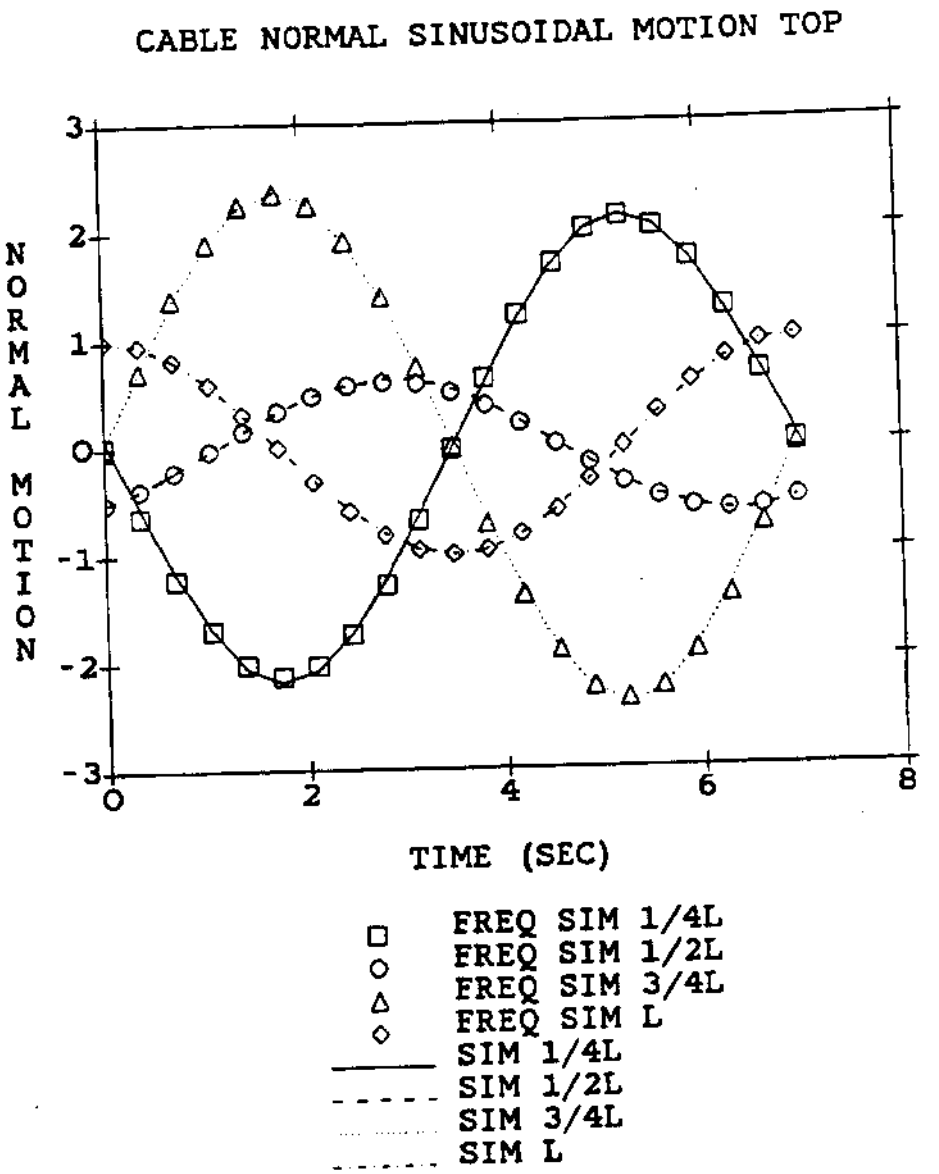

Figure 3-7: Linearization of the Drag Forces: Cable 1D

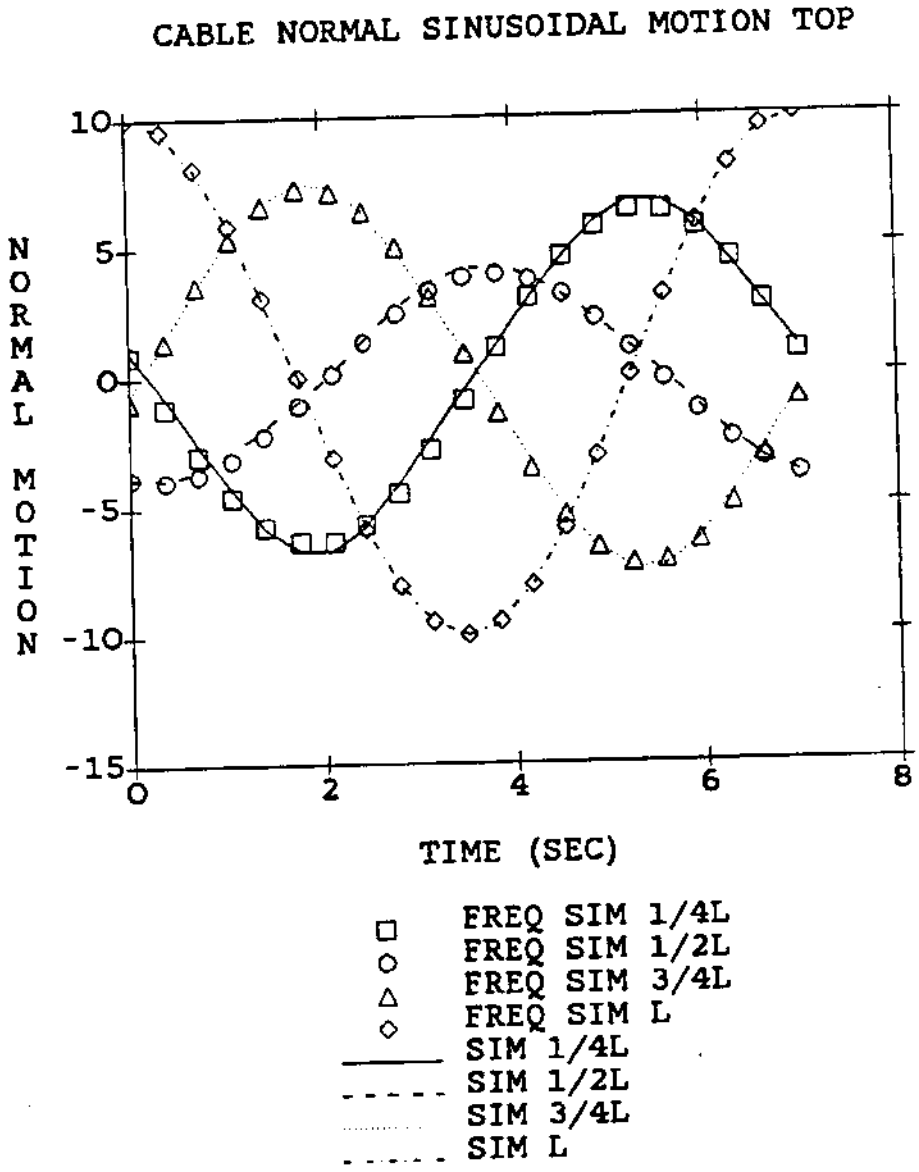

Figure 3-8: Linearization of the Drag Forces: Cable 10D

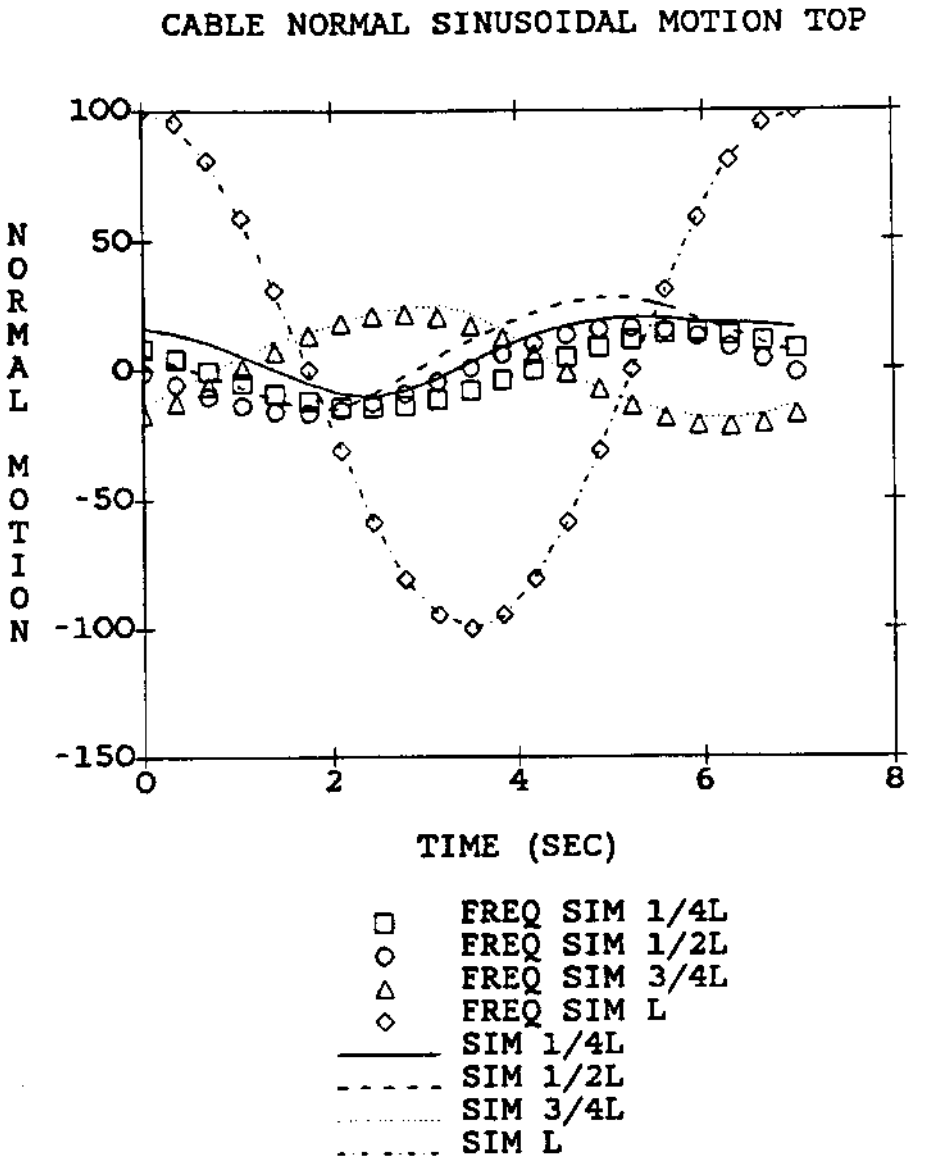

Figure 3-9: Linearization of the Drag Forces: Cable 100D

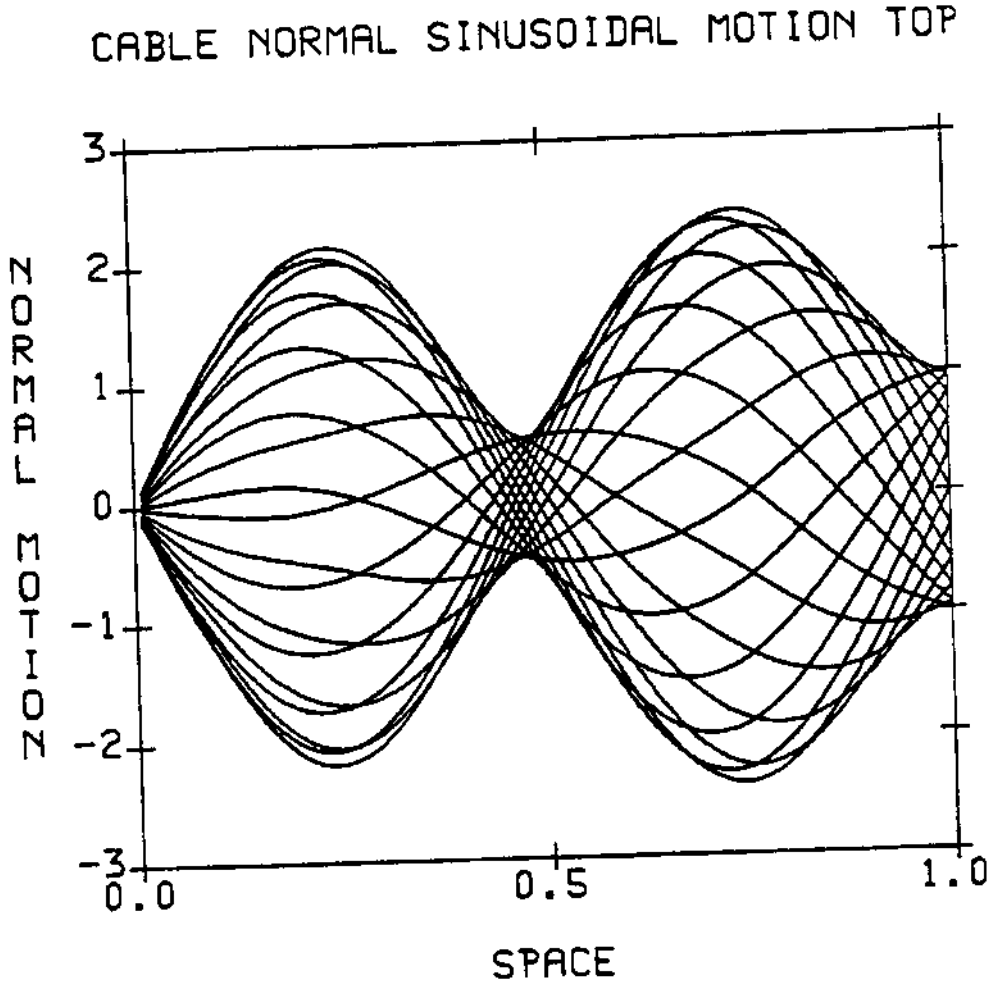

Figure 3-10: Displacement: Cable 1D

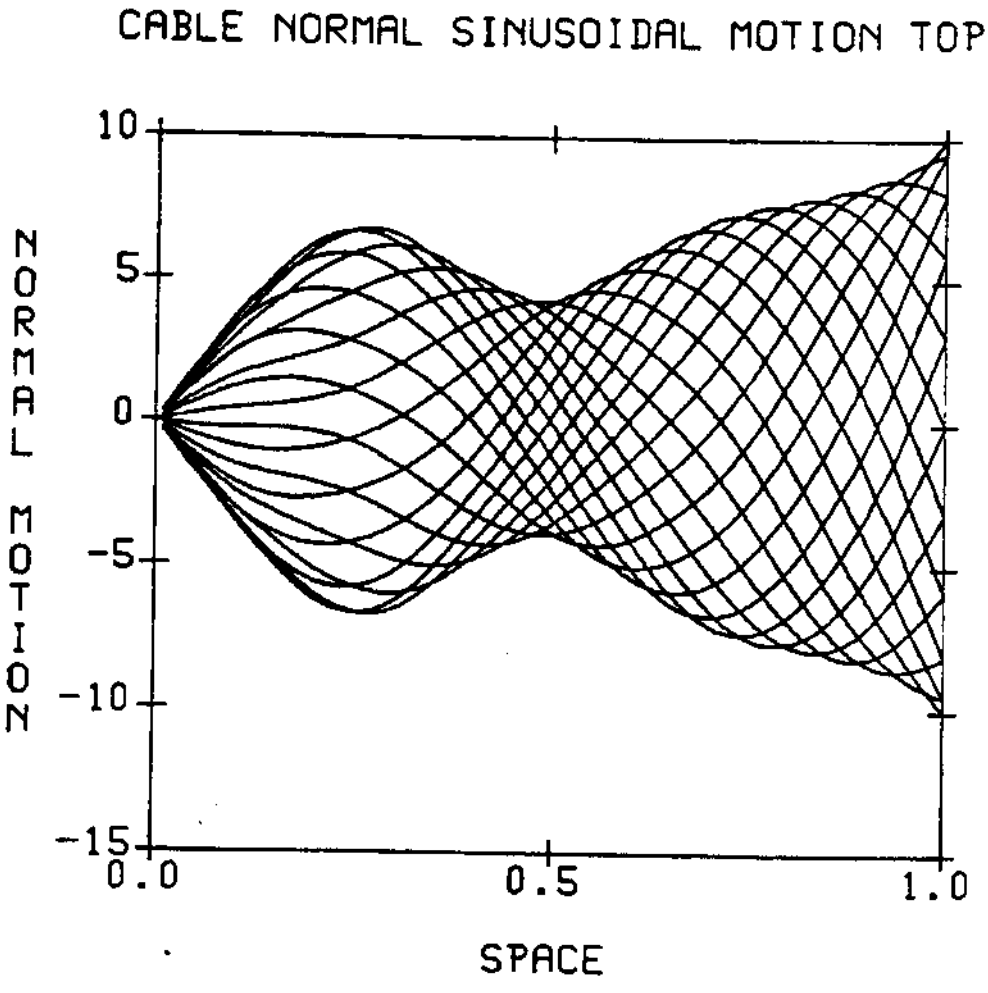

Figure 3-11: Displacement: Cable 10D

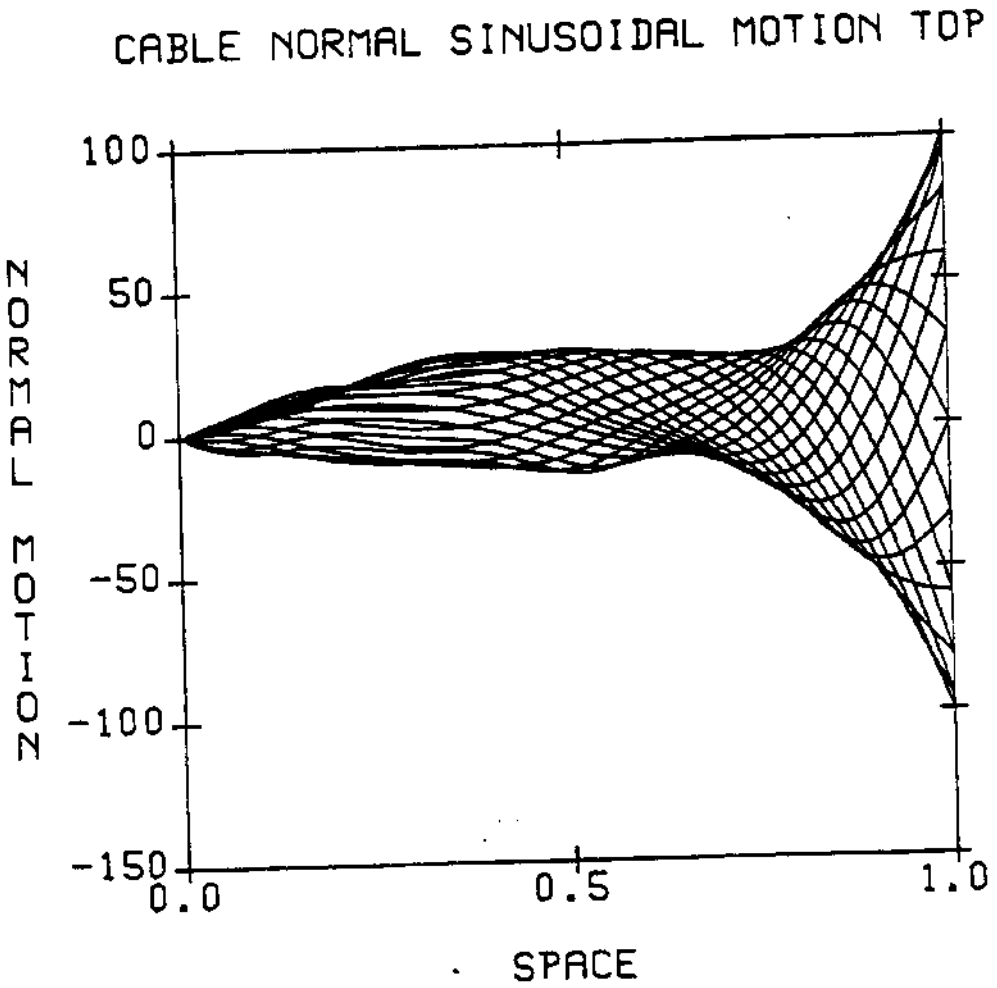

Figure 3-12: Displacement: Cable 100D

3.3 Equivalent Impedance functions

Using the equivalent linearization, equivalent impedance functions can be obtained for sinusoidal motion of the top. Two examples are analysed: The guyed tower example and a slacker mooring line used in a typical semi-submersible configuration. For the theory on impedance functions the reader is referred to part I.

3.3.1 S_{xx} for the Guy

The data for this case can be found in the previous section. Four horizontal top impedance functions are given for different amplitudes in figures 3-13, 3-14, 3-15 and 3-16. Figure 3-13 is only to show the undamped response of the system. In the case of such a small motion the drag force model used is of course not really valid. The impedance functions are substantially modified due to the strong effect of the drag forces. The dynamic response of the cable is dominated by the drag effects.

3.3.2 S_{Tx} for the Mooring Line of a Semi-submersible

The data for the selected mooring line are:

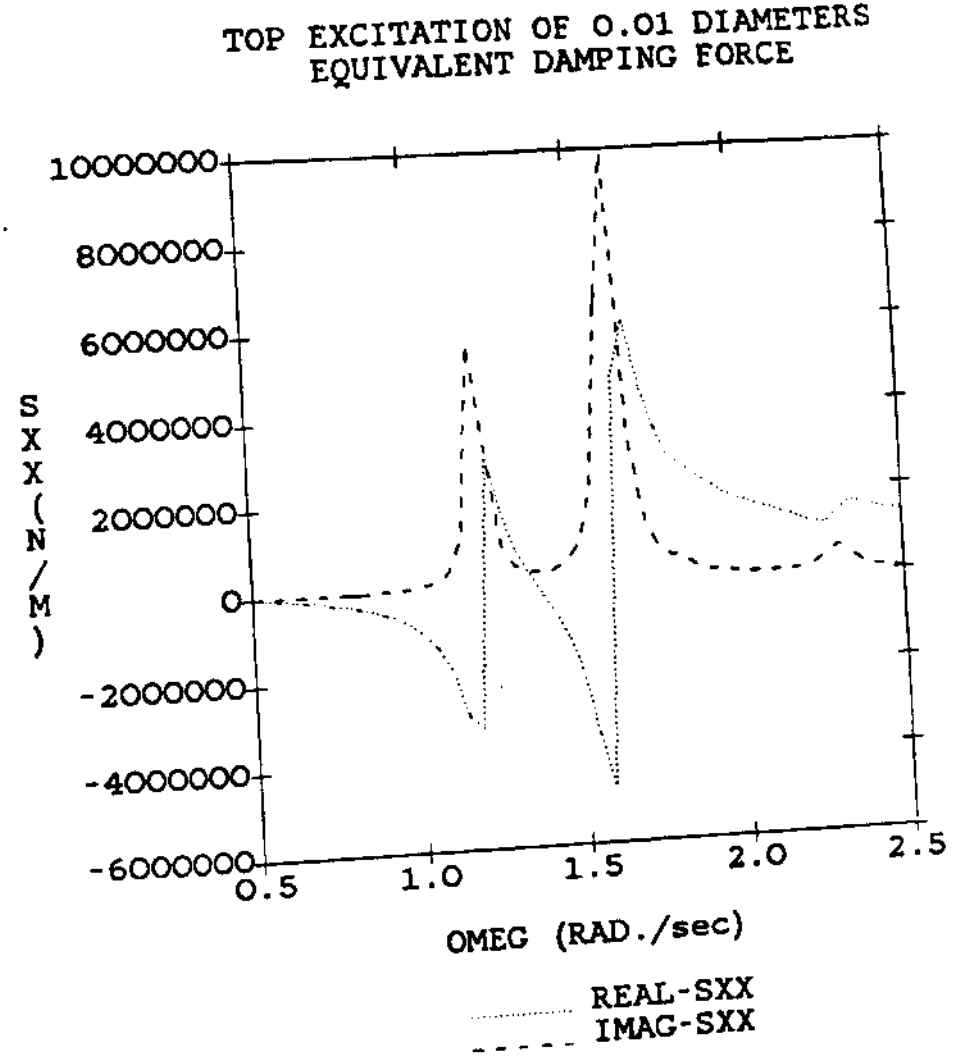

Figure 3-13: S_{xx} for a Guy of a Guyed Tower: 0.01D

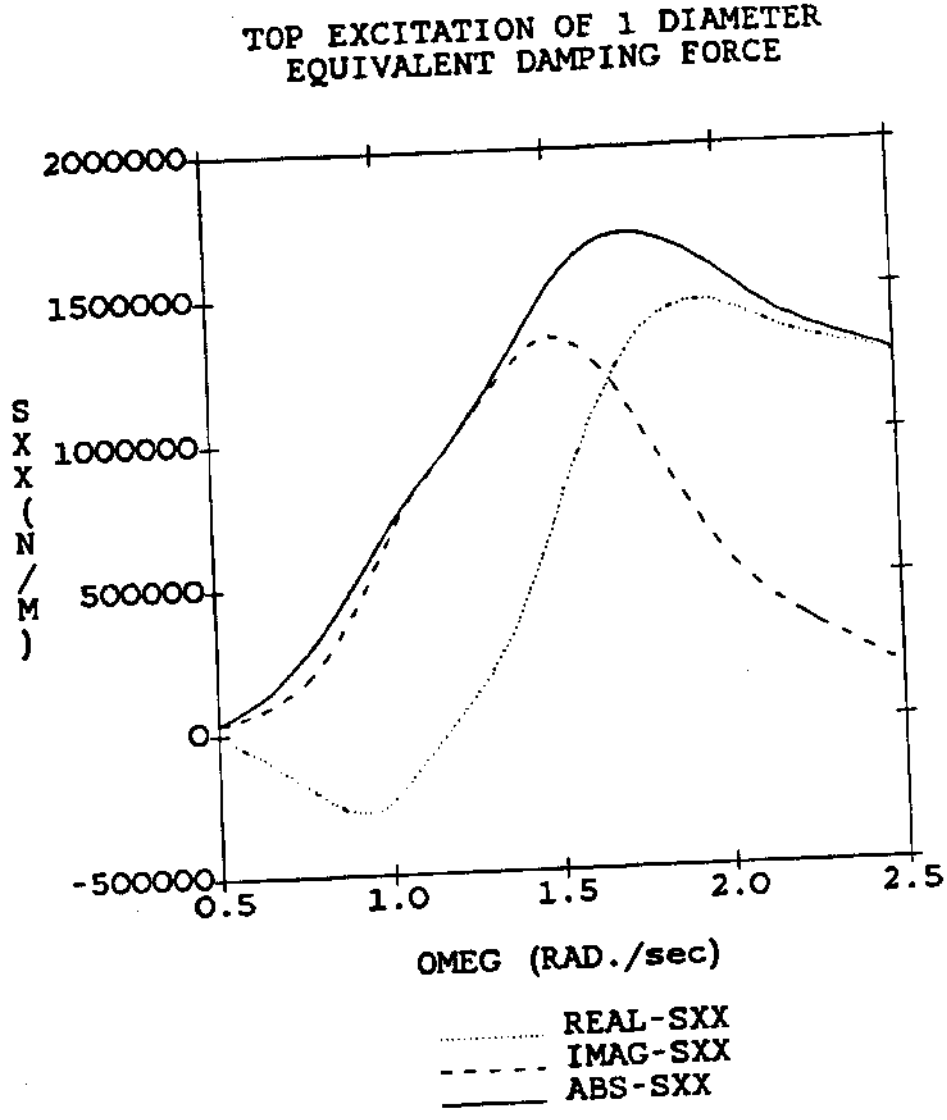

Figure 3-14: S_{xx} for a Guy of a Guyed Tower: 1D

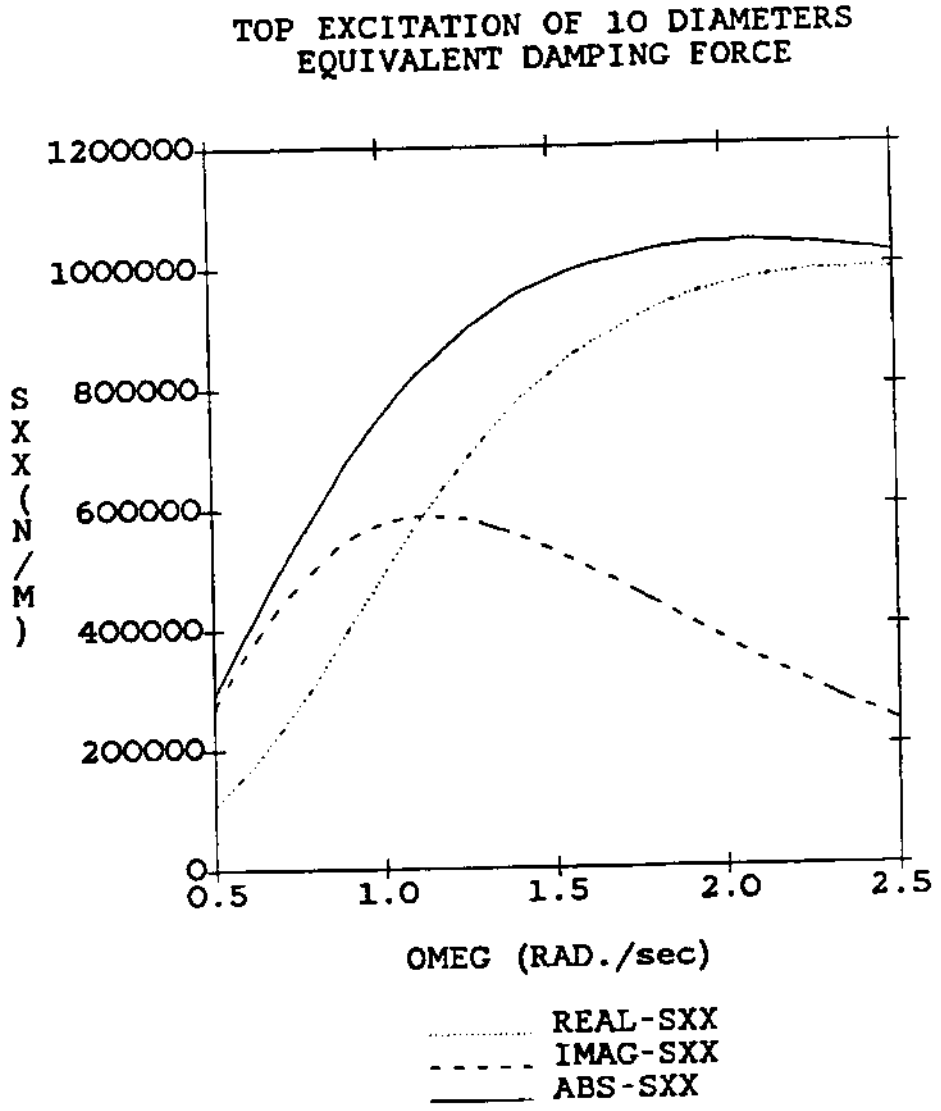

Figure 3-15: S_{xx} for a Guy of a Guyed Tower: 10D

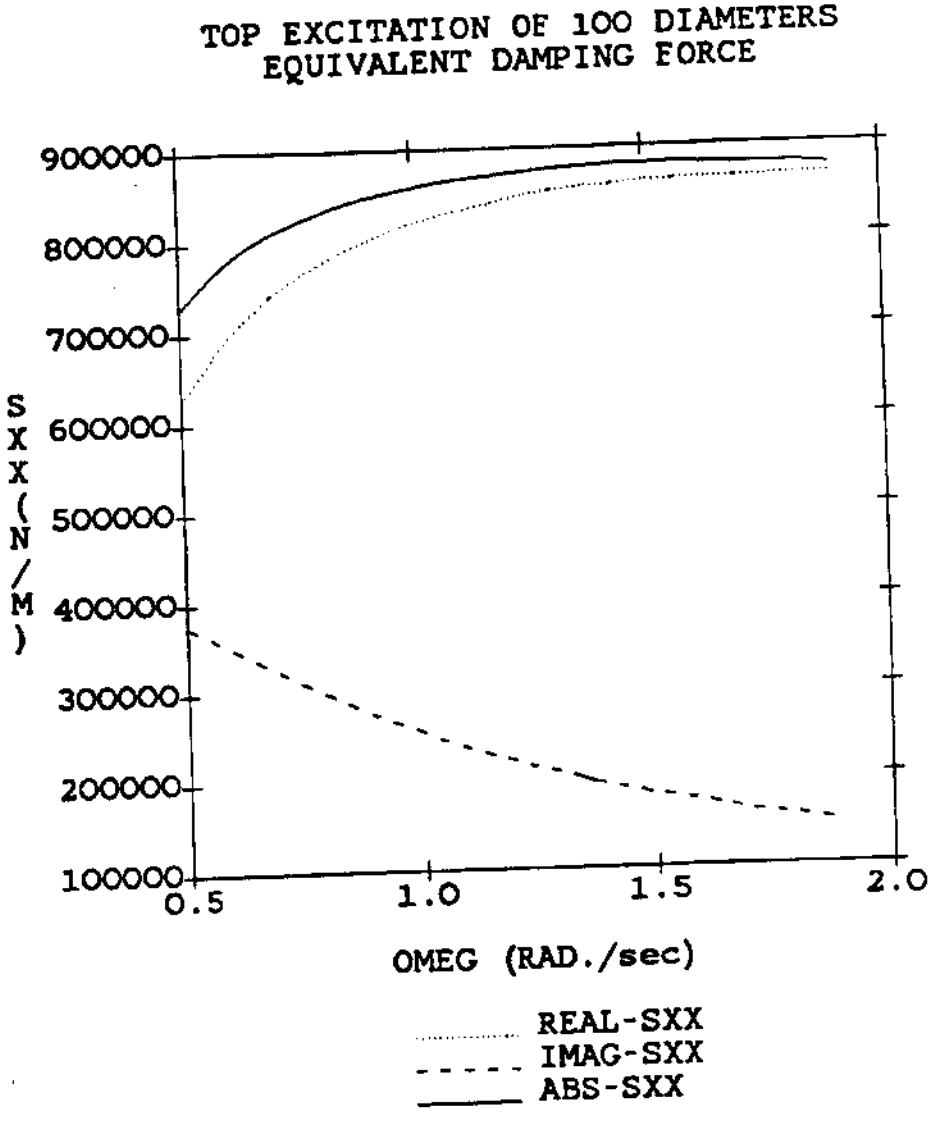

Figure 3-16: S_{xx} for a Guy of a Guyed Tower: 100D

T_{top}	=	700 000 N
T_{bot}	=	497 286 N
Mass	=	33.51 kg/m
Added mass	=	6.3 kg/m
Net weight	=	290 N/m
D_o	=	0.0889 m
E·A	=	0.424 10^9 N
Length	=	1 700 m
Depth	=	700 m
C_{Dn}	=	1.2
C_{Dt}	=	0.05
ϕ_{top}	=	44.73°
ϕ_{bot}	=	0.0°
ΔX	=	1503.22 m
ϕ_{av}	=	24.97°

No external current

In this case the dynamic tension per unit amplitude motion in the horizontal direction has been plotted for various amplitudes. The result can be found in figure 3-17. A limited number of results of time simulations have been superimposed on the plot. Agreement is good until a motion amplitude of 10D. At 100D motion amplitude the linearized theory predicts much lower values of dynamic tension as the time simulations. The figure shows also that the dynamic tension can increase due to drag effects in the low frequency range. The drag forces are the dominant forces on the cable, and therefore, induce significant dynamic tension as they reduce the motions.

3.4 Investigation of the Change of Tension Impedance function due to Lambda

It is well know that in linear theory large dynamic tensions are predicted near cross-over. In this example the stiffness of mooring line was varied continously to investigate how this behavior is influenced by the drag forces.

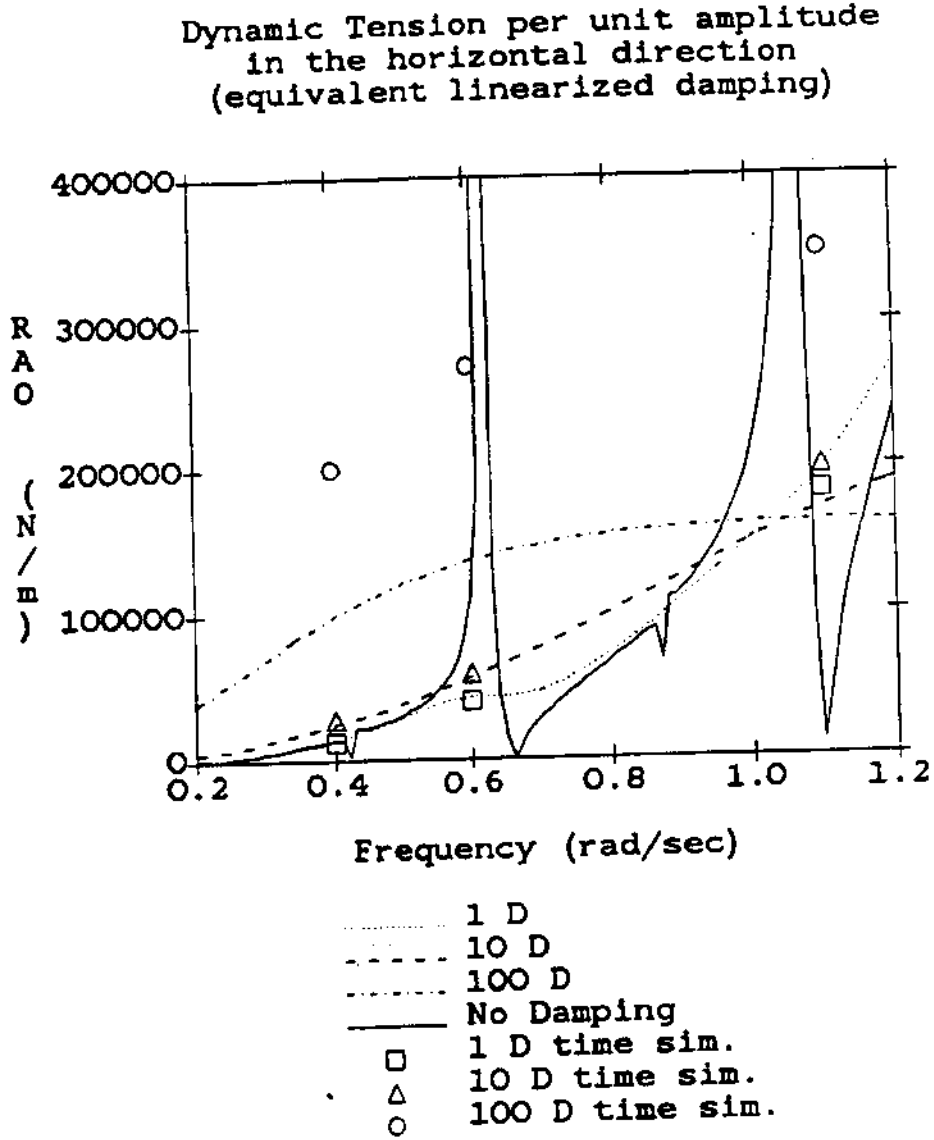

Figure 3-17: S_{Tx} for a Mooring Line

The data for the selected mooring lines are:

T_{top}	=	1 400 000 N
T_{bot}	=	1 197 618 N
Mass	=	33.51 kg/m
Added mass	=	6.3 kg/m
Net weight	=	290 N/m
D_o	=	0.0889 m
Length	=	1 700 m
Depth	=	700 m
C_{Dn}	=	1.2
C_{Dt}	=	0.05
ϕ_{top}	=	33.84°
ϕ_{bot}	=	13.84°
Δx	=	1545.31 m
ϕ_{av}	=	24.37°

No external current, the stiffness was varied so that λ_*^2 varied between 10 and 200.

The results can be found in figures 3-18, 3-19 and 3-20. The figures show the dynamic tension per unit horizontal and vertical motion at the first two eigenfrequencies when λ_*^2 is varied. When λ_*^2 is $4\pi^2$ the two eigenfrequencies are very close to each other and according to linear theory a significant dynamic tension can be generated. This linear prediction is confirmed qualitatively by figure 3-18. At larger motion amplitudes the dynamic tension is increasing when the line becomes less extensible. It should be emphasised that this are the results at two particular frequencies, and that these are not necessarily the frequencies where the generated dynamic tension has a maximum.

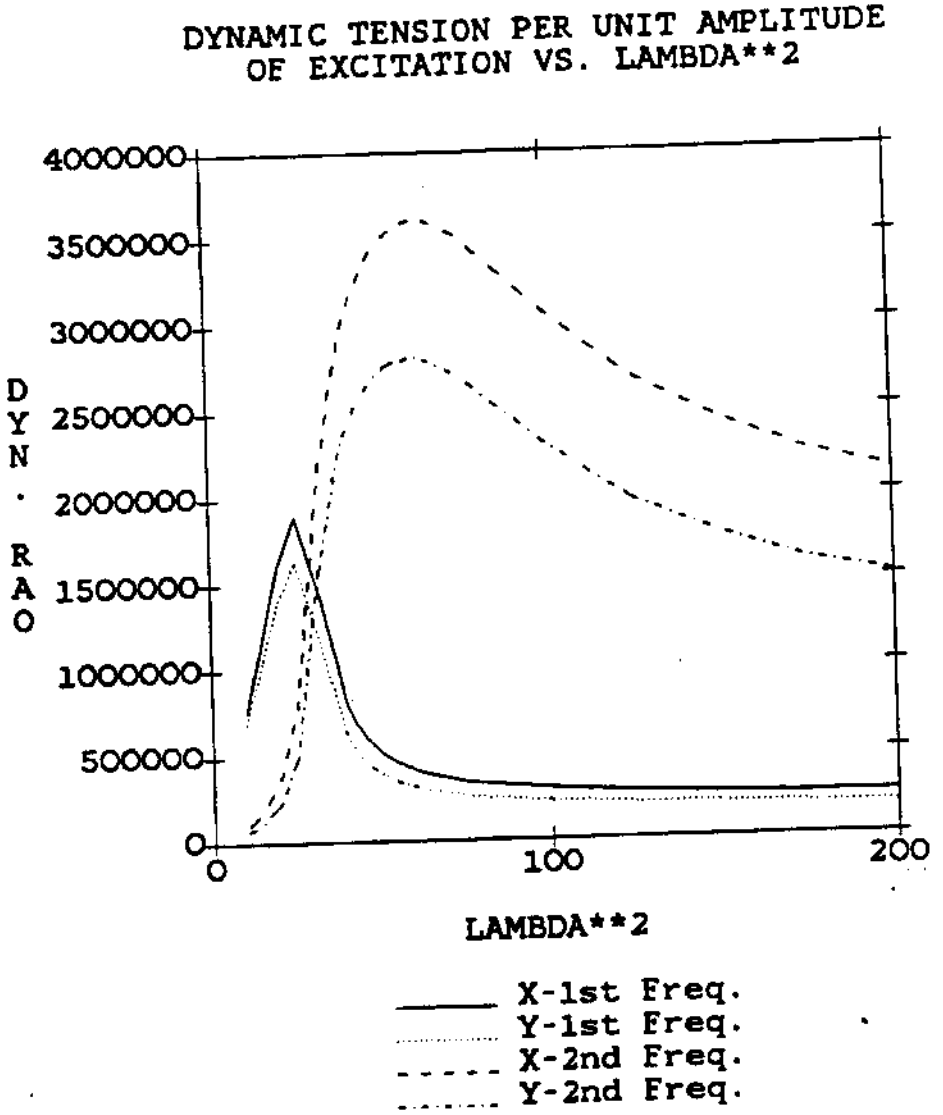

Figure 3-18: S_{Tx} for a Mooring Line in function of Lambda: 0.01D

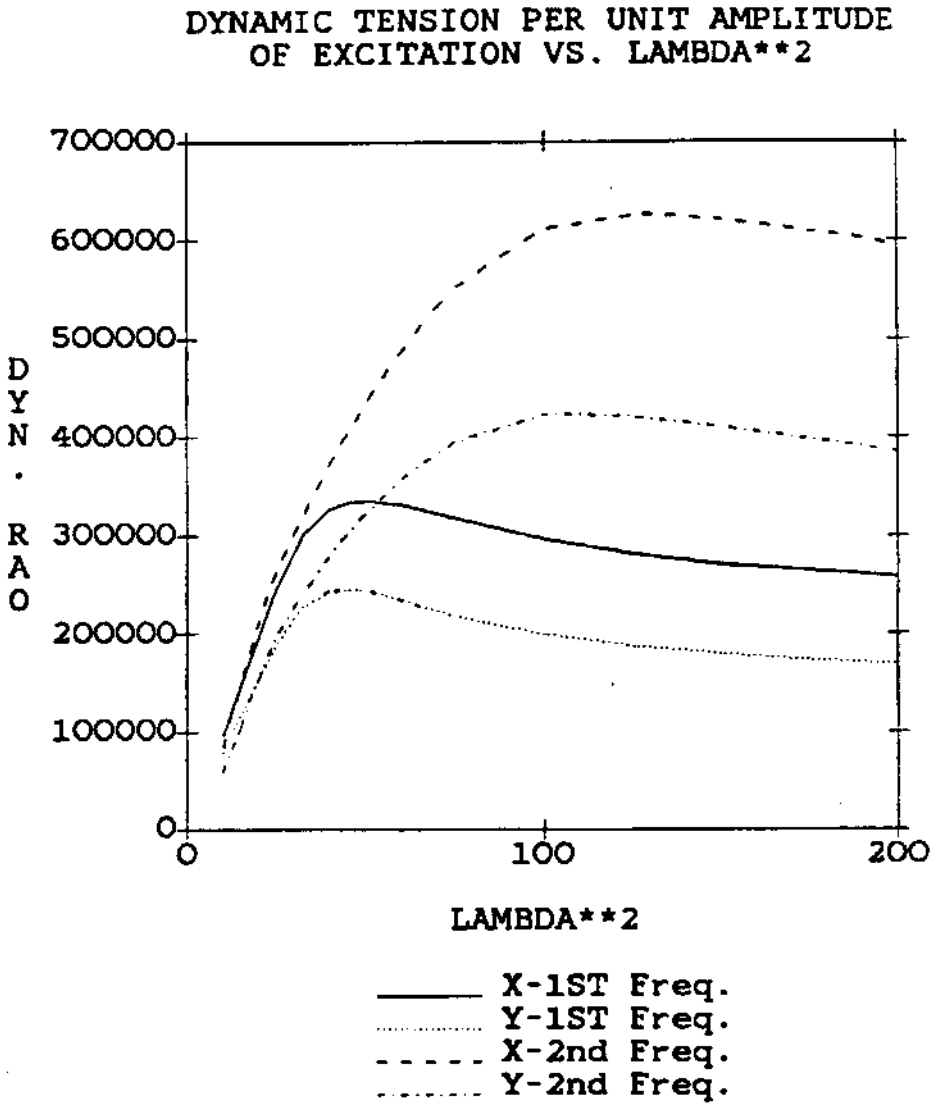

Figure 3-19: S_{Tx} for a Mooring Line in function of Lambda: 1D

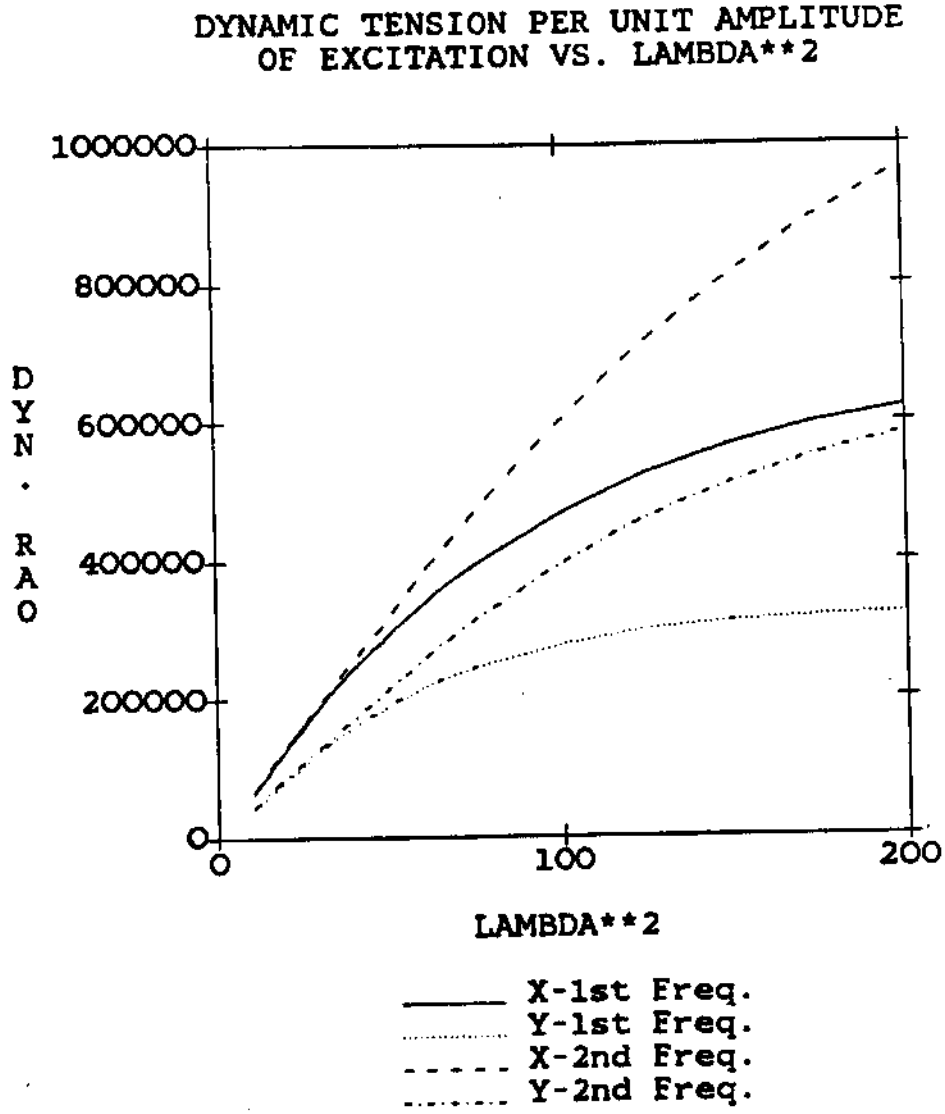

Figure 3-20: S_{Tx} for a Mooring Line in function of Lambda: 10D